國立交通大學

光電工程研究所

博士論文

利用弱共振腔費比布洛雷射二極體於
被動式分波多工光纖網路之研究

Studies on Weak-Resonant-Cavity-Fabry-Perot-Laser-Diode
-based Wavelength Division Multiplexer Passive Optical Network

研究生：廖育聖
指導教授：林恭如　教授
郭浩中　教授

中華民國一百年一月

利用弱共振腔費比布洛雷射二極體於被動式分波多工光纖網路之研究

Studies on Weak-Resonant-Cavity-Fabry-Perot -Laser-Diode-based Wavelength Division Multiplexer Passive Optical Network

研 究 生：廖育聖　　Student：Yu-Sheng Liao

指導教授：林恭如　　Advisor：Gong-Ru Lin

郭浩中　　Hao-Chung Kuo

國立交通大學 電機學院

光電工程研究所

博 士 論 文

A Dissertation

Submitted to Department of Photonics & Institute of Electro-Optical Engineering
College of Electrical Engineering
National Chiao Tung University
in partial Fulfillment of the Requirements
for the Degree of
Doctor
in

January 2011

Hsinchu, Taiwan, Republic of China

中華民國一百年一月

利用弱共振腔費比布洛雷射二極體於被動式分波多工光纖網路之研究

研究生：廖育聖　　指導教授：林恭如
郭浩中

國立交通大學 電機學院

光電工程研究所 博士班

摘　　要

本論文研究之弱共振腔費比布洛雷射二極體於被動式分波多工光纖網路系統，首先在可選擇的多通道傳輸上我們分析與展示側模注入鎖定費費比布洛雷射二極體，此外，我們使用直接調變方法的 1%反射率的弱共振腔費比布洛雷射二極體在注入鎖定效能於 2.5 千兆位元率與 25 公里傳輸討論與模擬了增強型注入鎖定頻寬的特性可達 0.48 奈米，此弱共振腔費比布洛雷射二極體可展示具有 25 個通道側模注入鎖定能力、鎖定範圍達 30 個奈米、最小注入光功率為-7 分貝毫瓦、以及高於 7 分貝的增益消滅比。同時，藉由使用增益切換式同調脈衝串列以及閥值電流降低的方式，我們展示了寬增益頻譜的近似無色特性的被動式分波多工光纖網路光源，在溫度 8 度的改變與誤碼率低於 10^{-10} 下接收靈敏度最多僅只差異 1 分貝，短線對傳的接收靈敏度可達-25.6 分貝毫瓦，傳輸 25 公里光纖的接收靈敏度在全 16 個通道最高僅有 2 分貝的光率靈敏度損失。最後，藉由使用已整合的監控感光二極體，我們展示一種嶄新的注入鎖定費比布洛雷射二極體自動回復機制，這樣的架構可以有效地植入於網路備援系統中，於 2.5 千兆位元率可達成的 50 秒內回覆 Q 值大於 8.2 以及側模抑制比達 35 分貝。這些研究將有助於未來的被動式分波多工光纖網路系統發展。

Studies on Weak-Resonant-Cavity-Fabry-Perot -Laser-Diode-based Wavelength Division Multiplexer Passive Optical Network

Student：Yu-Sheng Liao

Advisors：Dr. Gong-Ru Lin
Dr. Hao-Chung Kuo

Department of Photonics & Institute of Electro-Optical Engineering
College of Electrical Engineering
National Chiao Tung University

ABSTRACT

In this dissertation, we investigated the injection-locking wavelength-division-multiplexer passive optical network (WDM-PON) system. First, we introduced the side-mode injection-locked Fabry-Perot Laser Diode (FPLD) transmission diagnosis of a multi-channel selectable weak-resonant-cavity Fabry-Perot Laser Diode (WRC-FPLD). Moreover, the injection-locking performance of a 1% WRC-FPLD and demonstrate the 2.5-Gbit/s & 25-km WDM-PON application with the directly modulated WRC-FPLD based transmitter with enhanced injection-locking bandwidth of 0.48 nm was we discussed and simulated. A 25-channel locking capacity is reported for such a side-mode injection-locked WRC-FPLD with corresponding wavelength locking range of 30 nm, the minimal requested power of -7dBm and gain extinction ratio of <7 dB was demonstrated. Furthermore, we investigate quasi-color-free the WDM-PON transmitters with comparable broadband gain spectrum by using an optically gain-switching coherent pulse-train and threshold reduction of WRC-FPLDs. Nevertheless, such a degradation only induces a

power penalty of < 1dB at BER<10^{-10} over changing temperature of 9 degree. A receiving sensitivity back-to-back transmission can be -25.6 dBm, and 25-km transmission power penalties is up to 2 dB with 16 channels. At last, we demonstrated a novel in situ self-restoration scheme to track real time the injection locking of a FPLD by monitoring a built-in integrated photodiode. Such a scheme can be effectively implemented with a minimum amount of redundant network resources to achieve self-restoration within 50 seconds with Q factor >8.2 and side-mode suppression ratio (SMSR) >35 dB at 2.5 Gbit/s. These investigations would be useful in the next generation injection-locking based WDM-PON systems.

Acknowledgements
致謝

在博士班研究生的生涯中得到許多人的協助與支持，論文與學位方能順利完成。要特別感謝我的指導教授 林恭如老師在研究的過程中不斷的給予耐心的指導，在我低潮的時候給予我無私的協助支持與關懷，使我無論是在求學態度或是做人處世上都受益良多，您淵博的學識與為人師表的風範，將是我今後立身處世的標竿。除此之外，也感謝 郭浩中老師在學校時提供寶貴意見與協助，使我能夠順利完成我的博士學位，在此表達內心最誠摯的謝意。

感謝口試委員 賴賴暎杰教授、陳智弘教授、李柏璁教授、鄭木海教授、呂海涵教授、黃振發教授撥空來指導我的口試，提供許多寶貴的意見。實驗室博士班學長張詠誠、林俊榮對我教導與幫忙，無論在學識上、實驗上以及論文寫作上，都給我極大的幫助。 感謝中華電信研究所前瞻研究室廖虹惠、林恭政，因為你們的協助，才能讓我的實驗得以順利進行。還有學弟妹們邱奕祥、吳銘忠、林齊冠、陳家揚、張峻源、林螢聰、游昆潔、康榮瑞、紀裕傑、程子剛、彭國璿、林嘉琪、林奕宏、林俊儒、李宜錚與所有幫助過我的學弟妹們，在實驗上與生活上的協助，讓我在台北與新竹兩邊跑的情況下，能夠順順利利完成學業。

最後我要感謝我最摯愛的爸爸媽媽，給予我一個良好的學習環境，野果許多鼓勵與關懷，讓我可以順利完成我的博士學業。我哥哥、我姐姐的關心，以及其他好朋友，謝謝你們默默的給我全力的支持與關愛。在此與你們分享這份喜悅。謝謝！

CONTENTS

	Page
Chinese Abstract	i
English Abstract	ii
Acknowledgements	iv
Contents	v
List of Figures	vii
Chapter 1	1
Introduction	
1.1 Introduction of Fiber-to-the-Home (FTTH)	1
1.2 Introduction of Passive Optical Network (PON)	2
1.3 Introduction of Wavelength-Division-Multiplexer PON (WDM-PON)	3
1.4 Research Motivation	5
1.5 Organization of Dissertation	7
References	8
Chapter 2	10
Side-mode injection-locked FPLD transmission diagnosis	
2.1 Introduction and motivation	10
2.2 Side-mode suppressing ratio analysis	12
2.3 Degradation of linewidth enhancement factor on injection-locked side-mode	17
2.4 Experimental Setup	20
2.5 Data transmission diagnosis of side-mode injection-locked FPLD	22
2.6 Summary	25
References	27
Chapter 3	29
Weak-resonant-cavity Fabry-Perot laser diode with enhanced injection-locking bandwidth	
3.1 Introduction and motivation	29
3.2 System structure	30
3.3 Enhanced injection-locking bandwidth	32
3.4 Modeling and experimental results of WRC-FPLD	38

3.5 Data transmission performance of WRC-FPLD 45
3.6 Summary 50
References 52

Chapter 4 54
Pulsating master and injected slave weak-resonant-cavity laser diodes based quasi-color-free 2.5Gb/s WDM-PON
4.1 Introduction and motivation 54
4.2 Concept of coherent injection light source and quasi-color-free injection locking 56
4.3 Performances and discussions of quasi-color-free 2.5Gb/s RZ WDM-PON 58
4.4 Summary 68
References 70

Chapter 5 72
Self-restorable injection-locking monitor by integrated photodiode
5.1 Motivation and configuration 72
5.2 Modeling and experimental results of MPD-MCU based auto-restorable FPLD transmitter 75
5.3 Concept and Circuit Design 83
5.4 Injection-locking monitor of self-restoration 87
5.5 System performances of the MCU-based auto-restorable injection-locking transmitter 90
5.6 Summary 96
References 98

Chapter 6 100
Conclusions
6.1 Summary 100
6.2 Suggestions for Future Work 104
Curriculum Vitae
Publication list

Figure List

Fig. 1.1 Poin-to-point fiber networks access. 2
Fig. 1.2 Time-division-multiplexer PON fiber networks access. 3
Fig. 2.1 Wavelength locking range of the injection-locked mode in slave FPLD versus injection power. 12
Fig. 2.2 Measured SMSR curve on adjacent injected longitudinal mode and external optical power. 13
Fig. 2.3(a) Theoretically simulated SMSR of the side-mode injection-locked FPLD as function of the reflectivity change (ΔR) and the ratio of loss coefficient (Γ_m/Γ_0). 15
Fig. 2.3(b) Comparison on the theoretical and experimental results of the SMSR for one specific FPLD injection-locked mode. 17
Fig. 2.4 The simulated linewidth of the injection-locked FPLD as a function of the reflectivity change (ΔR). 18
Fig. 2.5 Spectral linewidths of the injection-locked FPLD in principle mode with (red line), without (blue line) modulation, and a reference laser source (black). 19
Fig. 2.6 The configuration of an experimental system with slave FPLD is side-mode injection-locked by a wavelength-sliced master FPLD. 21
Fig. 2.7 Measured injected power (hollow markers) and measured Q (solid markers) of the driving current at the principle longitudinal mode. 23
Fig. 2.8 BER analysis of wavelength injection-locked FPLD at different longitudinal modes and measured eye diagrams (inset) with and without injection. 25
Fig. 3.1 A DWDM-PON system with a WRC-FPLD based transmitter at the ONU end that is side-mode injection-locked by a wavelength-sliced master FPLD. 31
Fig. 3.2 A DWDM-PON system with a WRC-FPLD based transmitter at the ONU end that is side-mode injection-locked by a wavelength-sliced master FPLD. 32
Fig. 3.3 The output optical spectra of the free-running and injection-locking WRC-FPLD at different biased conditions. 33
Fig. 3.4 Injection-locking power dependent wavelength lock-in range of one longitudinal mode in the slave WRC-FPLD transmitter at the ONU end. 34
Fig. 3.5 Simulation of the normalized free-running spectra of WRC-FPLD with front-facet reflectivity of 30%, 10%, 1%, 0.1% and 0.01%. 36
Fig. 3.6 The gain spectral linewidth (solid squares) and the gain extinction (hollow squares) vs. the front-facet reflectivity of WRC-FPLD. 39
Fig. 3.7 The calculated Q factor and locking range of the injection locking WRC-FPLD with different reflectivity and injection power. 40
Fig. 3.8 The Q-factors of 1-% reflectivity WRC-FPLD and 30-% reflectivity FPLD with

injection power of +3dBm, -3dBm, -9 dBm. 42
Fig. 3.9 The requested injecting power (red solid square), corresponding the measured best Q-factor (red hollow square), and the minimal requested injecting power for Q=7.2 (blue solid square) at different driving currents. 43
Fig. 3.10 BER analysis of wavelength injection locked 1% WRC-FPLD at different longitudinal modes and measured eye diagrams (inset) with and without injection. 46
Fig. 3.11 P-I curve of the WRC-FPLD with the different optical power injection of -3dBm, -12dBm, and free-running. The inset shows the free-running optical spectrum. 48
Fig. 3.12 The numerically calculated small signal frequency response of laser with different Ibias/Ith of 1.5, 3.5, and 5. 49
Fig. 4.1 The WRC-FPLD based bi-directional quasi-color-free 2.5-Gb/s RZ WDM-PON with a pulsed WRC-FPLD coherent injection-locker. 57
Fig. 4.2. Configuration and band structure of the 1% front-facet AR-coated WRC FPLD. 58
Fig. 4.3(a) The P-I curve of the slave WRC-FPLD under master WRC-FPLD injection-locking with different power levels. 59
Fig. 4.3(b) Principle of the slave WRC-FPLD RZ transmitter triggered by externally injection from a pulsated master WRC-FPLD and directly modulated by a electrically PRBS data-stream. 60
Fig. 4.4 Left: optical spectra of the master WRC-FPLD operated at free-running (gray) and gain-switching (red) condition. Upper right: the normalized mode spectra at free-runing (gray) and gain-switching (red) conditions. Lower right: the linewidth and pulsewidth of the master WRC-FPLD with different RF modulation powers. 61
Fig. 4.5 Injection-locking power dependent wavelength lock-in range and corresponding SMSR of the slave WRC-FPLD transmitter. 62
Fig. 4.6 (a) Free-running AWG sliced WRC-FPLD. (b) Gain-switched AWG sliced WRC-FPLD. (c) Free-running slave WRC-FPLD injected by gain-switched WRC-FPLD. (d) NRZ modulated slave WRC-FPLD injected by gain-switched WRC-FPLD. 63
Fig. 4.7 the diagram of single-wavelength injection and gain-switched injection. 64
Fig. 4.8(a) Optical spectrum of injected WRC-FPLD at the temperature from 21oC to 29oC. 65
Fig. 4.8(b) BER of temperature-controlled WRC-FPLD with different injection locked mode number. 66
Fig. 4.9(a) Injection-locking power dependent wavelength lock-in range of one longitudinal mode in the slave WRC-FPLD transmitter at the ONU end. 67
Fig. 4.9(b) BER analysis of wavelength injection locked WRC-FPLD at different channels and measured pulsed RZ eye diagrams (inset). 68
Fig. 5.1 A self-restorable system for injection-locked FPLD with monitor photodiode. The MCU detects the MPD photocurrent and controls the TEC and the polarization controller. 74
Fig. 5.2 The frequency response of the directly modulated FPLD with 3-dB bandwidth of

4.2GHz 75
Fig. 5.3(a) Spectrum evolution of FPLD by detuning per 0.1-nm wavelength. 76
Fig. 5.3(b) Wavelength locking range of a side mode in the slave FPLD as a function of injection-locked power. 76
Fig. 5.4 (a) The photocurrent of MPD at the FPLD driving currents of 25, 30, and 35 mA as detuning wavelength. (b) The photocurrent of MPD at the injection power of + 3, 0, -3, -6, and -9 dBm as detuning wavelength 78
Fig. 5.5 The conceptual flow chart for designing the PD-MCU link based self-restoration. 84
Fig. 5.6 The circuit block for building a PD-MCU link based self-restoration unit. 85
Fig. 5.7 (a) The monitored PD current (upper, square-dotted curve) and the free-running FPLD spectrum (lower, block lines); (b) the spectra of the FPLD transmitter injection locked at different longitudinal modes (color lines at right part). 88
Fig. 5.8 The recovery experience of the self-restorable unlocked FPLD and corresponding MPD current controlled by MCU. 90
Fig. 5.9 The BER of the FPLD transmitter measured at three different conditions. 91
Fig. 5.10 Left: (a) Threshold current of FPLD before and after self-restoration. Right: The Optical eye-diagrams (b) before and (c) after auto-restoration. 92
Fig. 5.11 The BER of the FPLD transmitter before and after self-restoration at different wavelength-deviation conditions. 93
Fig. 5.12 Future system of the MPD-MCU based self-restoration unit. 95

利用弱共振腔費比布洛雷射二極體於被動式分波多工光纖網路之研究

研究生：廖育聖　　指導教授：林恭如
郭浩中

國立交通大學 電機學院

光電工程研究所 博士班

摘　　要

本論文研究之弱共振腔費比布洛雷射二極體於被動式分波多工光纖網路系統，首先在可選擇的多通道傳輸上我們分析與展示側模注入鎖定費費比布洛雷射二極體，此外，我們使用直接調變方法的1%反射率的弱共振腔費比布洛雷射二極體在注入鎖定效能於2.5 千兆位元率與25公里傳輸討論與模擬了增強型注入鎖定頻寬的特性可達 0.48 奈米，此弱共振腔費比布洛雷射二極體可展示具有 25 個通道側模注入鎖定能力、鎖定範圍達 30 個奈米、最小注入光功率為-7 分貝毫瓦、以及高於 7 分貝的增益消滅比。同時，藉由使用增益切換式同調脈衝串列以及閥值電流降低的方式，我們展示了寬增益頻譜的近似無色特性的被動式分波多工光纖網路光源，在溫度 8 度的改變與誤碼率低於 10^{-10} 下接收靈敏度最多僅只差異 1 分貝，短線對傳的接收靈敏度可達-25.6 分貝毫瓦，傳輸 25 公里光纖的接收靈敏度在全 16 個通道最高僅有 2 分貝的光率靈敏度損失。最後，藉由使用已整合的監控感光二極體，我們展示一種嶄新的注入鎖定費比布洛雷射二極體自動回復機制，這樣的架構可以有效地植入於網路備援系統中，於 2.5 千兆位元率可達成的 50 秒內回覆 Q 值大於 8.2 以及側模抑制比達 35 分貝。這些研究將有助於未來的被動式分波多工光纖網路系統發展。

Studies on Weak-Resonant-Cavity-Fabry-Perot -Laser-Diode-based Wavelength Division Multiplexer Passive Optical Network

Student：Yu-Sheng Liao

Advisors：Dr. Gong-Ru Lin
Dr. Hao-Chung Kuo

Department of Photonics & Institute of Electro-Optical Engineering
College of Electrical Engineering
National Chiao Tung University

ABSTRACT

In this dissertation, we investigated the injection-locking wavelength-division-multiplexer passive optical network (WDM-PON) system. First, we introduced the side-mode injection-locked Fabry-Perot Laser Diode (FPLD) transmission diagnosis of a multi-channel selectable weak-resonant-cavity Fabry-Perot Laser Diode (WRC-FPLD). Moreover, the injection-locking performance of a 1% WRC-FPLD and demonstrate the 2.5-Gbit/s & 25-km WDM-PON application with the directly modulated WRC-FPLD based transmitter with enhanced injection-locking bandwidth of 0.48 nm was we discussed and simulated. A 25-channel locking capacity is reported for such a side-mode injection-locked WRC-FPLD with corresponding wavelength locking range of 30 nm, the minimal requested power of -7dBm and gain extinction ratio of <7 dB was demonstrated. Furthermore, we investigate quasi-color-free the WDM-PON transmitters with comparable broadband gain spectrum by using an optically gain-switching coherent pulse-train and threshold reduction of WRC-FPLDs. Nevertheless, such a degradation only induces a

power penalty of < 1dB at BER<10^{-10} over changing temperature of 9 degree. A receiving sensitivity back-to-back transmission can be -25.6 dBm, and 25-km transmission power penalties is up to 2 dB with 16 channels. At last, we demonstrated a novel in situ self-restoration scheme to track real time the injection locking of a FPLD by monitoring a built-in integrated photodiode. Such a scheme can be effectively implemented with a minimum amount of redundant network resources to achieve self-restoration within 50 seconds with Q factor >8.2 and side-mode suppression ratio (SMSR) >35 dB at 2.5 Gbit/s. These investigations would be useful in the next generation injection-locking based WDM-PON systems.

Acknowledgements
致謝

在博士班研究生的生涯中得到許多人的協助與支持，論文與學位方能順利完成。要特別感謝我的指導教授 林恭如老師在研究的過程中不斷的給予耐心的指導，在我低潮的時候給予我無私的協助支持與關懷，使我無論是在求學態度或是做人處世上都受益良多，您淵博的學識與為人師表的風範，將是我今後立身處世的標竿。除此之外，也感謝 郭浩中老師在學校時提供寶貴意見與協助，使我能夠順利完成我的博士學位，在此表達內心最誠摯的謝意。

感謝口試委員 賴穎暘杰教授、陳智弘教授、李柏璁教授、鄭木海教授、呂海涵教授、黃振發教授撥空來指導我的口試，提供許多寶貴的意見。實驗室博士班學長張詠誠、林俊榮對我教導與幫忙，無論在學識上、實驗上以及論文寫作上，都給我極大的幫助。 感謝中華電信研究所前瞻研究室廖虹惠、林恭政，因為你們的協助，才能讓我的實驗得以順利進行。還有學弟妹們邱奕祥、吳銘忠、林齊冠、陳家揚、張峻源、林螢聰、游昆潔、康榮瑞、紀裕傑、程子剛、彭國璿、林嘉琪、林奕宏、林俊儒、李宜錚與所有幫助過我的學弟妹們，在實驗上與生活上的協助，讓我在台北與新竹兩邊跑的情況下，能夠順順利利完成學業。

最後我要感謝我最摯愛的爸爸媽媽，給予我一個良好的學習環境，野果許多鼓勵與關懷，讓我可以順利完成我的博士學業。我哥哥、我姐姐的關心，以及其他好朋友，謝謝你們默默的給我全力的支持與關愛。在此與你們分享這份喜悅。謝謝！

CONTENTS

	Page
Chinese Abstract	i
English Abstract	ii
Acknowledgements	iv
Contents	v
List of Figures	vii
Chapter 1 Introduction	1
1.1 Introduction of Fiber-to-the-Home (FTTH)	1
1.2 Introduction of Passive Optical Network (PON)	2
1.3 Introduction of Wavelength-Division-Multiplexer PON (WDM-PON)	3
1.4 Research Motivation	5
1.5 Organization of Dissertation	7
References	8
Chapter 2 Side-mode injection-locked FPLD transmission diagnosis	10
2.1 Introduction and motivation	10
2.2 Side-mode suppressing ratio analysis	12
2.3 Degradation of linewidth enhancement factor on injection-locked side-mode	17
2.4 Experimental Setup	20
2.5 Data transmission diagnosis of side-mode injection-locked FPLD	22
2.6 Summary	25
References	27
Chapter 3 Weak-resonant-cavity Fabry-Perot laser diode with enhanced injection-locking bandwidth	29
3.1 Introduction and motivation	29
3.2 System structure	30
3.3 Enhanced injection-locking bandwidth	32
3.4 Modeling and experimental results of WRC-FPLD	38

3.5 Data transmission performance of WRC-FPLD 45
3.6 Summary 50
References 52

Chapter 4 54
Pulsating master and injected slave weak-resonant-cavity laser diodes based quasi-color-free 2.5Gb/s WDM-PON
4.1 Introduction and motivation 54
4.2 Concept of coherent injection light source and quasi-color-free injection locking 55
4.3 Performances and discussions of quasi-color-free 2.5Gb/s RZ WDM-PON 58
4.4 Summary 68
References 70

Chapter 5 72
Self-restorable injection-locking monitor by integrated photodiode
5.1 Motivation and configuration 72
5.2 Modeling and experimental results of MPD-MCU based auto-restorable FPLD transmitter 75
5.3 Concept and Circuit Design 83
5.4 Injection-locking monitor of self-restoration 87
5.5 System performances of the MCU-based auto-restorable injection-locking transmitter 90
5.6 Summary 96
References 98

Chapter 6 100
Conclusions
6.1 Summary 100
6.2 Suggestions for Future Work 104
Curriculum Vitae
Publication list

Figure List

Fig. 1.1 Poin-to-point fiber networks access.
Fig. 1.2 Time-division-multiplexer PON fiber networks access.
Fig. 2.1 Wavelength locking range of the injection-locked mode in slave FPLD versus injection power.
Fig. 2.2 Measured SMSR curve on adjacent injected longitudinal mode and external optical power.
Fig. 2.3(a) Theoretically simulated SMSR of the side-mode injection-locked FPLD as function of the reflectivity change (ΔR) and the ratio of loss coefficient (Γ_m/Γ_0).
Fig. 2.3(b) Comparison on the theoretical and experimental results of the SMSR for one specific FPLD injection-locked mode.
Fig. 2.4 The simulated linewidth of the injection-locked FPLD as a function of the reflectivity change (ΔR).
Fig. 2.5 Spectral linewidths of the injection-locked FPLD in principle mode with (red line), without (blue line) modulation, and a reference laser source (black).
Fig. 2.6 The configuration of an experimental system with slave FPLD is side-mode injection-locked by a wavelength-sliced master FPLD.
Fig. 2.7 Measured injected power (hollow markers) and measured Q (solid markers) of the driving current at the principle longitudinal mode.
Fig. 2.8 BER analysis of wavelength injection-locked FPLD at different longitudinal modes and measured eye diagrams (inset) with and without injection.
Fig. 3.1 A DWDM-PON system with a WRC-FPLD based transmitter at the ONU end that is side-mode injection-locked by a wavelength-sliced master FPLD.
Fig. 3.2 A DWDM-PON system with a WRC-FPLD based transmitter at the ONU end that is side-mode injection-locked by a wavelength-sliced master FPLD.
Fig. 3.3 The output optical spectra of the free-running and injection-locking WRC-FPLD at different biased conditions.
Fig. 3.4 Injection-locking power dependent wavelength lock-in range of one longitudinal mode in the slave WRC-FPLD transmitter at the ONU end.
Fig. 3.5 Simulation of the normalized free-running spectra of WRC-FPLD with front-facet reflectivity of 30%, 10%, 1%, 0.1% and 0.01%.
Fig. 3.6 The gain spectral linewidth (solid squares) and the gain extinction (hollow squares) vs. the front-facet reflectivity of WRC-FPLD.
Fig. 3.7 The calculated Q factor and locking range of the injection locking WRC-FPLD with different reflectivity and injection power.
Fig. 3.8 The Q-factors of 1-% reflectivity WRC-FPLD and 30-% reflectivity FPLD with

injection power of +3dBm, -3dBm, -9 dBm.

Fig. 3.9 The requested injecting power (red solid square), corresponding the measured best Q-factor (red hollow square), and the minimal requested injecting power for Q=7.2 (blue solid square) at different driving currents.

Fig. 3.10 BER analysis of wavelength injection locked 1% WRC-FPLD at different longitudinal modes and measured eye diagrams (inset) with and without injection.

Fig. 3.11 P-I curve of the WRC-FPLD with the different optical power injection of -3dBm, -12dBm, and free-running. The inset shows the free-running optical spectrum.

Fig. 3.12 The numerically calculated small signal frequency response of laser with different Ibias/Ith of 1.5, 3.5, and 5.

Fig. 4.1 The WRC-FPLD based bi-directional quasi-color-free 2.5-Gb/s RZ WDM-PON with a pulsed WRC-FPLD coherent injection-locker.

Fig. 4.2. Configuration and band structure of the 1% front-facet AR-coated WRC FPLD.

Fig. 4.3(a) The P-I curve of the slave WRC-FPLD under master WRC-FPLD injection-locking with different power levels.

Fig. 4.3(b) Principle of the slave WRC-FPLD RZ transmitter triggered by externally injection from a pulsated master WRC-FPLD and directly modulated by a electrically PRBS data-stream.

Fig. 4.4 Left: optical spectra of the master WRC-FPLD operated at free-running (gray) and gain-switching (red) condition. Upper right: the normalized mode spectra at free-runing (gray) and gain-switching (red) conditions. Lower right: the linewidth and pulsewidth of the master WRC-FPLD with different RF modulation powers.

Fig. 4.5 Injection-locking power dependent wavelength lock-in range and corresponding SMSR of the slave WRC-FPLD transmitter.

Fig. 4.6 (a) Free-running AWG sliced WRC-FPLD. (b) Gain-switched AWG sliced WRC-FPLD. (c) Free-running slave WRC-FPLD injected by gain-switched WRC-FPLD. (d) NRZ modulated slave WRC-FPLD injected by gain-switched WRC-FPLD.

Fig. 4.7 the diagram of single-wavelength injection and gain-switched injection.

Fig. 4.8(a) Optical spectrum of injected WRC-FPLD at the temperature from 21oC to 29oC.

Fig. 4.8(b) BER of temperature-controlled WRC-FPLD with different injection locked mode number.

Fig. 4.9(a) Injection-locking power dependent wavelength lock-in range of one longitudinal mode in the slave WRC-FPLD transmitter at the ONU end.

Fig. 4.9(b) BER analysis of wavelength injection locked WRC-FPLD at different channels and measured pulsed RZ eye diagrams (inset).

Fig. 5.1 A self-restorable system for injection-locked FPLD with monitor photodiode. The MCU detects the MPD photocurrent and controls the TEC and the polarization controller.

Fig. 5.3(a) Spectrum evolution of FPLD by detuning per 0.1-nm wavelength.

Fig. 5.3(b) Wavelength locking range of a side mode in the slave FPLD as a function of injection-locked power.

Fig. 5.4 (a) The photocurrent of MPD at the FPLD driving currents of 25, 30, and 35 mA as detuning wavelength. (b) The photocurrent of MPD at the injection power of + 3, 0, -3, -6, and -9 dBm as detuning wavelength

Fig. 5.5 The conceptual flow chart for designing the PD-MCU link based self-restoration unit.

Fig. 5.6 The circuit block for building a PD-MCU link based self-restoration unit.

Fig. 5.7 (a) The monitored PD current (upper, square-dotted curve) and the free-running FPLD spectrum (lower, block lines); (b) the spectra of the FPLD transmitter injection locked at different longitudinal modes (color lines at right part).

Fig. 5.8 The recovery experience of the self-restorable unlocked FPLD and corresponding MPD current controlled by MCU.

Fig. 5.9 The BER of the FPLD transmitter measured at three different conditions.

Fig. 5.10 Left: (a) Threshold current of FPLD before and after self-restoration. Right: The Optical eye-diagrams (b) before and (c) after auto-restoration.

Fig. 5.11 The BER of the FPLD transmitter before and after self-restoration at different wavelength-deviation conditions.

Fig. 5.12 Future system of the MPD-MCU based self-restoration unit.

Chapter 1
Introduction

1.1 Introduction of Fiber-to-the-Home (FTTH)

The channel capacity requirement of high-speed access network inevitably accelerates the necessity in developing fiber-optics communication with narrower channel spacing and/or higher channel data rate. To accommodate upcoming demands due to the growing population in future broadband optical access networks, fiber-to-the-home (FTTH) [1.1-1.2] networks have been developed for business, education, communication, and entertainments services. Based on these applications, the requests of high definition (HD) image and video stream are greatly growing. Nowadays, many countries (such as United States, Japan, Korea, and China) define the broadband network access to be an important deployed point. In United States, over 6 million home have enjoyed the FTTH services, and grows quickly. Currently in Taiwan (2010), the dominated broadband service by internet service provider (ISP) is point-to-point (P2P) Ethernet-access network, so-called fiber-to-the-building (FTTB), system as following Fig.1.1. Between the central office and network end node, a power-supplied Ethernet switch is necessary equipment for such P2P structure [1.3-1.4]. The multi-service P2P structure uses the wavelength of 1550 nm for downstream service, and the wavelength of 1310 nm for upstream service. Most of P2P equipments are mature and related low cost which is the main reason chosen by ISP. Recently, the technology of passive optical network (PON) provides another option of broadband service for ISP. Without active components between central office and network end node is the premise of PON. By replacing the active devices, the maintaining cost of ISP can be significant reduced.

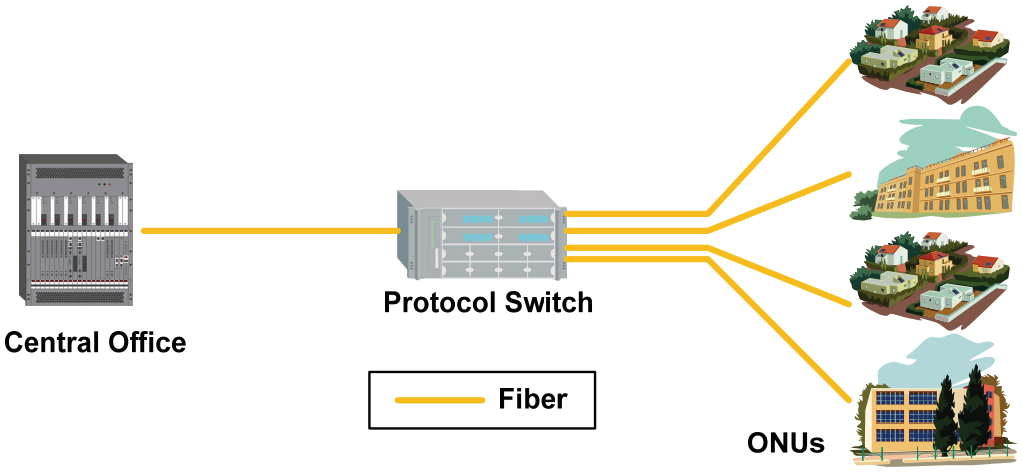

Fig. 1.1 Poin-to-point fiber networks access

1.2 Introduction of Passive Optical Network (PON)

The most popular multiplex technology of PON application is time division multiple (TDM) access. The principle of TDM-PON is that each of multiple subscribers used for downstream and upstream data transmission is assigned by individual time slot as illustrated in Fig. 1.2. One or two optical power splitter plays the role of separating and combing the connection of many subscribers. Recently, several alternative PON implementation scheme have been devised such as Ethernet passive optical network (EPON) and gigabit passive optical network (GPON) [1.5-1.6]. Fixed time slot for each subscriber can let central office differentiate the source and destination of data signal. However, due to this configuration, the subscriber cannot use the surplus bandwidth even if the other subscriber does not use. Burst-mode transmitter and receiver in optical network units (ONUs) and optical line terminals (OLTs), respectively, can turn-on and turn-off quickly if the time slot does not be possessed by the subscriber. Another issue of TDM-PON is caused by different transmission distance for each subscriber. For each incoming burst data signal, the time delay, synchronization, and a short guard time are necessary in this TDM-PON system. The management and control function of EPON/GPON application have been developed, and embedded into a high-density-silicon-based application-specified integrated circuit (ASIC)

chip which are namely OLT media access controller (MAC) and ONU MAC.

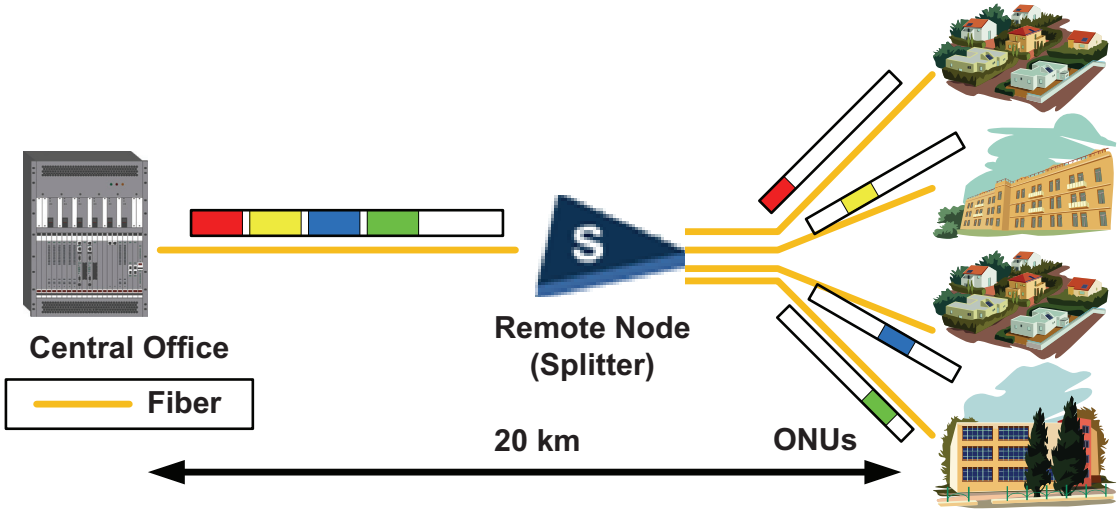

Fig. 1.2 Time-division-multiplexer PON fiber networks access

Table 1.1. FTTH access Technology Comparison

Attribute	**Active**	**PON**	
	Active Ethernet	EPON	GPON
Type of ODN	Active	Passive	Passive
Standardized	IEEE 802.3u	IEEE 802.3ah	ITU-T G.984
Capacity	1 user per passive tree	16 user per passive tree	32 user per passive tree
Bandwidth of upstream/downstream	100M/100M	1.25Gbps/1.25Gbps	1.25Gbps/2.5Gbps
Reach	10~80km	20km	20km

1.3 Introduction of Wavelength-Division-Multiplexer PON

Wavelength division multiplexed passive optical network (WDM-PON) is a popular technology for future broadband access networks because it provides large bandwidth, easy upgradability, high security and virtual point-to-point connection to end-users [1.7-1.8]. Each subscriber is assigned one or a pair wavelength, and the transmission data is continuous

at whole time. The multiplex and de-multiplex can be realized using arrayed waveguide gratings (AWGs) or thin-film dielectric filters. The channel spacing can reach as narrow as 50 or 100 GHz (0.4 or 0.8 nm), which is similar as the standard channel spacing of dense wavelength division multiplexer (DWDM) which defined by international telecommunication union (ITU-T) recommendation. A WDM component is used at the remote node (RN) instead of a power splitter, and an additional WDM multiplexer is located at central office to separate the wavelength from each subscriber. However, many challenges need to overcome in WDM-PON application. The specific wavelength of transmitter must be exactly the same as wavelength window of AWG. For such DWDM-PON application, retaining specific wavelength (such as thermal electric cooler (TEC) equipment) relatively cost too much, especially in sensitive FTTH market. For the deployment of practical WDM-PONs, the most critical issue is to develop the low cost WDM light sources for the optical network unit. To construct the low-cost WDM-PON, Lin *et. al.* demonstrate a bidirectional wavelength-division-multiplexed passive optical network with 1.25-Gb/s upstream and 2.5-Gb/s downstream over 20-km transmission distance by employing gain-saturated reflective semiconductor optical amplifiers (RSOAs) for wavelength- independent optical network terminals [1.9]. The upstream signals are generated by remodulating the downstream signals whose modulation amplitude is squeezed through gain-saturated RSOAs. On the other hand, Choi *et. al.* demonstrate color-free operation of a dense wavelength-division-multiplexing passive optical network based on the wavelength-locked Fabry–Pérot laser diodes with injection of a low-noise broadband light source (BLS) at Manchester coded data rate of 100-Mb/s [1.10]. The color-free operation, i.e., wavelength-independent operation, was obtained at 50-GHz channel spacing with the help of a narrow injection bandwidth of the low-noise BLS. Such injection-locked optical sources (Fabry-Perot laser diodes (FPLDs) and reflective semiconductor optical amplifiers (RSOAs)) have recently become one of the practical solutions for the next-generation WDM-PON

system due to their promising features of broadband wavelength tenability, enhanced side-mode suppressing ratio, and improved modulation bandwidth performances.

1.4 Research Motivation

Most of previous works established the WDM-PON system with broadband injecting source (Amplified spontaneous emission (ASE)) at central office, and such a WDM-PON induces the intra-band crosstalk. The ASE source inherently suffers from large intensity noise (IN) caused by spontaneous-spontaneous beat noise, such that the spontaneous–spontaneous beating noise injects into the WRC-FPLD, which degrades the signal-to-noise ratio (SNR) and causes the penalty in receiving power for obtaining error-free data. However, the spectrally sliced incoherent ASE suffers from large intensity noise to limit the transmission bit-rate at 2.5 Gb/s. With over 2.5-Gbps WDM-PON, the coherence injection-locked sources is inevitable. Nonetheless, it was seldom addressed that the FPLD under side-mode injection-locking condition can also be approached as a high-quality optical light source in particular conditions. Although most of the transmission performances have been comprehensively investigated, some of the important parameters such as the SMSR, the spectral linewidth and its enhancement factor, and the bit-error-rate (BER) power penalty of the optical carrier based on the injection-locked side modes were never discussed. In order to increase the injection efficiency, reducing the front-face reflectivity could let FPLDs be close to ROSA. However, the injection-locked RSOAs of previous works suffer a drawback of serious intensity noise from high bit-rate operation. Most of the proposed WDM-PON works on a FPLD injection-locked scheme, which still meets the problems of wavelength discontinuity and finite injection-locking wavelength range due to the limitation on lasing mode selected by the resonant cavity of the FPLD. To overcome the problems, making the RSOA like a FPLD has thus emerged to deal the trade-off between noise reduction and color-free operation. Therefore, the weak-resonant-cavity FPLD placed at the ONUs enable

a more cost-effective and high-performance infrastructure for WDM-PONS.

All these coherence-injection applications require precisely controlling the wavelength matching between the master and the slave laser, and the shortcoming of maintenance and stability is accompanied in practical WDM-PON systems. Currently, the proposed approaches are limited by colorless issue, low operation bandwidth, power budget and high intensity noise when applying to the optical link. The coherent master BLS injection-locked slave laser diode has oriented new solution towards high-bit-rate WDM-PONs. By the threshold current reduction of injection locked WRC-FPLD, the return-to-zero (RZ) data-format at 2.5 Gb/s using the slave WRC-FPLDs coherently injection-locked by a pulsated WRC-FPLD based quasi-colorless master source is interesting. Without using data-format transformer circuit, both the down- and up-stream slave WRC-FPLDs are directly modulated by the PRBS NRZ data, and coherently injection-locked by the gain-switched master WRC-FPLD after 200-GHz AWG channelization.

At last, even though, all these coherence-injection applications require precisely controlling the wavelength matching between the master and the slave laser, and the shortcoming of maintenance and stability is accompanied in practical WDM-PON systems. The relatively high cost of the transmitters with specified wavelengths has hindered market acceptance. In principle, the injection-locking lasers strictly rely on external seeding or self-feedback injecting a continuous-wave (CW) laser to achieve single-mode pulsed generation. Many versatile injection-locking techniques, such as the clock frequency division [1.11], the 10-Gbps WDM passive optical network (PON) [1.12], the parallel transmission and wavelength routing network (Para-Wave NET) [1.13], and the all-optical non-return-to-zero (NRZ) to pseudo-return-to-zero (PRZ) format transformation [1.14], have been demonstrated. All these applications require precisely controlled injection-locked FPLD, but the maintenance as regards its stability and reliability usually requires complicated modules. Therefore, fault management is one of the crucial aspects in network management

to enhance the network reliability. Of late, many efforts have been focused on the fault-monitoring methods [1.15] and the self-restorable networks [1.16] to achieve network protection. We are interested in investigating a novel injection-locking monitor for real-time and self-restorable tracking the FPLD-based WDM-PON transmitter. Without employing high-speed electronics and instruments, the proposed in situ monitoring and self-restorable architecture uses the integrated MPD, which is usually employed to monitor the optical power illuminated by the FPLD.

1.5 Organization of this Dissertation

The dissertation is organized into six chapters. The present chapter, being the first, introduces the research history of the WDM-PON and motivation of the dissertation. Chapter 2 introduces the side-mode injection-locked FPLD transmission diagnosis of a multi-channel selectable injection-locked Fabry-Perot Laser Diode with anti-reflection coated front facet. The Chapter 3 discusses and simulates the injection-locking performance of a 1% WRC-FPLD and demonstrates the 2.5-Gbit/s WDM-PON application with the directly modulated WRC-FPLD based ONU transmitter with enhanced injection-locking bandwidth. The Chapter 4 demonstrates quasi-color-free the WDM-PON transmitters with comparable broadband gain spectrum by using an optically gain-switching coherent pulse-train and threshold reduction of WRC-FPLDs. Without using data-format transformer circuit, both the down- and up-stream slave WRC-FPLDs are directly modulated by the PRBS NRZ data, and coherently injection-locked by the gain-switched master WRC-FPLD after 200-GHz AWG channelization to perform bi-directional RZ transmission at 2.5 Gb/s over 25 km. The Chapter 5 shows a novel in situ self-restoration scheme to track real time the injection locking of a FPLD by monitoring a built-in integrated photodiode. Finally a brief conclusion for these researched is given in the sixth chapter.

References

[1.1] G. Kesier, FTTX concepts and Applications, *Wiley-Interscience*, (2006).

[1.2] J. George, "Application compelling fiber to the home," *The Prism FTTH*, **3**, 47, (2006).

[1.3] D. Meis, "Fiber Terminal Distribution Systems Cut Develop Cost and Risk," *Broadband Properties*, 64, (2006).

[1.4] G. P. Agrawal, "Fiber-optic Communication Systems", *2nd Ed., John Wiley & Sons, New York*, **3**, 121, (1997).

[1.5] E. Shraga, "GPON and EPON Economical Comparison," *Flexlight Network White Paper*, (2004).

[1.6] D. Parsons, "GPON vs. EPON Cost Comparison," *Broadlight White Paper*, (2005).

[1.7] H. D. Kim, S.-G. Kang, and C.-H. Lee, "A low-cost WDM source with an ASE injected Fabry-Perot semiconductor laser," *IEEE Photon. Technol. Lett.*, **12**, 1067 (2000).

[1.8] S. J. Park, C. H. Lee, K. T. Jeong, H. J. Park, J. G. Ahn, and K. H. Song, "Fiber-to-the-home services based on wavelength-division-multiplexing passive optical network," *IEEE J. Lightw. Technol.*, **22**, 2582, (2004).

[1.9] S.-C. Lin, S.-L. Lee, and C.-K. Liu, "Simple approach for bidirectional performance enhancement on WDM-PONs with directmodulation lasers and RSOAs," *Opt. Express,* **16**, 3636, (2008).

[1.10] K.-M. Choi, J.-S. Baik, and C.-H. Lee, "Broad-band light source using mutually injected Fabry–Pérot laser diodes for WDM-PON," *IEEE Photon. Technol. Lett.*, **17**, 2529, (2005).

[1.11] Y. Matsui, S. Kutsuzawa, S. Arahira, Y. Ogawa, and A. Suzuki, "Bifurcation in 20-GHz gain-switched 1.55-μm MQW lasers and its control by CW injection seeding," *IEEE J. Quantum Electron.*, **34**, 1213, (1998).

[1.12] Z. Xu, Y.-J. Wen, W.-D. Zhong, C.-J. Chae, X.-F. Cheng, Y. Wang, C. Lu, and J. Shankar, "High-speed WDM-PON using CW injectionlocked Fabry-Pérot laser diodes," *Opt. Express.*, **15**, 2953, (2007).

[1.13] N. Kashima, S. Yamaguchi, and S. Ishii, "Optical transmitter using side-mode injection locking for high-speed photonic LANs," *IEEE J. Lightwave Technol.*, **22**, 550, (2004).

[1.14] Y.-C. Chang, Y.-H. Lin, J. H. Chen, and G.-R. Lin, "All-optical NRZ-to-PRZ format transformer with an injection-locked Fabry-Perot laser diode at unlasing condition", *Opt. Express*, **12**, 4449, (2004).

[1.15] C. K. Chan, F. Tong, L. K. Chen, K. P. Ho, and D. Lam, "Fiber-fault identification for

branched access networks using a wavelength-sweeping monitoring source," *IEEE Photon. Technol. Lett.*, **5**, 614, (1999).

[1.16] K. Lee, S. B. Lee, J. H. Lee, Y. -G. Han, S. -G. Mun, S. -M. Lee, and C. -H. Lee, "A self-restorable architecture for bidirectional wavelength-division-multiplexed passive optical network with colorless ONUs," *Opt. Express*, **15**, 4863, (2007).

Chapter 2
Side-mode injection-locked FPLD transmission diagnosis

2.1 Introduction and motivation

To meet increasing demand, the single-longitudinal-mode and low-noise operation of the laser sources with selectable channel wavelengths [2.1-2.6] are critical issues for such a wavelength-division-multiplexing (WDM) optical access system. Some of the previous works focused on developing the specific broadcasting architectures to release the cost issue of the rather expensive DFB laser transmitters by sharing over a large customer base. One solution is the use of 1.5-μm DFB in conjunction with optical amplifiers to achieve larger link budgets [2.1]. Alternatively, a high-power diode-pumped erbium-doped fiber amplifier (EDFA) based ring laser using an intra-cavity liquid-crystal fiber etalon filter was proposed with its output wavelength electrically tunable from 1525 to 1586 nm [2.2]. In particular, a transmission experiment at 2.5 Gbit/s over 30 km using a wavelength-locked Fabry–Perot laser diode (FPLD) externally controlled by another spectrally sliced Fabry–Perot laser diode was also performed [2.3]. Under such kind of injection-locking, the suppression on second/third harmonic distortion and third-order inter-modulation distortion was demonstrated [2.4]. Moreover, a distinguished and cost-effective method for generation a channel-selectable single-mode FPLD by self-seeding it with low-level injection power was ever reported [2.5]. Nearly single-mode source with side-mode suppressing ratio (SMSR) of higher than 40 dB over all selectable channels with a wavelength tuning range covering 11.5 nm was demonstrated with such a self-seeding FPLD [2.6]. Typically, the aforementioned technology is achieved by use of a tunable linearly-chirped fiber Bragg grating or an active

Fabry–Perot filter to provide wavelength-selective injection and output filtering function. Alternatively, the other approaches using an FPLD injection-locked with a coherent optical source have also been presented in previous works. For example, a spectrally sliced amplified-spontaneous–emission (ASE) light source and a spectrally sliced FPLD have also been proposed as the WDM optical sources, [2.7] which were in connection with the add–drop modules that are composed of "4skip0" and add-drop filters. The experiments in a novel optical distribution network for multistage access with multiple remote nodes (RNs) have shown error-free transmission with simultaneous bidirectional 1.25 Gbit/s per channel up to 20 km. Not long ago, we have also demonstrated a single-longitudinal-mode optical source generated using a mode-beating noise-suppressed FPLD-EDFA link under mutually injection–locking condition [2.8]. Similar FPLD-FPLD injection-locked sources were emerged as the WDM passive optical network (PON) transmitters [2.9], and the high-speed-uplink WDM-PON architecture at 10 Gbit/s with 15-km transmission capability has been demonstrated using the injection-locked FPLDs [2.10]. Up to now, most researching efforts are focused on the injecting architectures of the FPLD at its principle longitudinal mode under high-gain competition. Nonetheless, it was seldom addressed that the FPLD under side-mode injection-locking condition can also be approached as a high-quality optical light source in particular conditions. Although most of the transmission performances have been comprehensively investigated, some of the important parameters such as the SMSR, the spectral linewidth and its enhancement factor, and the bit-error-rate (BER) power penalty of the optical carrier based on the injection-locked side modes were never discussed. In this chapter, we analyze the performances of a side-mode injection-locked FPLD by externally injecting with another spectrally sliced FPLD. The effects of the biased current and the external injection power on the optimization of a side-mode injection-locked FPLD at different longitudinal modes are discussed. The transmission performances such as extinction ratio, Q factor, and BER at 2.5 Gbit/s over 25

km are also characterized.

2.2 Side-mode suppressing ratio analysis

The wavelength locking range of the slave FPLD measured by using a modified delayed-self-homodyne (MDSH) scheme is shown in Fig. 2.1, which is defined as the wavelength injection-locking range for one specific longitudinal mode of the slave FPLD with its SMSR >35 dB.

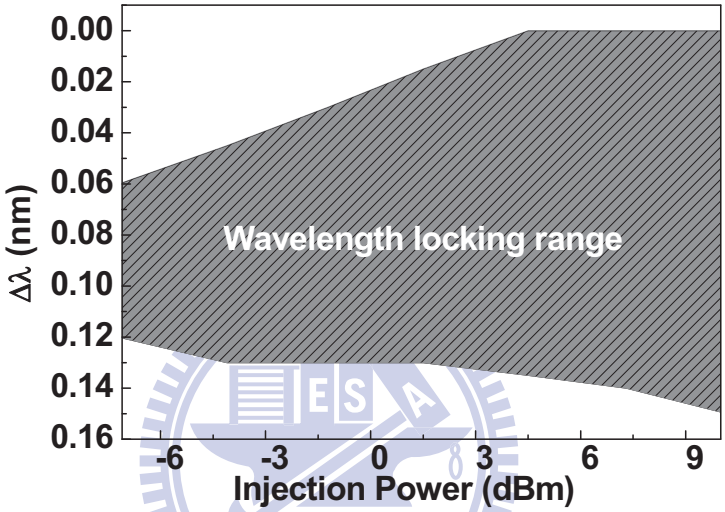

Fig. 2.1 Wavelength locking range of the injection-locked mode in slave FPLD versus injection power.

The detuning wavelength is defined as the wavelength shift on the longitudinal mode of the master FPLD with respect to that of the slave FPLD. The stable injection-locking region is bounded by two solid curves and the slave FPLD is operated at higher injection ratio to reach larger injection-locking range under such conditions, where the injection ratio is defined as the power ratio of the injected signal to the free-running optical signal inside FPLD cavity. In addition, a relatively weak signal with considerable noise has also been observed as the injection wavelength is detuned away from the slave FPLD's longitudinal mode by 0.15 nm. After injection-locking with the master FPLD, the SMSR of the slave FPLD as a function of the detuning external injection power and the order of the side longitudinal mode is shown in Fig. 2.2. The measured SMSR of injection-locked FPLD is at without-modulation condition.

For modulated FPLD, the SMSR will decay up to 3 dB. This figure provides the minimum optical power at all longitudinal modes to initiate the wavelength injection-locking. Note that a higher ordered longitudinal mode acquires larger injecting power to achieve a SMSR > 35 dB. In more detail, the SMSR of the slave FPLD with the seeding from the master FPLD is theoretically discussed as below.

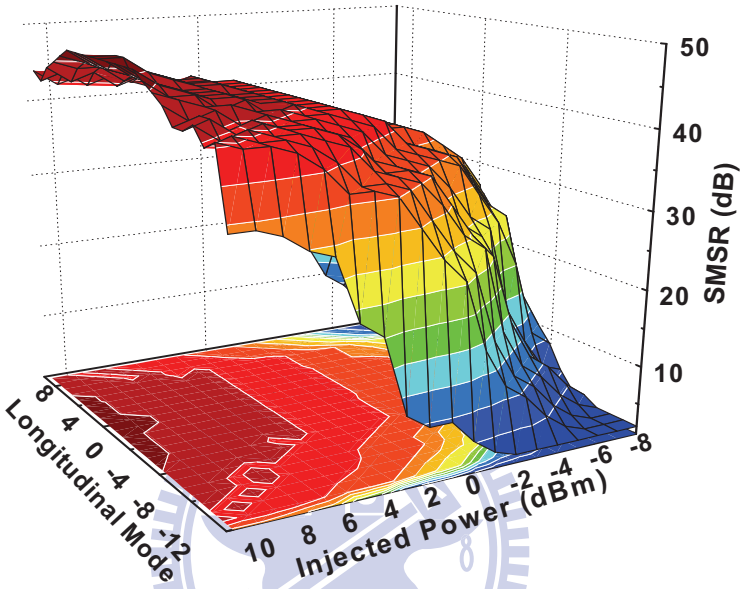

Fig. 2.2 Measured SMSR curve on adjacent injected longitudinal mode and external optical power.

Typically, the SMSR of the FPLD longitudinal mode under external injection-locking condition can be expressed by [2.11]

$$SMSR = \frac{I_m}{I_0} = \frac{g_m}{(\Gamma'_m - g_m)} \times \frac{(\Gamma'_0 - g_0)}{g_0} = \frac{\dfrac{g_m}{(1+\dfrac{I_m}{I_S(m)})}}{\Gamma'_m - \dfrac{g_m}{(1+\dfrac{I_m}{I_S(m)})}} \times \frac{\Gamma'_0 - \dfrac{g_0}{(1+\dfrac{I_0}{I_S(0)})}}{\dfrac{g_0}{(1+\dfrac{I_0}{I_S(0)})}}, \qquad (1)$$

where the optical intensity of the fundamental (the largest) mode and the desired side-mode to be injection-locked in the slave FPLD are denoted as I_0 and I_m, the index j defines each parameter, g_j denotes the gain coefficient, Γ_j denotes the loss coefficient, and I_S denotes the saturation intensity. We assume that only the intensities of the external injection at λ_0 (the

central wavelength of principle mode) and λ_m (the injection-locked side-mode) can contribute to the slave FPLD. In our case, a new parameter Δm is employed to describe the wavelength difference between the injection-locked m^{th} side-mode and the principle mode ($\Delta m=0$) naturally lasing at the gain peak of the slave FPLD. The material gain spectrum is approximated by a Lorentzian shape function to model the spectral roll-off of the slave FPLD gain profile. The gain of each m^{th} side-mode can thus be described by $g_m=g_0/[2.1+(\Delta m/M^2)]$, where M denotes the total mode number related to the full-width-at-half-maximum of the slave FPLD gain spectrum. If we assume that the saturation conditions of the principle and side modes are equivalent (i.e. $I_s(0) = I_s(m)$), the SMSR, I_0/I_m, can thus be described as a function of the ratio of loss coefficients.

$$SMSR = \frac{I_m}{I_0} = \frac{C_1(\Gamma'_0/(1+\Delta m/M^2) - C_2\Gamma'_m)}{\Gamma'_m} = \frac{C_1(1 - C_2\,\Gamma'_m(1+\Delta m/M^2)/\Gamma'_0)}{\Gamma'_m(1+\Delta m/M^2)/\Gamma'_0}$$

$$= \frac{C_1\left[1 - C_2\ln\left(R'_{eff,m}\right)(1+\Delta m/M^2)/\ln\left(R'_{eff,0}\right)\right]}{\ln\left(R'_{eff,m}\right)(1+\Delta m/M^2)/\ln\left(R'_{eff,0}\right)}, \qquad (2)$$

where C_1 and C_2 are constants. In addition, the relationship between the loss coefficient Γ and the reflectivity R can be correlated each other by writing the following formula $\Gamma_j = -\ln(R'_{eff,j})/2L$, where $R'_{eff,}$ denotes the effective reflectivity of the slave FPLD cavity under external injection. Hereafter, we define the reflectivity change (ΔR) in term of external injection power as

$$\Delta R = \frac{I_{ext}}{\Gamma_F} \Big/ \frac{I_o}{1-R}, \qquad (3)$$

where I_{ext} is the optical intensity of the external injection, and the Γ_F is the coupling loss between the slave FPLD and the coupled SMF. Thus, the change of the loss coefficient for the slave FPLD can be described as

$$\Delta\Gamma = -\frac{\partial}{\partial R}\left[\frac{\ln\left(R'_{eff}\right)}{2L}\right]\cdot\Delta R = -\frac{\Delta R}{2LR'_{eff}}, \tag{4}$$

Consequently, the SMSR of the slave FPLD under external injection-locking can be re-written as a function of the reflectivity change. The ratio of loss coefficients Γ_0'/Γ_m' can be represented as

$$\frac{\Gamma_m'}{\Gamma_0'} \Rightarrow \frac{\Gamma_m+\Delta\Gamma_m}{\Gamma_0+\Delta\Gamma_0} = \frac{\Gamma_m - \dfrac{\Delta R}{2LR_{eff,m}}}{\Gamma_0 - \dfrac{\Delta R}{2LR_{eff,0}}} = \frac{-\dfrac{\ln(R_{eff,m})}{2L} - \dfrac{\Delta R}{2LR_{eff,m}}}{-\dfrac{\ln(R_{eff,0})}{2L} - \dfrac{\Delta R}{2LR_{eff,0}}},$$

$$\cong \frac{[\ln(R_{eff,m} + \dfrac{\Delta R_{eff,m}}{R_{eff,m}})]}{[\ln(R_{eff,0})]}, \tag{5}$$

in which the effective reflectivity of the principle mode is assumed to be equivalent to the largest side mode, and the reflectivity change of the side mode is far stronger than that of the principle mode ($\Delta R_{eff,0} >> \Delta R_{eff,m} \cong 0$).

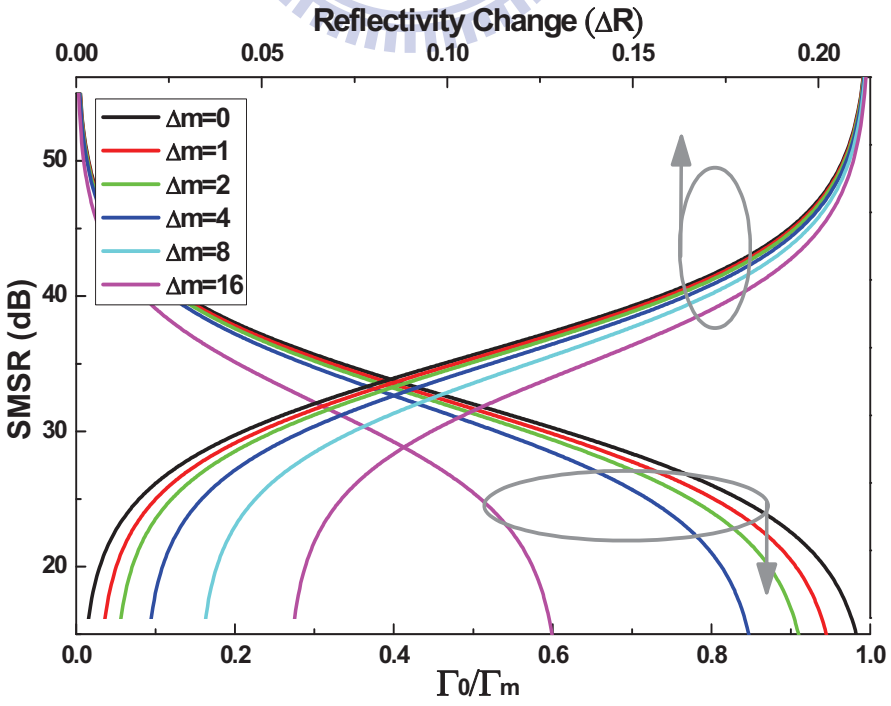

Fig. 2.3(a) Theoretically simulated SMSR of the side-mode injection-locked

FPLD as function of the reflectivity change (ΔR) and the ratio of loss coefficient (Γ_m/Γ_0).

By setting the output power of the slave FPLD as 0.1 mW under external injection, the cavity length (L) as 250 μm, the refractive index (n) as 3.5, and the photon lifetime (T_R) as 5.8 ps, the SMSR of the slave FPLD under external injection-locking is simulated and shown in Fig. 2.4. The SMSR of the slave FPLD as a function of the reflectivity change can also be obtained as shown in Fig. 2.3(a). Obviously, the SMSR of the slave FPLD can be up to 50 dB as the loss of the principle mode is far smaller than that of the injection-locked side-mode (i.e., the Γ_m/Γ_0 is infinitely small). To elucidate the injection-locking performance, we further compare the experimentally obtained and theoretical simulated SMSRs for one side-mode of the slave FPLD under external injection, as shown in Fig. 2.3(b). As illustrated in Fig. 2.2, we have already shown that the experimentally measured SMSR is well proportional to the externally injection-locking power. Since there is a linear relationship between the effective reflectivity change (ΔR) and the external injection power (I_{ext}), a relatively high injection could result in an increasing reflectivity change as well as an enhanced SMSR. The obtained reflectivity changing (ΔR) is caused by an external injection into the slave FPLD. Between the ΔR from 0 to 0.16, the experimental result meets with our simulation. Beyond ΔR of 0.16, the injection power should be higher than 8 mW to induce the reflectivity changing, and the experimental result does not meet with simulation result. The reflectivity changing distinctly is dominated by another effect with the high optical injection.

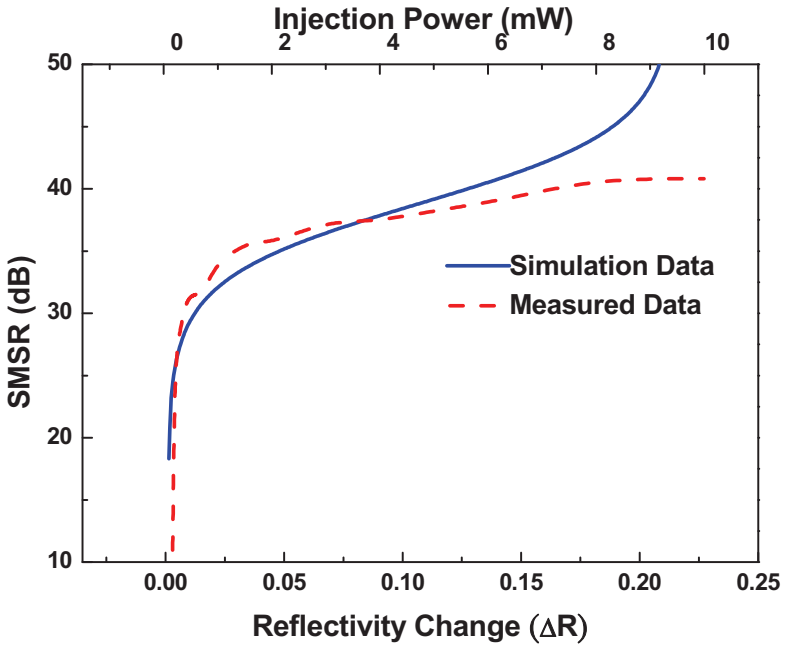

Fig. 2.3(b) Comparison on the theoretical and experimental results of the SMSR for one specific FPLD injection-locked mode.

2.3 Degradation of linewidth enhancement factor on injection-locked side-mode

If we consider the Fabry-Perot etalon effect of the slave FPLD, the 3-dB linewidth of the lasing side-mode from the slave FPLD under external injection can thus be described as

$$\Delta\lambda = \frac{\lambda_m^2}{2\pi nL}\frac{\left(1-R_{eff}G_{eff}\right)}{\sqrt{R_{eff}}\sqrt{G_{eff}}}, \tag{6}$$

when the effective reflectivity of the slave FPLD is slightly changed due to the external injection-locking, this may give rise to a change in the longitudinal-mode linewidth of the slave FPLD. That is

$$\Delta\lambda = \frac{\lambda_m^2}{2\pi nL}\frac{\left[1-R'_{eff,m}G_{eff}\right]}{\sqrt{R'_{eff,m}}\sqrt{G_{eff}}} = \frac{\lambda_m^2}{2\pi nL}\frac{\left[1-(R_m+\Delta R)G_1/\left(1+\left(\Delta m/M^2\right)\right)\right]}{\sqrt{\left(R_m+\Delta R\right)}\sqrt{G_1/\left(1+\left(\Delta m/M^2\right)\right)}}, \tag{7}$$

Thus, the simulated linewidth of the FPLD can also be plotted as a function of the change in

reflectivity for the slave FPLD due to the side-mode injection, as shown in Fig. 2.4.

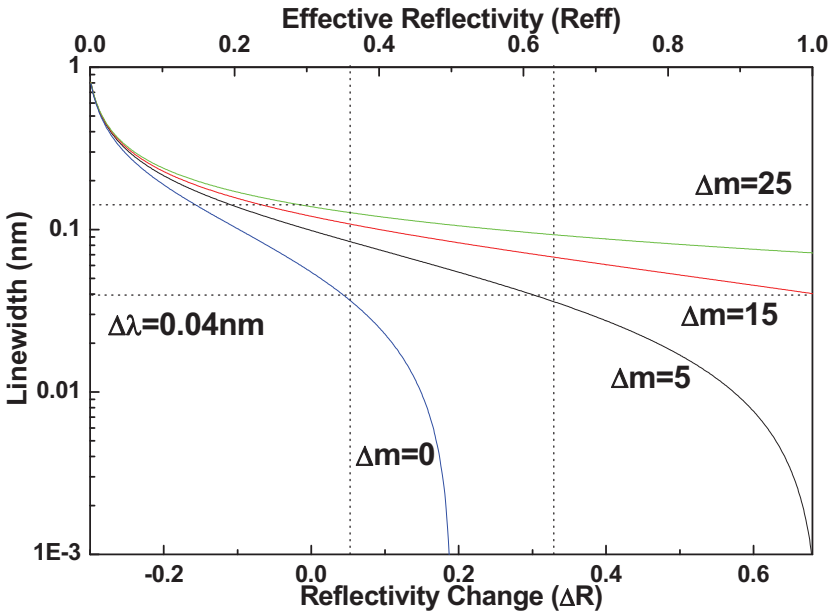

Fig. 2.4 The simulated linewidth of the injection-locked FPLD as a function of the reflectivity change (ΔR).

Therefore, the linewidth reduction and side-mode suppression of the slave FPLD can be understood through the theoretical modeling shown above. The measured 3-dB spectral linewidth for one longitudinal mode of the CW free-running and the directly modulated FPLD are 0.024 and 0.04 nm, respectively. These results correlate well with the theory since that the transient variation in carrier density simultaneously affects the refractive index and the linewidth of the slave FPLD. However, the linewidth of the directly modulated FPLD under external injection-locking are reduced from 0.04 to 0.018 nm, respectively, as shown in Fig. 2.5.

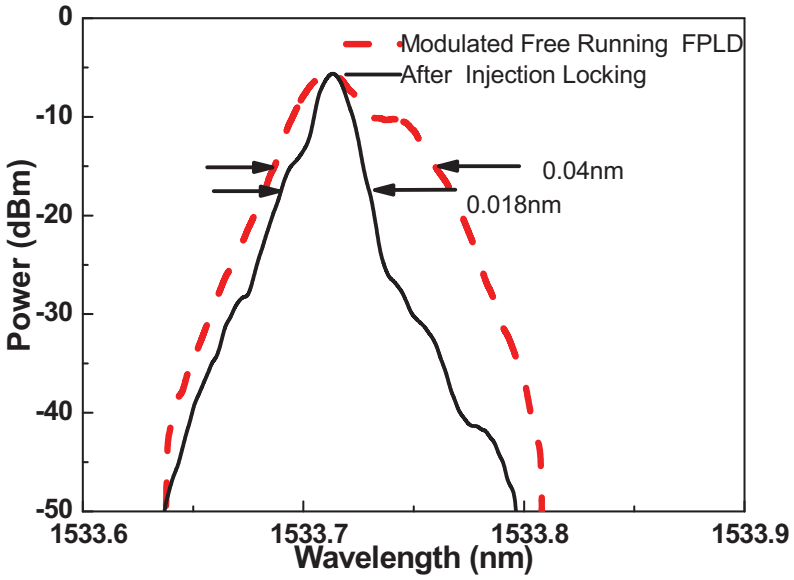

Fig. 2.5 Spectral linewidths of the injection-locked FPLD in principle mode with (red line), without (blue line) modulation, and a reference laser source (black).

In particular, the linewidth reduction effect of the injection-locked side modes is significantly degraded with increasing side-mode order (Δm). That is, the side-mode exhibits greatly broadened spectrum as compared to the principle mode of the slave FPLD even under injection-locked condition. In digital communication systems, the product of the bit rate of B and the full-width-at-half-maximum of the propagated data bit of ΔT must be under 1. If we consider the dispersion effect in fiber, the limitation on the side-mode linewidth of the injection-locked slave FPLD can be derived by using the equation of $B\Delta T<1$ => $BL|D|\Delta\lambda<1$, where L is the fiber length, D is the dispersion, and $\Delta\lambda$ is the spectral linewidth. Under a mode-linewidth of 0.025 nm, the transmission limitation of the injection-locked FPLD at the data rate of 2.5 Gbit/s can be over 1000 km. Nevertheless, even the side-mode with Δm up to 25, the degraded linewidth can still support the OC192 transmission over 80 km or longer. In our case, the obtained linewidth of the side-mode injection-locked FPLD is 0.022 nm, which completely meets the requirement for the middle-short WDM optical access system even though the injection-locked side-mode is far

from the principle mode of the FPLD (for example, Δm > 15).

By adopting the linewidth formula, the injection-locked side mode linewidth of the slave FPLD with side-mode order of Δm can thus be modified as [2.12]

$$\Delta\lambda = C\lambda^2 R_{sp,m}(1+\alpha^2)/(4\pi P) = \frac{C\lambda^2 R'_{sp,0}(1+\alpha^2)}{(4\pi P)\left(1+\left(\Delta m / M^2\right)\right)}, \quad (8)$$

where Δν denotes the linewidth of the slave FPLD under side-mode injection-locking condition, R_{sp} is the rate of the spontaneous emission coupled into the lasing mode, α is the linewidth enhancement factor, P is the average power, Δm is the order of the side-mode away from the central wavelength, *M* is the total mode number where the gain has fallen to half of its peak value. Note that R_{sp} is much smaller than the total spontaneous emission rate, since only a little part of the spontaneous emission is contributed to the injection-locked side-mode. The R_{sp} can be modified as $R'_{sp,0}/(1+(\Delta m/M^2))$ by using the gain-profile approximation, and the linewidth is enhanced by $1+\alpha^2$ with a decreasing linewidth enhancement factor due to the amplitude-phase coupling. If the side mode with an increasing mode number Δm away from the principle mode is considered in our case, the rate of the spontaneous emission (R_{sp}) corresponding to the injection-locked side mode is gradually reduced due to the shift of the material gain profile. That is, the narrowest linewidth should be located at the peak of the material gain profile under injection-locking. By assuming the parameters of the slave FPLD as the optical power of 5 mW, the wavelength of 1550 nm, the spontaneous emission (R_{sp}) of 10^8, the linewidth (Δλ) of 0.04 nm, we obtain the linewidth enhancement factor of 1.5 for the principle mode of the slave FPLD under injection-locking. In contrast, the linewidth enhancement factor for the injection-locked side mode of the slave FPLD in same condition is inevitably increasing up to 2.1.

2.4 Experimental Setup

Figure 2.6 schematically illustrates the WDM-PON system based on the side-mode injection-locked FPLDs. A FPLD with an integrated isolator is employed as the master laser for injection-locking the other slave FPLDs used as WM-PON transmitters. The master FPLD is a commercially available one with mode spacing of 1.1~1.2 nm (corresponding to 150 GHz), which could be replaced by a specially designed long-cavity one for obtaining the 50-GHz longitudinal mode spacing. The relative intensity noise (RIN) of the master FPLD as low as -140 dBm/Hz at biased current of 40 mA was measured with a lightwave signal analyzer (Agilent 71401C). The longitudinal mode of the master FPLD is detuned to match the ITU-T DWDM channel by adjusting its temperature, which is further amplified by an EDFA at the central office for obtaining higher modal power. The master FPLD output is filtered by arrayed waveguide grating (AWG) multiplexer with the channel spacing of 100 GHz.

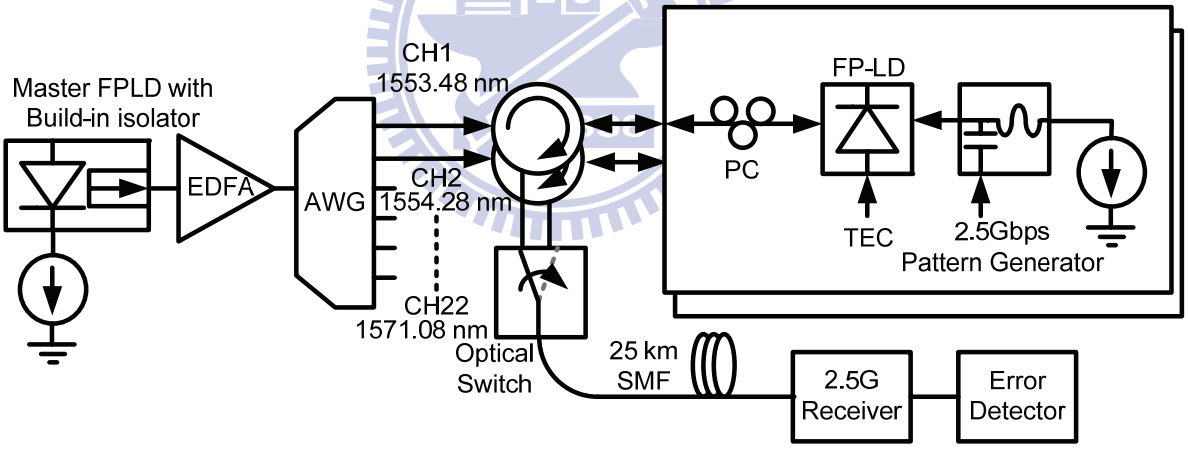

Fig. 2.6 The configuration of an experimental system with slave FPLD is side-mode injection-locked by a wavelength-sliced master FPLD.

The side-mode injection-locking transmissions of the multi-channel selectable FPLD up to 22 wavelengths from 1553.48 nm (CH 1) to 1571.08 nm (CH 22) are demonstrated. The slave FPLD exhibits a threshold current of 8.5 mA, a longitudinal mode spacing of 1.1 nm, and a cavity length of 250 μm. The temperature of all FPLDs are controlled at 25^{o}C with a fluctuation of <0.1^{o}C to prevent any wavelength drift on the longitudinal modes. The total

insertion loss of the injection-locked FPLD-FPLD link during transmission is 18 dB coming from the AWG (4 dB), the 25-km single-mode fiber (SMF) (6 dB), and the other excessive loss (8 dB). When the externally injection-locking condition between the wavelength-sliced master FPLD and the slave FPLDs is achieved, the slave one can be operated just as a single-longitudinal-mode optical source with high SMSR. Each slave FPLD is directly modulated by a 2.5 Gbit/s PRBS data stream with a pattern length of 2^{31}-1 for transmission diagnosis.

2.5 Data transmission diagnosis of side-mode injection-locked FPLD

We also evaluate the transmission performance with a BER evaluation method previously demonstrated by Bergano *et al.*, which is approached by measuring the signal-to-noise ratio at the decision circuit of an optical transmission and receiving system.[2.13] The equivalent mean value and standard deviation of the marks and spaces are determined by fitting this data to Gaussian function, and the measured BER of the optical transmitting eye-diagram can be accurately calculated from the recorded Q factor at a desired data rate. The measured Q factor of the slave FPLD with optimized injection-locking condition can be as high as 9.2, providing a reachable BER of 1.8×10^{-20} at the data rate of 2.5 Gbit/s. By increasing the biased current of the slave FPLD to 20 mA, the wavelength locking at the data rate of >2.5 Gbit/s can be achieved, which is eventually limited by the transient gain contribution to each longitudinal mode. On the other hand, the injection power required to maintain the slave FPLD within the injection-locking range as a function of the biased current, and the corresponding Q factor are also measured and shown in Fig. 2.7. The calculated Q-factor of the injection-locked slave FPLD based transmitter at different driving currents and injection-locking powers was illustrated. The effective transmission is obtainable within

blue-shaped region of an estimated Q > 7 corresponding to a BER of about 10^{-12}. The red-shaped region represents the practical implementation of such an injection-locked slave FPLD at an injecting power below 2 dBm. That is, the optimized operating parameters for concurrently achieving high-Q and low-injection are determined at the driving current for FPLD between 12 and 17 mA.

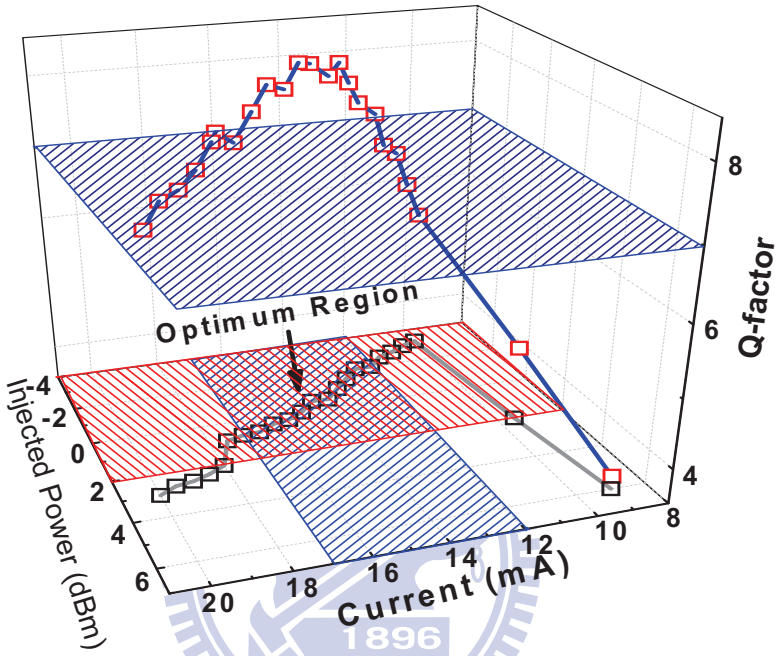

Fig. 2.7 Measured injected power (hollow markers) and measured Q (solid markers) of the driving current at the principle longitudinal mode.

Later on, the BER analysis at 2.5 Gbit/s is also performed to characterize the data transmitting performance of a simulated multi-channel DWDM fiber-optic network using the directly NRZ-modulated FPLD under side-mode injection-locking regime. The PRBS data pattern length for modulating the injection-locked FPLD is 2^{31}-1. Figure 8 shows the measured BER for the channels at 1st, 9th, 13th, 14th, 15th, and 21th orders, which are corresponding to the mode number (Δm) of -12, -4, 0, 1, 2, and 8, respectively, away from the central mode. The power of the downstream signal injected into the slave FPLD was fixed to -3 dBm by using an optical attenuator, and the biased current of the injection-locked FPLD was fixed at 15 mA. The maximum usable channel of the side-mode injection-locking slave FPLD is 22,

covering a wavelength range up to 24 nm. A BER of $<10^{-12}$ is obtained for the nearest 13 side-modes and a BER of 10^{-10} can be achieved for all of the 22 injection-locked side-modes. Without any chirping compensation, the data streams exhibit a power penalty of about 1.1 dB at a BER of 10^{-12} after 25-km transmission. In particular, there is a measured positive power penalty of 0.7 dB at a BER of 10^{-12}, which is mostly attributed to the reduction of the relaxation oscillation of the slave FPLD from the competition among longitudinal modes as shown in the inset of Fig. 2.8. As the transient situation of the carrier density changing from the bit 0 to bit 1, the photon density of the desired longitudinal mode reaches a stable gain by external optical injection, whereas the carrier density continuously depletes and cannot form relaxation oscillation. Consequently, the rising time and falling time (defined as the duration between 20% and 80% of the on-level amplitude) are 118 ps and 125 ps, respectively, and a well-opened eye pattern can be obtained with a relatively large dynamic range as shown in inset of Fig. 2.8. Both the nearly error-free (BER $< 10^{-12}$) back-to-back transmissions with and without optical injection can be detected at the received optical power of larger than -24.4 and -23.7 dBm, respectively. Up to 7 dB power penalty is observed at BER of 10^{-9} when changing the injection-locking from principle to the largest side mode, however, the corresponding receiving power level is still beyond the requirement for data communication.

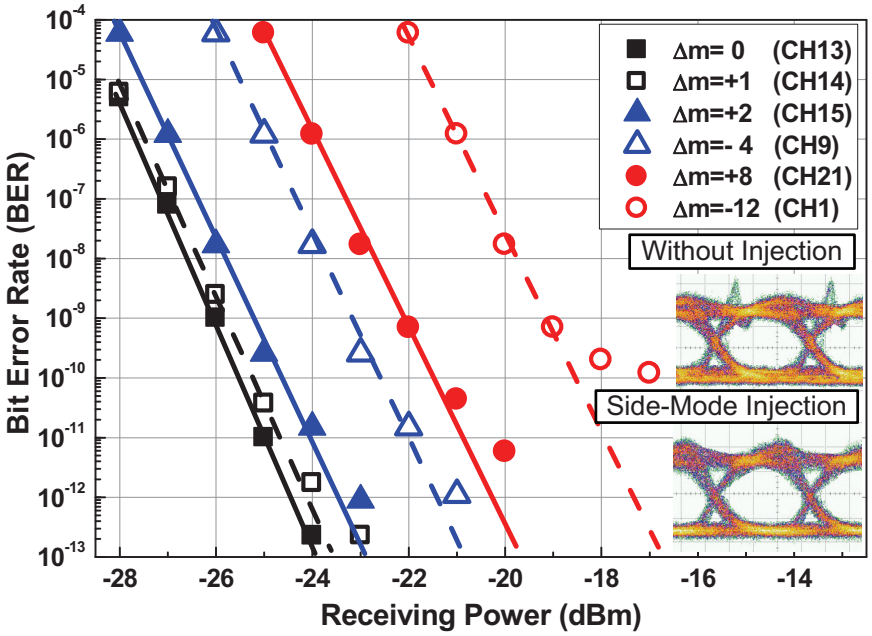

Fig. 2.8 BER analysis of wavelength injection-locked FPLD at different longitudinal modes and measured eye diagrams (inset) with and without injection

2.6 Summary

In this chapter, we theoretically analyzed the effect of the injection-locking power and side-longitudinal-mode order on the linewidth, SMSR, and BER characteristics of a slave FPLD injected by another spectrally sliced master FPLD. The SMSR and 3-dB linewidth of such a FPLD-FPLD link as a function of the injection-locking power dependent reflectivity change are simulated. The back-to-back and 25km-SMF transmission performances of the 2.5-Gbit/s directly modulated FPLD based WDM-PON transmitter under side-mode injection-locking is demonstrated. Such a wavelength injection-locked FPLD shows a largest SMSR of 35 dB and a Q factor ranging from 9.2 to 7.5 as the injection-locked channel extends to the 12th side-mode with respect to the central carrier. Degradation on the linewidth enhancement factor from 1.5 to 2.1 corresponding to the principle- and side-mode injection-locking conditions of the slave FPLD injection-locked are observed. The

maximum usable channels of the side-mode injection-locking FPLD are 22, covering a wavelength-locking range up to 24 nm. A BER of $<10^{-12}$ is obtained for the nearest 13 modes and a 10^{-10} error rate can be achieved for all of the 22 injection-locked modes, providing a negative power penalty of -0.7 dB due to the reduction on relaxation oscillation of the FPLD. These results indicates that the demonstrated side-mode injection-locked FPLD can be a potential candidate of unified WDM-PON transmitter to achieve the cost effective and high-capability 2.5 Gbit/s WDM systems.

References

[2.1] R. Olshansky, V. A. Lanzisera, S. F. Su, R. Cross, A. M. Forucci, and A. H. Oakes, "Subcarrier multiplexed broad-band service network: A flexible platform for broad-band subscriber services," *IEEE J. Lightwave Technol*. **11**, (1993).

[2.2] J. L. Zyskind, J. W. Sulhoff, J. Stone, D. J. Digiovanni, L. W. Stulz, H. M. Presby, A. Piccirilli, P. E. Pramayon, "Electrically Tunable, Diode-Pumped Erbium-Doped Fibre Ring Laser with Fibre Fabry-Perot Etalon," *Electron. Lett.* **27**, 1950, (1991).

[2.3] H. C. Kwon and S. K. Han, "Performance analysis of a wavelength-locked Fabry-Perot laser diode by light injection of an external spectrally sliced Fabry-Perot laser diode," *Appl. Opt.* **45**, 6175, (2006).

[2.4] X. J. Meng, T. Chau, and M. C. Wu, "Improved intrinsic dynamic distortions in directly modulated semiconductor lasers by optical injection-locking," *IEEE Trans. Microwave Theory Tech.* **47**, 1172, (1999).

[2.5] S. Li, K. S. Chiang, and W. A. Gambling, "Fast Wavelength Tuning of a Self-Seeded Fabry–Pérot Laser Diode with a Fabry–Pérot Semiconductor Filter," *IEEE Photon. Technol. Lett.* **13**, 1364, (2001).

[2.6] S. Li, K. S. Chiang, W. A. Gambling, Y. Liu, L. Zhang, and I. Bennion, "Self-seeding of Fabry–Perot laser diode for generating wavelength-tunable chirp-compensated single-mode pulses with high-side mode suppression ratio," *IEEE Photon. Technol. Lett*. **12**, 1441, (2000).

[2.7] K. Lee, J. H. Song, H. K. Lee, and W. V. Sorin, "Multistage access network for bidirectional DWDM transmission using ASE-injected FP-LD," *IEEE Photon. Technol. Lett*. **18**, 761 (2006).

[2.8] G.-R. Lin, Y.-H. Lin, and Y.-C. Chang, "Theory and Experiments of a Mode Beating Noise Suppressed and Mutually Injection-Locked Fabry-Perot Laser Diode and Erbium-Doped Fiber Amplifier Link" *IEEE J. Quantum Electron*. **40**, 1014, (2004).

[2.9] N. Kashima, "Dynamic properties of FP-LD transmitters using side-mode injection-locking for LANs and WDM-PONs," *IEEE J. Lightwave Technol.* **24**, 3045, (2006).

[2.10] Z. Xu, Y.-J. Wen, W.-D. Zhong, C.-J. Chae, X.-F. Cheng, Y. Wang, C. Lu, and J. Shankar, "High-speed WDM-PON usi.ng CW injection-locked Fabry-Pérot laser diodes," *Opt. Express* **15**, 2953, (2007)

[2.11] S. Noda, K. Kojima, and K. Kyuma, "Mutual injection-locking properties of

monolithically integrated surface-emitting multiple-quantum-well distributed feedback lasers," *IEEE J. Quantum Electron*. **26**, 1883, (1990).

[2.12] G. P. Agrawal, "Fiber-optic Communication Systems", 2nd Ed., John Wiley & Sons, New York, 1997, Ch. 3, p.121.

[2.13] N. S. Bergano, F. W. Kerfoot, C. R. Davidsion, "Margin measurements in optical amplifier system," *IEEE Photon. Technol. Lett.* **5**, 304, (1992).

Chapter 3
Weak-resonant-cavity Fabry-Perot laser diode with enhanced injection-locking bandwidth

3.1 Introduction and motivation

The wavelength-division-multiplexed passive optical network (WDM-PON) is a promising candidate of the low-cost subscriber networks for the fiber-to-the-home systems due to its large capacity and flexibility. For the deployment of practical WDM-PONs, the most critical issue is to develop the low cost WDM light sources for the optical network unit (ONU). A multistage access network for bi-directional WDM transmission using AWG-sliced ASE-injected Fabry-Perot laser diode (FPLD) with simultaneous bidirectional 1.25-Gbit/s transmission per channel up to 20 km has been reported [3.1, 3.2]. The slave FPLDs used in these references were injected by an ASE light source which is sliced by an AWG based wavelength division demultiplexer. To solve the mode-selection problem, a bidirectional WDM-PON based on gain-saturated colorless reflective semiconductor optical amplifiers (RSOA) was demonstrated for 1.25-Gbit/s upstream and 2.5-Gbit/s downstream transmission over 20 km [3.3, 3.4]. One alternative approach is employing the FPLDs with single-mode output under the injection-locking with a coherent light source of a mutually injection-locked FPLD amplified by an Erbium-doped fiber amplifier (EDFA) [3.5, 3.6]. In particular, a broad-band light source (BLS) emerged by mutual injection between two antireflection-coated FPLDs is used to injection-lock the FPLDs for obtaining 125-Mb/s transmission with 50-GHz channel spacing limited by the FPLD cavity length and the injection efficiency. Shin *et al.* have reported a hybrid WDM/TDM PON with each WDM

channel sharing by eight subscribers to simultaneously accommodate 128 subscribers [3.7]. However, this method requires the complicated media access control, the high-cost burst mode receivers, and the link-bandwidth sharing. All of these achievements meet the demand of the rapidly increased capacity in the fiber-to-the-home (FTTH) communication systems based on gigabit Ethernet protocol [3.8-3.10]. Currently, the proposed approaches are limited by low bandwidth, power budget and high intensity noise when applying to the optical link.

In this chapter, we theoretically analyze and experimentally demonstrate the transmission performance of a side-mode injection-locked weak-resonant-cavity Fabry-Perot laser diode (WRC-FPLD). By spectrally slicing and externally injecting the side-mode of such an WRC-FPLD, the parameters of the front-facet reflectivity, the injection-locking range, the spontaneous emission dependent Q-factor, the eye diagram and the bit error rate (BER) are determined and discussed.

3.2 System structure

Figure 3.1 schematically illustrates a DWDM-PON system based on the side-mode injection-locked WRC-FPLDs. A standard FPLD with an integrated optical isolator is employed as the master laser for injection-locking the WRC-FPLD with a longitudinal mode spacing of 0.6 nm. The front-facet reflectivity of the WRC-FPLD was coated as low as 1%, and the rear-facet reflectivity was increasing to 99%. Such a highly asymmetric coating allows the efficient injection of ASE, which also reduces undesirable backward reflection at front-facet and avoids the power consumption at rear-facet. To facilitate the injection-locking scheme, the design and fabrication procedures of the WRC-FPLD were modified from a conventional FPLD without significantly increasing the production cost. The threshold current of the WRC-FPLD is 13 mA. A long-term test of the WRC-FPLDs biased at 80 mA and 85^{o}C with output power of 5 mW for more than 4500 hrs was employed

for the stable operation of 40 devices used in our experiments.

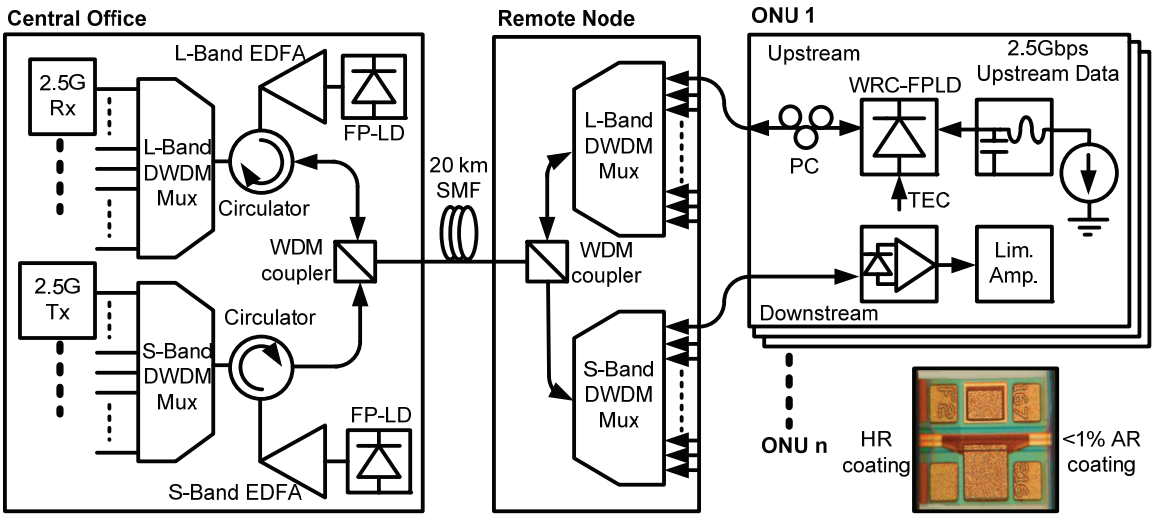

Fig. 3.1. A DWDM-PON system with a WRC-FPLD based transmitter at the ONU end that is side-mode injection-locked by a wavelength-sliced master FPLD.

At the ONU end shown in Fig. 3.1, each transmitter consists of a polarization controller (PC) that is adjusted to maximize the efficiency of injection from the master FPLD. At the central office, the master FPLD can be replaced by a specially designed long-cavity device with 50-GHz longitudinal mode spacing to match the ITU-T defined DWDM channels. Before injecting into each WRC-FPLD at the ONU end, the master FPLD output is channelized by a DWDM multiplexer built-in with the DWDM-PON and amplified by a EDFA (SDO, OAS-1000) with maximum output power of +18 dBm, which consequently causes a reduction on threshold current of the slave WRC-FPLD. The external injection-locking condition is easily achieved by matching the slave WRC-FPLD wavelength with the incoming master signal via a slight temperature and current detuning. The side-mode injection-locked WRC-FPLD acts like a single-mode source with high side-mode suppression ratio (SMSR), which is directly modulated by a 2.5-Gbit/s pseudo-random binary-sequence (PRBS) data-stream for transmission performance diagnosis.

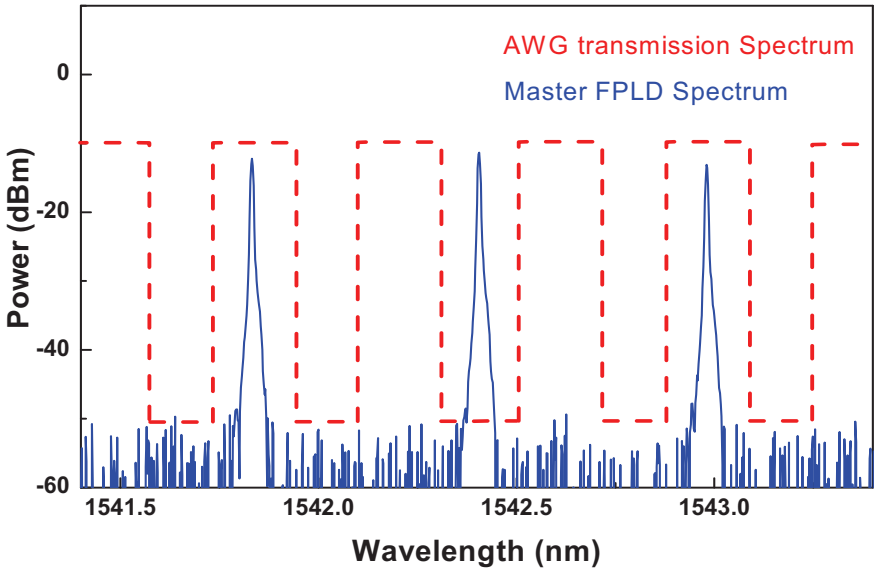

Fig. 3.2 A DWDM-PON system with a WRC-FPLD based transmitter at the ONU end that is side-mode injection-locked by a wavelength-sliced master FPLD.

The FPLD used in our experiment exhibits a long-cavity to shrink its longitudinal mode spacing to 0.6 nm, which is not coincident with the channel spacing of 50 GHz (or 0.4 nm) set by the AWG based DWDM. The FPLD emits numerous modes before passing through the DWDM, which is filtered into a single-mode spectrum for injection-lock the WRC-FPLD afterwards. Technically, the DWDM channels with number of (3n-1) were used in our case. Such a mismatch can be solved by precisely dicing the FPLD chip by the manufacturer.

3.3 Enhanced injection-locking bandwidth

In comparison with conventional FPLDs, the mode spacing of the WRC-FPLD is reduced to ensure that the injected narrowband ASE can spectrally overlap with at least one lasing mode of the WRC-FPLD. Such a design easily maintains the wavelength locking regardless of the thermally drifting wavelength of the WRC-FPLD modes. The channel spacing of the arrayed waveguide gratings (AWGs) based DWDM multiplexer and demultiplexer nearly rectangular passband shape was chosen to fit the mode spacing of the WRC-FPLD. Figure

3.3 shows the optical spectrum of the free-running WRC-FPLD at biases of 20, 30, and 40 mA. A less distinct and broadened longitudinal mode response can be observed from the WRC-FPLD output when biasing below 30 mA. The FWHM of the free-running WRC-FPLD output spectrum remains as large as 35 nm even at biased current up to 40 mA. Note that there is still a weak Fabry–Perot effect in the WRC-FPLD chip but the major lasing peak is relatively hard to be built up without external injection. After injecting with the spectrally sliced master FPLD signal, the WRC-FPLD reveals a perfectly injecting-locking peak with SMSR up to 40 dB (see Fig. 3.3).

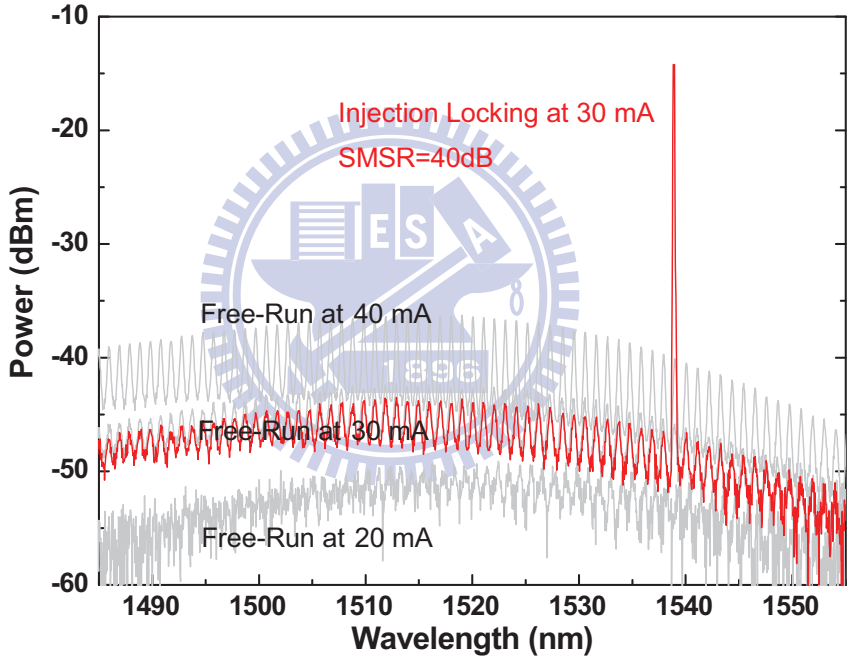

Fig. 3.3 The output optical spectra of the free-running and injection-locking WRC-FPLD at different biased conditions.

The WRC-FPLD exhibits a wide injected-locking range from 1510 nm to 1540 nm at low biased current, which can extend to the S-band if the WRC-FPLD bias further enlarges up to 40 mA. As the wavelength of one longitudinal mode in WRC-FPLD exactly coincides with that of the incoming FPLD source, the WRC-FPLD output the largest peak power with lowest noise. The detuning wavelength is the wavelength shift of the injected signal from the

master FPLD with respect to the free-running wavelength of one longitudinal mode of the slave WRC-FPLD. As a result, the wavelength locking range of the slave WRC-FPLD measured by adopting the modified delaying self-homodyne (MDSH) scheme is shown in Fig. 3.4. The locking range was defined as the wavelength tunable range needed for retaining the SMSR of the WRC-FPLD lasing mode at >35 dB. The stable lock-in region for injection-locking one longitudinal mode is found to be bounded by two solid curves shown in Fig. 3.4.

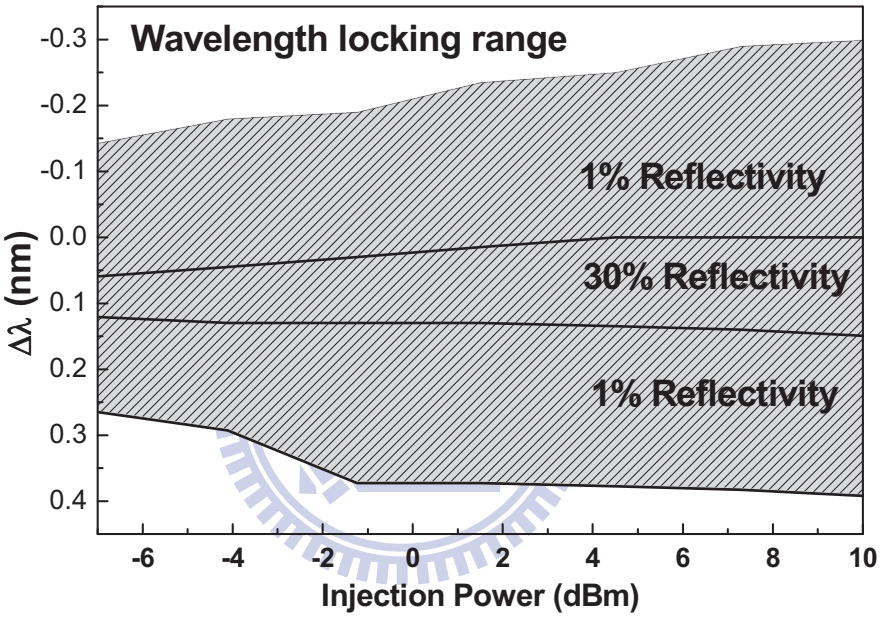

Fig. 3.4. Injection-locking power dependent wavelength lock-in range of one longitudinal mode in the slave WRC-FPLD transmitter at the ONU end.

Under a low-level injection condition, a broadened lock-in range for each longitudinal mode is observed for the WRC-FPLD as compared to that of the standard FPLD with front-facet reflectivity of 30%. A relatively weak injection-locked signal with considerable noise has also been found even the injecting wavelength is detuned away from the slave WRC-FPLD's longitudinal mode by 0.6 nm. The lock-in range of WRC-FPLD is greatly increased to be 7-8 times larger than that of a standard FPLD at extremely high bias. Such a

less tolerant injection-locking performance essentially benefits the easier lock-in of WRC-FPLD from worse wavelength mismatching condition. The wide lock-in range greatly release the need of any restorable wavelength locker set for the commercial FPLD based up-stream transmitter. Moreover, the maximum side-mode injected-locking range of up to 45 nm was limited by the gain profile of the WRC-FPLD.

In more detail, the injection-locking dynamics of the AR-FPLD under external injection can be described with the following rate equations. A traveling-wave rate-equation model [3.12, 3.13] is constructed to simulate the gain profile of WRC-FPLD initiated from the amplified spontaneous emission (ASE). In particular, the opposite-direction parts of the traveling-wave equations are neglected due to the unidirectional propagation of light in WRC-FPLD with high reflectivity at the rear facet. Both the ASE and injection locking induced gain-depletion effects are considered, and the asymmetric gain characteristic is also taken into account during simulation. The differential rate equation of carrier density (denoted as *dN/dt*) and the propagation equations which describe the time-varied powers of the injection-locked WRC-FPLD (denoting as $dP_{\lambda 0}/dt$ and $dP_{\lambda i}/dt$) are listed as below:

$$\frac{dN}{dt} = \frac{I}{qV} - \frac{N}{\tau_C} - \Gamma v_g g\left(\lambda_0\right)(N - N_0)P_{\lambda_0} - \sum_i \Gamma v_g g\left(\lambda_i\right)(N - N_0)P_{\lambda_i}, \tag{1}$$

$$\frac{dP_{\lambda_0}}{dt} = \Gamma v_g g(\lambda_0)(N - N_0)\left[(P_{\text{int}} + P_{ext}) + \frac{h\omega n_{sp}}{2\pi\tau_c}\right], \tag{2}$$

$$\frac{dP_{\lambda_i}}{dt} = \Gamma v_g g\left(\lambda_i\right)(N - N_0)\left[P_{\text{int}} + \frac{h\omega n_{sp}}{2\pi\tau_c}\right], \tag{3}$$

where I is the injection current, V is the volume of WRC-FPLD, q is the electron charge, $\hbar\omega$ is the photon energy, v_g is the group velocity, w is the angular frequency, $g(\lambda)$ is the gain coefficient, Γ is the optical confinement factor, h is the Planck's constant, P_{int} is the internal photon density, P_{ext} is the external injection photon density, and n_{sp} is the photon number of

spontaneous emission. The spontaneous emission lifetime is defined as $\tau_c = (A+BN_j+CN_j^2)^{-1}$ with A, B, and C coefficients denoting the nonradiative, bimolecular, and auger recombination coefficients, respectively. In Eq. (2), the last term of $\Gamma v_g g(\lambda)(N-N_0)\hbar\omega n_{sp}/2\pi\tau_c$ denotes the spontaneous emission noises in WRC-FPLD. The solution of these rate equations is numerically solved by the fourth-order Runge-Kutta method.

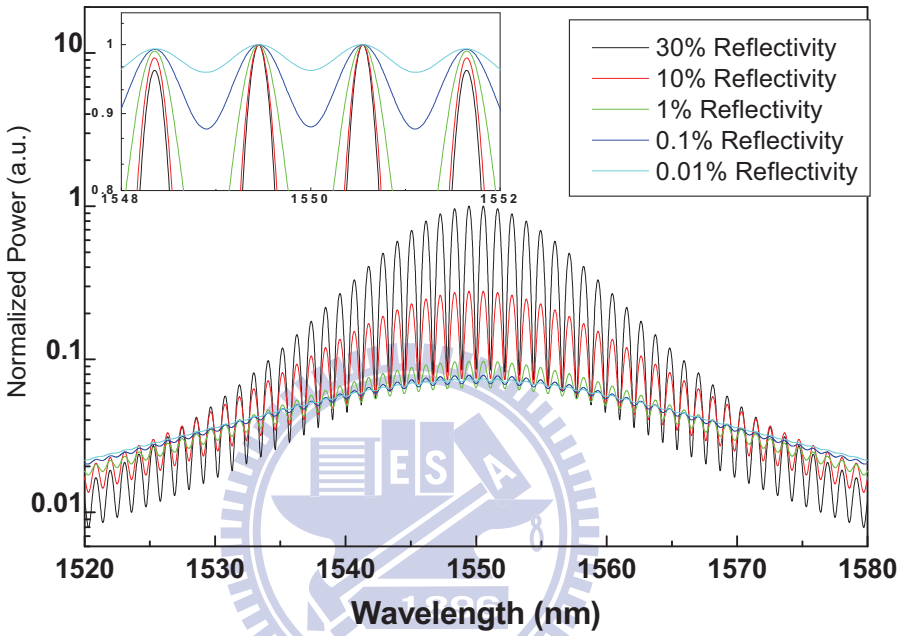

Fig. 3.5. Simulation of the normalized free-running spectra of WRC-FPLD with front-facet reflectivity of 30%, 10%, 1%, 0.1% and 0.01%.

A Lorentzian gain shape function is employed to describe the spectral roll-off of the WRC-FPLD gain profile by $g(\lambda, N)=g_0(1+((\lambda-\lambda_0)/\Delta\lambda_g)^2)$, where $\Delta\lambda_g$ = 40 nm is assumed as the gain bandwidth. If we consider that only the free-running ASE and the external injection are propagated in the injection-locked WRC-FPLD, the power gain of the WRC-FPLD lasing mode spectrum by involving the weak Fabry-Perot etalon effect happened in the WRC-FPLD can thus be modified as,

$$E_T = E_0 t_1 e^{gd} r_2 e^{gd} + E_0 t_1 r_2 e^{2gd} + \cdots = \frac{E_0 r_2 t_1^{\,2} e^{2gd}}{1 - r_1 r_2 e^{2gd} e^{i\delta}}, \tag{4}$$

$$I_T = I_0 G(\lambda) = I_0 e^{g(\lambda,N)d} \left[\frac{\dfrac{1-R_1}{\left(1-\sqrt{R_1 R_2}\, e^{g(\lambda,N)d}\right)^2}}{1 + \dfrac{4\sqrt{R_1 R_2}\, e^{g(\lambda,N)d}}{\left(1-\sqrt{R_1 R_2}\, e^{g(\lambda,N)d}\right)^2} \sin^2 \dfrac{\lambda\pi}{\Delta\lambda_m}} \right] \tag{5}$$

where $\delta = (2\pi/\lambda)2nL$, $\Delta\lambda_m = \lambda^2/2nL$, R_1 and R_2 are the reflectivity of the front and rear facets, respectively. The simulated gain spectral profiles for the WRC-FPLD with different front-facet reflectivity are illustrated in Fig. 3.5, which are obtained by assuming the gain of WRC-FPLD is equivalent to the loss of cavity at threshold condition, the output power of WRC-FPLD is 0.5 mW under the injection, the cavity length (L) is 600 μm, and the refractive index (n) is 3.5. The rear-facet reflectivity (R_2) is assumed to be a 100% perfect reflection, whereas five AR-coated front-facet reflectivity of R_1 = 30%, 10%, 1%, 0.1% and 0.01% are employed for simulation. As compared with other simulated gain spectra, the 10-% FPLD with a front-facet reflectivity of 10% exhibit narrow gain profiles with a spectral linewidth of 20 nm and a gain extinction ratio of 12 dB. The simulation exhibits that the WRC-FPLD with front-facet reflectivity of <1% benefits from more injection-locked channels. The longitudinal modes with a relatively large mode extinction ratio (>2 dB) occurs when coating the WRC-FPLD front-facet with 1% reflectivity. rf By taking the WRC-FPLD with its farthest side mode injection-locked by the incoming FPLD signal as an example, the Q factor of the injection-locked WRC-FPLD transmitted data-stream can reach 8.5 under a biased current of 30 mA and an injection power below -1 dBm. Even setting the dc biasing current of the slave WRC-FPLD as low as 20 mA, the data transmission of WRC-FPLD with a Q-factor >6.0 at data rate >2.5 Gbit/s can be achieved by injection-locking farthest side-mode, corresponding to a reachable BER of 10^{-9}.

3.4 Modeling and experimental results of WRC-FPLD

In our experiments, the WRC-FPLD with end-face AR coating reflectance is only 1%. To our best knowledge, the ultralow facet reflectance below 0.1% cannot be reached by only implanting an AR-coating on the facet of a FPLD. The extremely low facet reflectance ($R<10^{-5}$) has been demonstrated in commercially available RSOA product (CIP, SOA-RL-OEC-1550) [3.14], which is approached by concurrently designing an angled facet SOA facet and depositing an AR coating to minimize the end-face reflectance. In principle, a perfect RSOA with an R_1 of <0.01% can perfectly achieve color-free operation due to its reflectless cavity and mode-free gain spectrum. As compared with other simulated gain spectra, the ROSA with a front-facet reflectivity of 0.01% and 0.1% exhibit similar flattened gain profiles with a spectral linewidth of 39.5 nm and a smallest gain extinction ratio of <3.3 dB within 60 nm range, as shown in Fig. 3.6. The simulation supports that the WRC-FPLD with front-facet reflectivity of <0.5% benefits from more injection-locked channels. The simulating results also show that the longitudinal modes with a relatively large mode extinction ratio (>2 dB) occurs when coating the WRC-FPLD front-facet with 1% reflectivity. Without greatly sacrificing the linewidth of gain spectrum, such an WRC-FPLD benefits from a weak Fabry-Perot etalon effect with a slightly larger efficiency at the central gain peak in comparison with the standard RSOA with front-facet reflectivity of 0.01%. As shown in Fig. 3.6, the simulated gain-spectral linewidth and gain extinction ratio for the 1% front-facet-reflectivity coated WRC-FPLD are 32 nm and 7 dB, respectively.

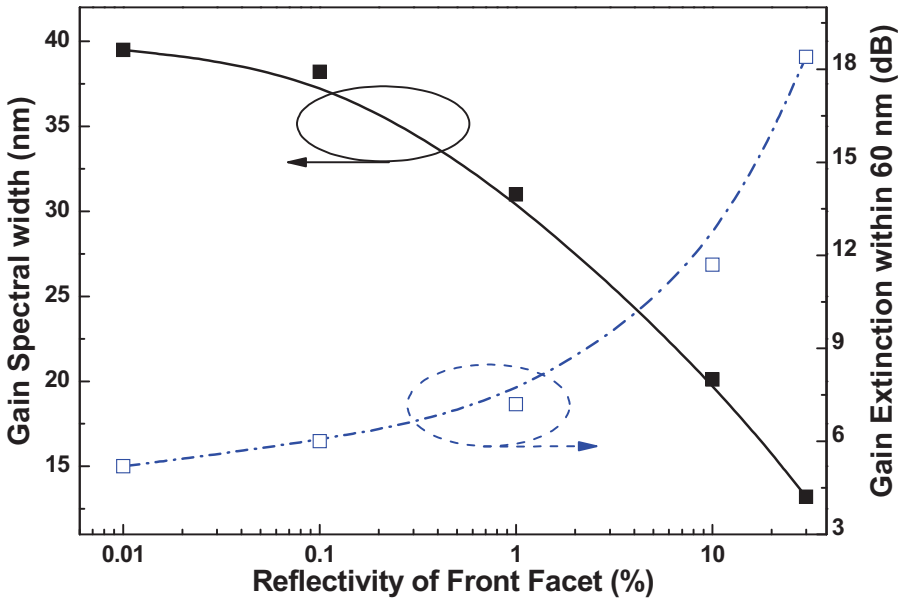

Fig. 3.6 The gain spectral linewidth (solid squares) and the gain extinction (hollow squares) vs. the front-facet reflectivity of WRC-FPLD.

Numerous WDM-PON works have previously emerged with the spectral-sliced ASE injection-locking of RSOA transmitters. However, the spectrum-sliced ASE injection is a detrimental source to the RSOAs or FPLDs due to its relatively large intensity noise and randomized polarization characteristics. Although the ASE injection-locking technique supplies a broadband incoherent light source for multi-channel injection, such an approach usually exhibits high intensity noise to limit its data rate at <1.25 Gbit/s. To enhance the transmission performance, we employ a master FPLD in front of the EDFA to change the broadband light source from incoherent to coherent. The FPLD-EDFA link plays the role of a multi-channel coherent source to avoid the drawback of an excessive intensity noise generated from the ASE-ASE beating accompanied with the broadband incoherent source. Typically, the spectrally sliced ASE source contains a RIN of -100 dB/Hz to limit the modulation bandwidth of the injection-locked FPLD or WRC-FPLD. In contrast, the filtered single-mode-sliced FPLD amplified by EDFA can provide a RIN as low as -135 dB/Hz, which facilitates a lower BER and a better transmission performance in WDM-PON system. In comparison with the spectrum-sliced ASE source, the high-frequency intensity noise of the

FPLD injection-locked WRC-FPLD can be efficiently suppressed, thus providing a better signal-to-noise (SNR) performance than the spectrum-sliced ASE source for gigabit data transmission in WDM-PON. By modifying the signal-to-noise ratio (SNR) previously demonstrated for an optical transmitter [3.15], the SNR of the WRC-FPLD transmitted data-stream can be correlated with the amplified spontaneous emission of the WRC-FPLD by

$$SNR = G(\lambda)\frac{P_{ext}}{P_{noise}} = \frac{\dfrac{1-R_1}{\left(1-\sqrt{R_1}\sqrt{R_2}e^{g(\lambda,N)}\right)^2}}{\dfrac{h\omega n_{sp}}{2\sqrt{2}\pi\tau_c}\left[1+\dfrac{4\sqrt{R_1}\sqrt{R_2}e^{g(\lambda,N)}}{\left(1-\sqrt{R_1}\sqrt{R_2}e^{g(\lambda,N)}\right)^2}\sin^2\dfrac{\lambda\pi}{\Delta\lambda_m}\right]}, \quad (6)$$

With the modified SNR model, the measured BER of the data-stream received by the WRC-FPLD can also be accurately calculated from the simulated Q factor of the received eye pattern at a desired data rate. Figure 7 shows the calculated Q factor and locking range of the injection-locked WRC-FPLD with different front-facet reflectivity.

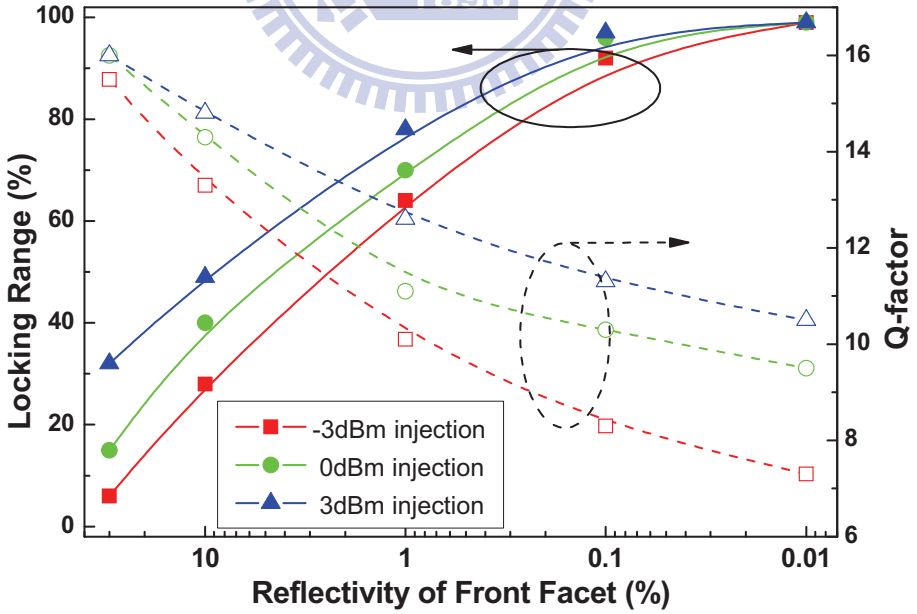

Fig. 3.7. The calculated Q factor and locking range of the injection locking WRC-FPLD with different reflectivity and injection power.

In order to evaluate the effects of optical signal performance, intensity noise, and phase noise, the frequency detuning characteristic of the 1% WRC-FPLD and 30% FPLD were measured and shown as below. By injecting the optical power of +3dBm, -3dBm, and -9dBm, the measured BER of the optical transmitting eye diagram performance can be correlated with the recorded Q factor according to the calculation given by Bergano *et al*. In principle, the signal-to-noise ratio can be measured at the decision circuit of an optical transmission system [3.15], which is described as $Q=(I_1-I_0)/(\sigma_1+\sigma_0)$ and $BER=0.5\mathrm{erfc}(Q/2^{0.5})$, where $I_{1,0}$ denote mean amplitudes of on-level and off-level bit-stream, $\sigma_{1,0}$ the corresponding standard deviation of the marked optical signal rail, and erfc(x) the complementary error function. When comparing with a commercial FPLD with 30% end-facet reflectance, the WRC-FPLD shows a great tolerance on the injection-locking wavelength range. Even with an injection power of -3 dBm, the WRC-FPLD still exhibits a locking range as wide as 0.48 nm for maintaining the Q factor higher than 7.2 requested for $BER<10^{-12}$. The injection locking range is significantly reduced as 0.34 nm while the optically injecting -9 dBm signal. The transmission performance is not affected too much when attenuating the injection level from +3 dBm to -3 dBm. With detuning injection wavelength (frequency), the performances of the 2.5 Gbps data transmitted by the WRC-FPLD exhibits some degradation. For example, the relative intensity noise (RIN) and the phase noise are inevitably increased from -129 dB/Hz to -120 dB/Hz and from -103 dBc/Hz to -97 dBc/Hz, respectively, when offsetting the $\Delta\lambda$ from 0.1 nm to 0.3 nm. This results in the degradation on calculated Q factor from 8.5 to 8.1 at central wavelength, giving rise to a receiving power penalty of 0.4 dB at BER of 10^{-12}.

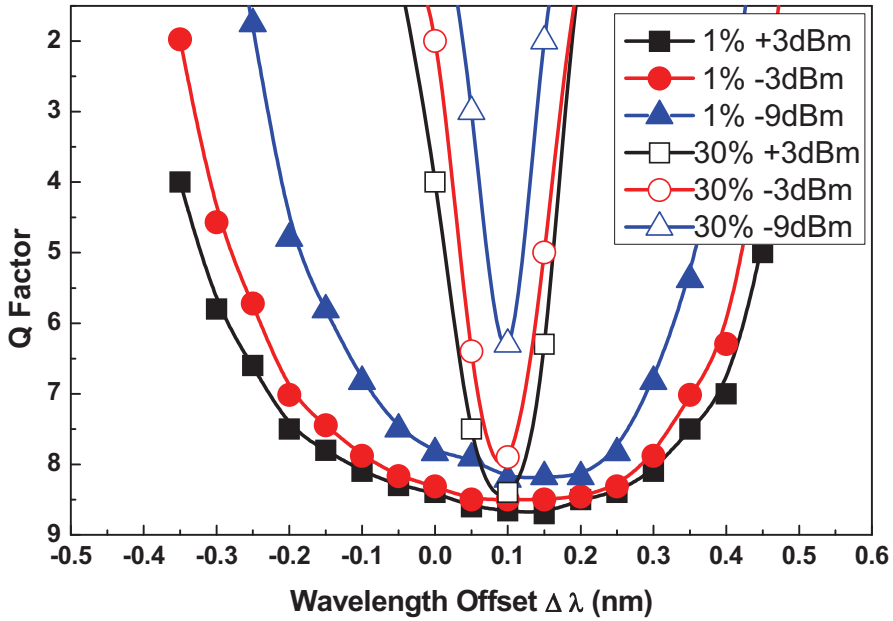

Fig. 3.8. The Q-factors of 1-% reflectivity WRC-FPLD and 30-% reflectivity FPLD with injection power of +3dBm, -3dBm, -9 dBm.

According to the simulations, a higher front-facet reflectivity could result in a larger Q-factor to guarantee the transmission of good-quality data-stream at the expense of a narrower locking range as well as a smaller side-mode quantity. The shrinkage on locking range arises from the failure of gain competition when detuning the injection wavelength away from the gain peak of the etalon cavity with restrained optical confinement factor. The front-facet reflectivity of the WRC-FPLD should be slightly reduced in order to promote the side-mode injection-locking flexibility of the WRC-FPLD. With lowest front-facet reflectivity (R=0.01%) and weak injection (-3 dBm), the worst Q factor can still be as high as 7.2 to provide a theoretically predicted BER reaching 1.1×10^{-12} at a data rate of 2.5 Gbit/s. In practical design of the WRC-FPLD with R_1=1%, the error-free transmission with BER $<10^{-12}$ is easily obtainable since the evaluated Q factor is already larger than 9.5 dB even at a low injection level of -3 dBm. In Fig. 3.9, the Y-axis of injecting power denotes the requested optical power for the best Q factor and error-free eye diagram. The best Q factor as high as 8.5 can only be reached by operating the WRC-FPLD at 22 mA with optical

injection level of -1 dBm at least. The maximum obtainable Q factor and the requested injection power are shown as the hollow- and solid-square curves, respectively. In a practical application, the Q factor minimum requested for standard data-communication with BER under 10^{-12} is only 7.2, which greatly releases the operating conditions of the WRC-FPLD for approaching an extremely high Q factor. In order to keep the BER performance at different biased conditions of the WRC-FPLD, the minimum injection power required to maintain the Q factor of transmission data above its marginal value (fixing Q=7.2 at all biased condition) is measured and plotted as the blue-square curve in Fig. 3.9. In comparison with the operating conditions for best Q factor obtained at biased current of 22 mA, it is observed that only an optical injection power of -6.9 dBm is required to achieve the Q factor of 7.2.

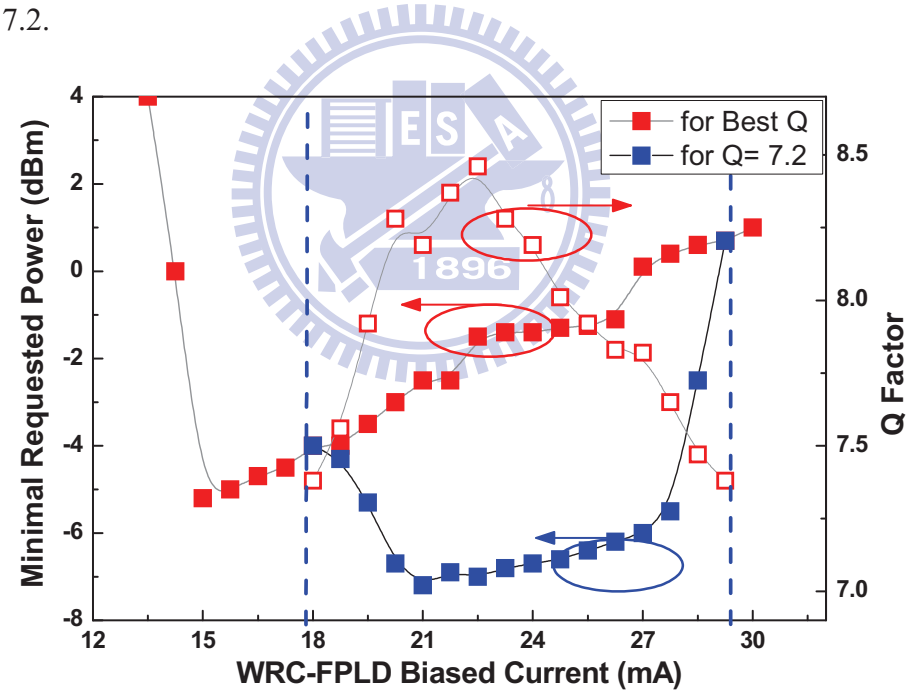

Fig. 3.9. The requested injecting power (red solid square), corresponding the measured best Q-factor (red hollow square), and the minimal requested injecting power for Q=7.2 (blue solid square) at different driving currents.

As the bias current increases beyond 22 mA, the larger intra-cavity carrier density

forces the WRC-FPLD to fix its lasing wavelength at preferred mode, thus the injection-locking can only be achieved by externally feeding a higher photon density into the WRC-FPLD cavity. As a result, the WRC-FPLD needs a higher injection power to obtain single-wavelength output and to optimize Q-factor and eye-diagrams. The minimum requested power need to be increased at higher biased current at a fixing Q of 7.2, which is a tradeoff between the gain depletion and the noise suppression for the single-mode injection-locked WRC-FPLD or FPLD typically used in the WDM-PON architectures. Therefore, the power budget in our system could be considered to allow an additional 11-dB loss for the whole WDM-PON link, including the fiber loss of 5 dB, the AWG loss of 15 dB, the WDM coupler loss of 2 dB, and the circulator loss of 1 dB. As the minimum required injection power is as low as -7 dBm (at I_{bias}=21 mA), the required maser FPLD power for such a 32-channel WDM-PON can be estimated to be about 16 dBm after EDFA. By taking the WRC-FPLD with its farthest side mode injection-locked by the incoming FPLD signal as an example, the Q factor of the injection-locked WRC-FPLD transmitted data-stream can reach 8.5 under a biased current of 30 mA and an injection power below -1 dBm. Even setting the dc biasing current of the slave WRC-FPLD as low as 20 mA, the data transmission of WRC-FPLD with a Q-factor >6.0 at data rate >2.5 Gbit/s can be achieved by injection-locking farthest side-mode, corresponding to a reachable BER of 10^{-9}. On the other hand, the actual injecting level requested for the WRC-FPLD injection-locked at different side-modes is strongly dependent with the transient gain contribution of the side-mode in the WRC-FPLD. It is clearly seen that the requested injecting power level for obtaining highest Q factor show an inverse hyperbolic function with increasing WRC-FPLD bias. At WRC-FPLD bias higher than 24 mA, the requested injecting level oppositely decreases from +1 to -1 dBm. That is, the optimized operating current of the WRC-FPLD for concurrently achieving high-Q (>7.2) and low-injection (<0 dBm) are determined as 25±2 mA.

3.5 Data transmission performance of WRC-FPLD

At last, the data transmitting performance of the directly modulated WRC-FPLD with its side-mode injection-locked by a filtered FPLD source in a simulated 2.5-Gbit/s WDM-PON system is characterized. Previously, the FPLD wavelength-locked by the spectrum-sliced incoherent light source has been investigated for low-capacity WDM-PON realization, which unfortunately exhibits a limited data rate at 622 Mbit/s for a single channel due to its relatively high RIN. The similar WDM-PON transmitter based on the directly modulated RSOA operating in linear regime has also been proposed with allowable extinction ratio (ER) less than 3 dB [3.3,10]. In comparison, the clear eye diagram of the WRC-FPLD transmitted data with high extinction ratio (>8 dB) can be obtained, as shown in the inset of Fig. 3.10. The rising time and falling time (defined as the duration between 20% and 80% of on-level amplitude) are 118 ps and 125 ps, respectively. By injection-locking the central mode, a nearly error-free (BER<10^{-12}) back-to-back transmission of the WRC-FPLD carried Pseudo Random Binary Sequence (PRBS) data-stream with pattern length of a 2^{31}-1 can be detected at receiving optical power of -24.4 dBm. In comparison with a free-running WRC-FPLD based transmitter, a negative receiving power penalty is observed for detecting the data-stream with BER of less than 10^{-12}, which is due to the relaxation on the relaxation oscillation and the increasing bandwidth of the WRC-FPLD after injection-locking. Alternatively, if the farthest side-mode (the 12^{th} modes away from the central mode) of the WRC-FPLD is injection-locked, the receiving sensitivity at BER of 10^{-12} dramatically degrades to -17.4 dBm with a power penalty of 7 dB, which is mainly attributed to the greatly reduced SNR of the side-mode injection-locked WRC-FPLD. For practical application of being the universal ONU transmitter in the WDM-PON system, nearly 17 modes of the WRC-FPLD can be used to achieve a data communication with BER<10^{-9} at receiving power of larger than -22 dBm at 2.5 Gbit/s. At same BER criterion, there are at least 25 side modes

applicable for data transmission with their maximum receiving sensitivity degrading to -19 dBm.

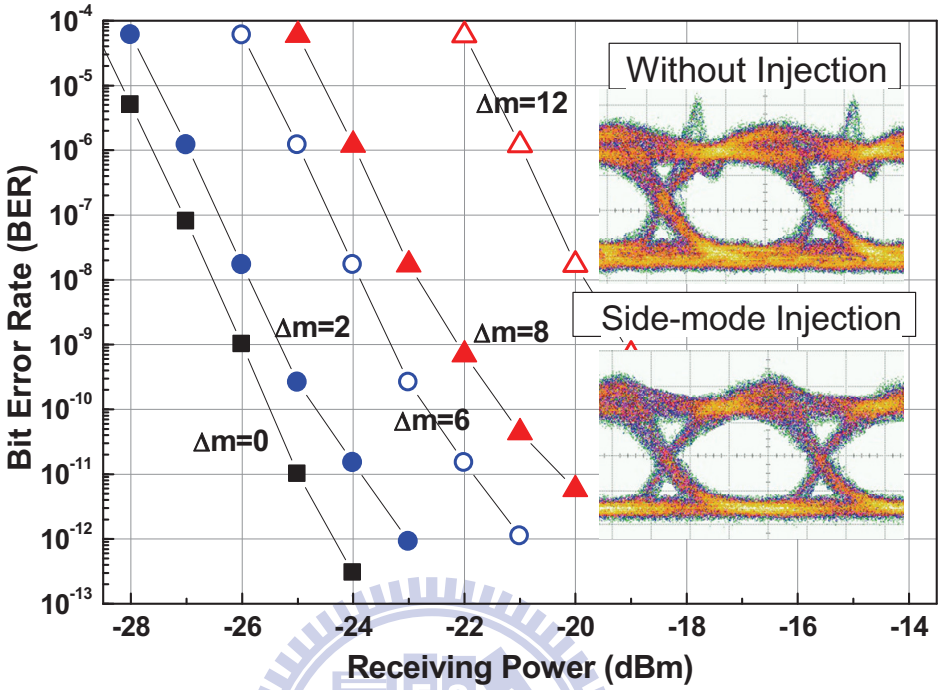

Fig. 3.10.BER analysis of wavelength injection locked 1% WRC-FPLD at different longitudinal modes and measured eye diagrams (inset) with and without injection.

The overshooting effect on the rising edge of on-bit data can be eliminated by stabilizing the gain of WRC-FPLD via the assistance of external optical injection. As the transient current changes from bit "0" to bit "1", the damping effect on photon density of the injection-locked longitudinal mode diminishes due to external injection-locking operation, since incoming photons are incorporated with those of the injection-locked longitude mode to equivalently offset the biased point of WRC-FPLD beyond its threshold. The threshold current reduction phenomenon of a laser diode under externally optical injection was previously demonstrated by Chang *et al* [3.16]. In principle, the threshold current is a nonlinear function of the external injection power or photon density, as described by

$$I_{th,ui} = \frac{qV}{\eta_i \tau} n_{th,ui} = \frac{qV}{\eta_i \tau}\left(\frac{g_{th}}{a} + n_{tr}\right) - \frac{qV}{\tau \eta_i a}\left(\frac{R_{sp}}{S_B} + \sqrt{\frac{4\alpha^2}{\left(1+\alpha^2\right)}}\sqrt{S_i}\right) \quad , \qquad (7)$$
$$= I_{th,\,free-running} - \Delta I_{injection}$$

where q denotes the unit charge of a electron, V the volume of the active region, η_i the internal quantum efficiency, τ_{eth} the carrier lifetime at threshold, $N_{th,ui}$ the carrier number in the active region, g_{th} the gain at threshold condition, a the differential gain coefficient, n_{tr} the carrier density at transparent condition, R_{sp} denotes the spontaneous emission rate, S_B the maximum photon number in the locked mode, α the linewidth broadening factor, k_c the coupling coefficient, and S_i the photon number injected into the laser diode cavity. As a result, **the Fig. 3.11** shows the P-I curves of our WRC-FPLD sample with reducing threshold current obtained by increasing the optical injection power. Obviously, the lower reflectivity on the emitting face can improve the coupling efficiency of optical injection and enhance the corresponding effect. On the other hand, the threshold current reduction significantly affects the damping and the relaxation oscillation of the laser which can be described by modifying a set of regular rate equations with external injection term as below.

$$\begin{cases} \dfrac{dN}{dt} = \dfrac{I}{qV} - \dfrac{N}{\tau_{eth}} - \nu_g g(N)(S_B + S_i) \\ \dfrac{dS_B}{dt} = \Gamma \nu_g g(N) S_B - \dfrac{(S_B + S_i)}{\tau_p} + S_i \end{cases}, \qquad (8)$$

where Γ denotes the optical confinement factor. By using the nonlinear gain model of $g(N)=\sigma_g(N-N_{tr})/(1+\varepsilon S)$, the small signal frequency response of laser is given by

$$S(\omega) = \frac{\Gamma \nu_g \sigma_g S_B \dfrac{i(\omega)}{qd}}{\left(\dfrac{\varepsilon S_B}{\tau_{eth}\tau_p} + \omega_r^2\right) - \left(\tau_p + \dfrac{\varepsilon}{\nu_g \sigma_g}\right)\omega_r \omega - (1+\varepsilon S_B)\omega^2} \quad , \qquad (9)$$

where d denotes the thickness of active region. The normalized transfer function, $H(\omega)=[3.S(\omega)/I(\omega)]/[3.S(0)/I(0)]$, can be numerically calculated and plotted in Fig. 3.12. The Eq. (9) results in a proportionality between the relaxation oscillation frequency and the externally injected photon density or the effective bias current, that is, $\omega_r \propto (S+S_i)^{0.5} \propto (I-I_{th})^{0.5}$. The simulation of Eq. (9) reveals that the damping effect on the $H(\omega)$ is relatively significant with increasing I/I_{th}. Similar phenomenon was also observed by Z. Xu *et al.* [3.11] Under the external injection with a photon density of $S+S_i$, the threshold current of the WRC-FPLD is shrinking from 13 mA to 8mA by increasing the optical injection power up to -3 dBm. The I_{bias}/I_{th} is dynamically increased from 2.3 to 3.75 to enlarge the relaxation frequency in this case, which effectively suppress the overshooting problem on the rising edge of the optical eye-diagram.

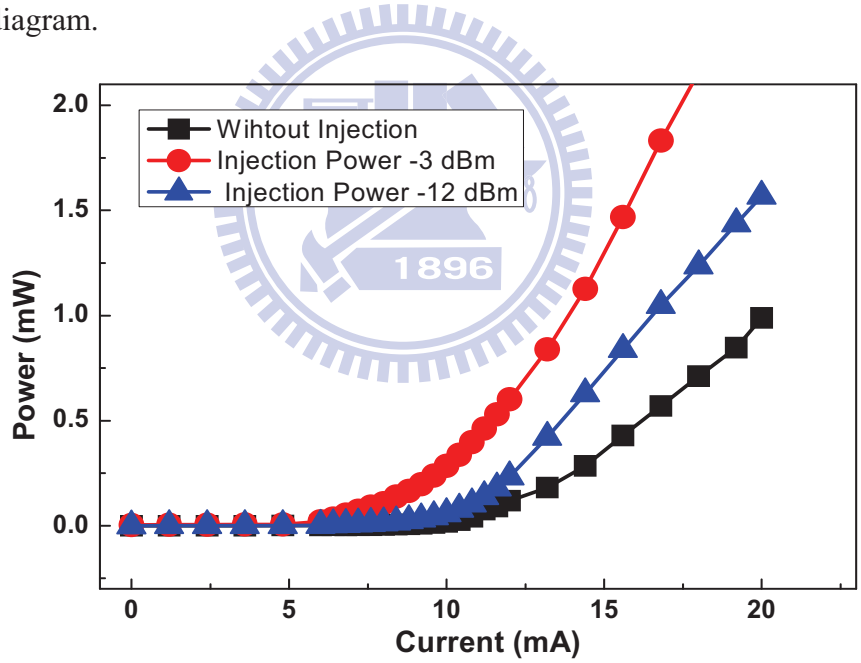

Fig.11 P-I curve of the WRC-FPLD with the different optical power injection of -3dBm, -12dBm, and free-running. The inset shows the free-running optical spectrum.

In comparison with the results of ASE light source injected FPLD, the incoherent light injection usually brings a relatively high intensity noise to limit the achievable bit rate or transmission distance. The WDM-PON transmitters based on such an injection source can

provide a highest data rate up to 1.25 Gbps with the minimum DWDM channel spacing of 100 GHz. With the use of coherent light source injection, the WRC-FPLD based WDM-PON transmitter becomes a potential candidate for achieving 2.5-Gbit/s transmission in DWDM-PON system with channel spacing of 50 GHz. Although a 10-Gbps WDM-PON injected by DFB laser diode was previously demonstrated by Z. Xu *et al*. [3.11], which only allows a wavelength-detuning range of 3.6 GHz (0.029 nm) at BER of 10^{-9}. The wavelength matching and temperature controlling circuitry is mandatory for this approach. Since the temperature-dependent wavelength shifting slope of a regular commercial FPLD is 0.06 nm/^{o}C, and the temperature of FPLD with locking range of 0.029 nm should be maintained within ±0.25 ^{o}C. This is not an easy approach to deal with the locking range and the BER performance within such a tiny temperature tolerance. There is always a tradeoff between intensity noise and coherence of the injection-locked FPLD or WRC-FPLD based transmitters in the WDM-PON architectures.

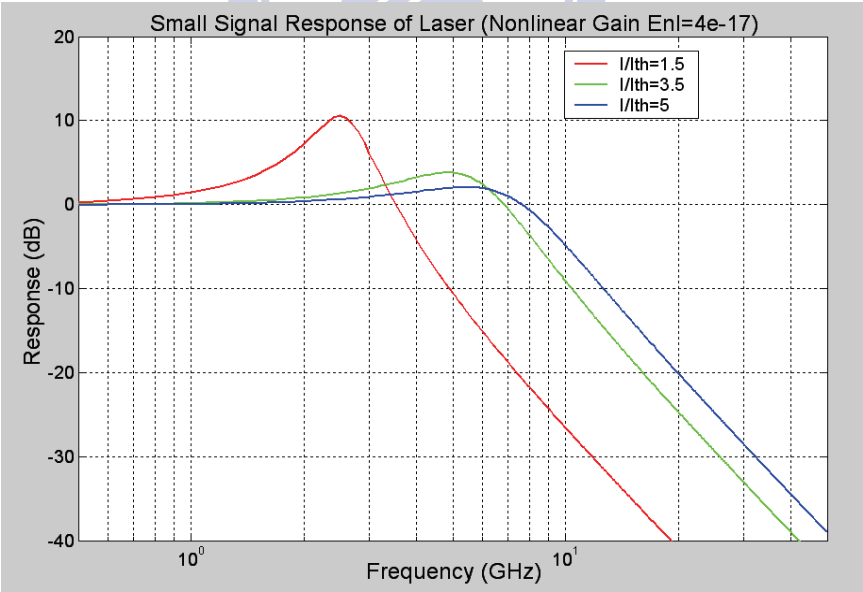

Fig. 3.12 The numerically calculated small signal frequency response of laser with different I_{bias}/I_{th} of 1.5, 3.5, and 5.

In addition, a slight degradation on the eye-diagram and BER when detuning the polarization state of the external injection to be orthogonal to the preferred polarization state of the

WRC-FPLD was observed. At free-running case, the requested power of optical injection into the WRC-FPLD could be greatly increased due to the deviation of the injected polarization from the preferred state of the WRC-FPLD. In practical application, such a problem relies on the self-restoration of the preferred polarization for the injection-locked WRC-FPLD, which can be achieved by feedback controlling an electronically tunable polarization controller added prior to the WRC-FPLD. Although such a proposed scheme cannot eliminate the common problem on the polarization sensitivity accompanied with the injection-locked FPLD or WRC-FPLD, the wavelength locking and polarization matching can be designed within a feedback control loop to implement a practical self-restorable injection locker. This experiment is demonstrated and discussed at next chapter as we are lack of an electrically controlled polarization controller to set up such a wavelength/polarization auto-restoration injection-locker.

3.6 Summary

In this chapter, we theoretically and experimentally investigate the effect of the front-facet reflectivity of the WRC-FPLD on the injection locking range, the spontaneous emission dependent SNR and Q-factor, and the BER transmission response. The front-facet reflectivity of WRC-FPLD is theoretically analyzed to be smaller than 1% in order to obtain a wide gain spectral linewidth and low gain extinction ratio, which benefits from the largest number of injection-lockable side modes. As a result, the 30-nm wavelength-locking capacity of the directly modulated WRC-FPLD based ONU transmitter with 1% front0facet reflectivity under side-mode injection-locking condition is demonstrated for 2.5-Gbit/s DWDM-PON application. The largest SMSR up to 40 dB and a least Q factor of 9.5 dB is achieved when injection-locking the central mode with a seeding power level of -3 dBm, which provides a receiving sensitivity of -24.4 dBm at BER of 10^{-12}. Even injecting-locking the farthest lockable side modes of the WRC-FPLD can reach a SMAR >35 dB and a Q factor

of 8.5. The maximum usable ONU channels of the side-mode injection-locking WRC-FPLD are 25, corresponding to a wavelength locking range of 30 nm. A BER of $<10^{-12}$ is obtained for the nearest 17 channels with worst receiving sensitivity of -21 dBm, and all of the injection-locked side-modes in the WRC-FPLD can reach a BER of 10^{-9}, providing a largest power penalty of 7 dB as compared to the central-mode injection-locking condition. The simulating and experimental results indicate the flexibility and the limitation of the side-mode injection-locked WRC-FPLD based transmitter, which can still be a potential candidate of the cost-effective universal ONU transmitter for 2.5Gbit/s DWDM-PON systems.

References

[3.1] H. D. Kim, S. G. Kang, and C. H. Lee, "A low-cost WDM source with an ASE injected Fabry–Pérot semiconductor laser," *IEEE Photon. Technol. Lett*. **12**, 1067, (2000).

[3.2] K. Lee, J.-H. Song, H.-K. Lee, and W.-V. Sorin, "Multistage access network for bidirectional DWDM transmission using ASE-injected FPLD," *IEEE Photon. Technol. Lett.* **18**, 761, (2006).

[3.3] W. Lee, M.-Y. Park, S.-H. Cho, J. Lee, C. Kim, G. Jeong, and B.-W. Kim, "Bidirectional WDM-PON Based on Gain-Saturated Reflective Semiconductor Optical Amplifiers," *IEEE Photon. Technol. Lett.* **17**, 2460, (2005).

[3.4] P. Healey, P. Townsend, C. Ford, L. Johnston, P. Townley, I. Lealman, L. Rivers, S. Perrin and R. Moore, "Spectral slicing WDM-PON using wavelength-seeded reflective SOAs," *Electron. Lett.* **5**, 1181, (2001).

[3.5] K.-M. Choi, J.-S. Baik, and C.-H. Lee, "Color-free operation of dense WDM-PON based on the wavelength-locked Fabry–Pérot laser diodes injecting a low-noise BLS," *IEEE Photon. Technol. Lett.* **18**, 1167, (2006).

[3.6] H.-C. Kwon, and S-K. Han, "Performance analysis of a wavelength-locked Fabry-Perot laser diode by light injection of an external spectrally sliced Fabry-Perot laser diode," *Applied Optics*. **45**, 6175, (2006).

[3.7] D. J. Shin, D. K. Jung, H. S. Shin, J. W. Kwon, S. Hwang, Y. Oh, and C. Shim, "Hybrid WDM/TDM-PON with wavelength-selection free transmitters," *IEEE J. Lightwave Technol.* **23**, 187, (2005).

[3.8] X. J. Meng, T. Chau, and M. C. Wu, "Improved intrinsic dynamic distortions in directly modulated semiconductor lasers by optical injection locking," *IEEE Trans. Microwave Theory Tech.* 47, 1172, (1999).

[3.9] G.-R. Lin, Y.-H. Lin, and Y.-C. Chang, "Theory and experiments of a mode-beating noise-suppressed and mutually injection-locked Fabry–Pérot laser diode and erbium-doped fiber amplifier link," *IEEE J. Quantum Electron.* **40**, 1014, (2004).

[3.10] S.-M. Lee, K.-M. Choi, S.-G. Mun, J.-H. Moon, and C.-H. Lee, "Dense WDM-PON based on wavelength-locked Fabry-Pérot laser diodes," *IEEE Photon. Technol. Lett.* **17**, 1579, (2005).

[3.11] Z. Xu, Y.-J. Wen, W.-D. Zhong, C.-J. Chae, X.-F. Cheng, Y. Wang, C. Lu, and J.

Shankar, “High-speed WDM-PON using CW injectionlocked Fabry-Pérot laser diodes,” *Opt. Exp*. **15**, 2953, (2007).

[3.12] K.-Y. Park, S.-G. Mun, K.-M. Choi, and C.-H. Lee, “A Theoretical Model of a Wavelength-Locked Fabry–Pérot Laser Diode to the Externally Injected Narrow-Band ASE,” *IEEE Photon. Technol. Lett.* **17**, 1797, (2005).

[3.13] G.-R. Lin, Y.-S. Liao, and G.-Q. Xia, “Dynamics of optical backward-injection-induced gain-depletion modulation and mode locking in semiconductor optical amplifier fiber lasers,” *Opt. Exp.* **12**, 2017, (2004).

[3.14] P. Healey, P. Townsend, C. Ford, L. Johnston, P. Townley, I. Lealman, L. Rivers, S. Perrin, and R. Moore, “Spectral slicing WDM-PON using wavelength-seeded reflective SOAs”, *Electron. Lett.* **37**, 1181, (2001).

[3.15] N. S. Bergano, F. W. Kerfoot, C. R. Davidsion, “Margin measurements in optical amplifier system,” *IEEE Photon. Technol. Lett.* **5**, 304, (1992).

[3.16] Y.-C. Chang, Y.-H. Lin, J. Chen, and G.-R. Lin, “All-optical NRZ-to-PRZ format transformer with an injection-locked Fabry–Perot laser diode at unlasing condition,” *Opt. Exp.* **12**, 4449, (2004).

[3.17] G.-R. Lin, H.-L. Wang, G.-C. Lin, Y.-H. Huang, Y.-H. Lin, and T.-K. Cheng, “Comparison on Injection-Locked Fabry–Perot Laser Diode With Front-Facet Reflectivity of 1% and 30% for Optical Data Transmission in WDM-PON System,” IEEE J. Lightwave Technol., vol. 27, pp. 2779–2785, 2009.

Chapter 4
Pulsating master and injected slave weak-resonant-cavity laser diodes based quasi-color-free 2.5Gb/s WDM-PON

4.1 Introduction and motivation

Versatile DWDM-PON architectures with acceptable capacity and flexibility have emerged as the subscriber networks to meet the demand of the next-generation fiber-to-the-home application [4.1]. With the amplified spontaneous emission (ASE) injection-locking of the Fabry-Perot laser diode (FPLD) [4.2], or the reflective semiconductor optical amplifiers (RSOA) [4.3-4.5], or the WRC-FPLD [4.6] several kinds of the quasi-color-free transmitters were considered to overcome the mode-selection problem happened in conventional laser diode based transmitters. However, the spectrally sliced incoherent ASE suffers from large intensity noise to limit the transmission bit-rate below 2.5 Gb/s. Alternatively, the coherent injection-locking schemes by using the new master broad-band light sources (BLSs) such as a mutually injection-locked FPLD [4.7] or a quantum-dash passively mode-locked laser (QD-MLL) [4.8] have been proposed recently. The mutually injected antireflection-coated FPLDs has been a employed as master BLS to injection-lock the slave FPLDs for 125-Mb/s transmission with 50-GHz channel spacing. Later on, a highly coherent CW light injection-locked FPLD based 10-Gb/s bi-directional WDM-PON architectures was reported [4.9]. Nevertheless, all these coherence-injection applications require a precisely controlling wavelength match between the master and the slave lasers such that the shortcomings on the wavelength maintenance and stability are accompanied for practical WDM-PON systems. Currently, the proposed approaches are limited issues of their colorless transmitter, low

operation bandwidth, power budget and high intensity noise when applying to the WDM-PON link. In comparison with the results of PRZ injection-locking and CW injection locking, the CW injection locking need incoherent light injection (sliced ASE) for colorless operation, and incoherent light injection usually brings a relatively high intensity noise to limit the achievable bit rate or transmission distance. The WDM-PON transmitters based on such an injection source can provide a highest data rate up to 1.25 Gbps with the minimum WDM channel spacing of 100 GHz. With the use of coherent light source injection, the WRC-FPLD based WDM-PON transmitter becomes a potential candidate for achieving 2.5-Gbit/s transmission in WDM-PON system with channel spacing of 50 GHz. There is always a tradeoff between intensity noise and coherence of the injection-locked FPLD or WRC-FPLD based transmitters in the WDM-PON architectures. Nowadays, most of the proposed WDM-PON works on a FPLD-FPLD injection-locked scheme, which CW injection locking still faces problems of wavelength discontinuity and finite injection-locking wavelength range due to the limitation on lasing mode selected by the resonant cavity of the FPLD.

Nevertheless, the coherent master BLS injection-locked slave laser diode has oriented a new solution towards high-bit-rate WDM-PONs. In this chapter, we demonstrate a novel bi-directional WDM-PON with RZ data-format at 2.5 Gb/s by using the slave WRC-FPLDs coherently injection-locked by a pulsated master WRC-FPLD based quasi-colorless source. In particular, the on-off-keying RZ encoding is achieved by reducing the biased current of slave WRC-FPLD at below threshold current that is a nonlinear function of the external injection power or photon density [4.10-4.11]. Without using any data-format transformer circuit, both the down- and up-stream slave WRC-FPLDs are directly modulated by the PRBS NRZ data and coherently injection-locked by the gain-switched master WRC-FPLD. After 200-GHz AWG channelization, both the back-to-back and 25-km transmitted performances bi-directional RZ transmission at 2.5 Gb/s are analyzed.

4.2 Concept of coherent injection light source and quasi-color-free injection locking

The bi-directional 2.5-Gb/s RZ WDM-PON is contrasted quasi-color-free with the slave WRC-FPLDs which are coherently injection-locked by the pulsating master WRC-FPLD, as illustrated in Fig. 4.1. The WRC-FPLD is a general buried heterostructure FPLD with different end-face reflectivity. First of all, the WRC-FPLD was fabricated by growing a 2000-A-thick n-type InP layer with dopant concentration of $5x10^{18}$ cm^{-3} on substrate, and two n-type InP films containing with dopant concentrations of $N=2x10^{18}$ cm^{-3} (2000-A thick) and $N=2x10^{18}$ cm^{-3} (1000-A thick) were employed as the cladding layers. The active InGaAsP layer composed of the 0.9% compress-strain multi-quantum wells with thickness of 50 A at emission wavelength of 1.55 μm and the 0.6% tensile-strain barriers with thickness of 85 A at 1.1 μm. The design of such a WRC-FPLD can greatly suppress the temperature-dependent wavelength shift with a $\Delta\lambda/\Delta T$ slope as low as 0.08 nm/^{o}C, which is very close with that obtained from common quantum-well-based LDs. Afterwards, the p-type cladding layers including a 5000-A-thick intrinsic InP and a 1000-A-thick / 1.2μm-thick p-type InP layers with corresponding doped concentrations of $1x10^{17}$ / $1x10^{18}$ cm^{-3}, respectively were grown upon the gain region. Finally, a 2000-A-thick p-type InGaAs layer with dopant concentration of $2x10^{18}$ cm^{-3} was deposited as a contact layer.

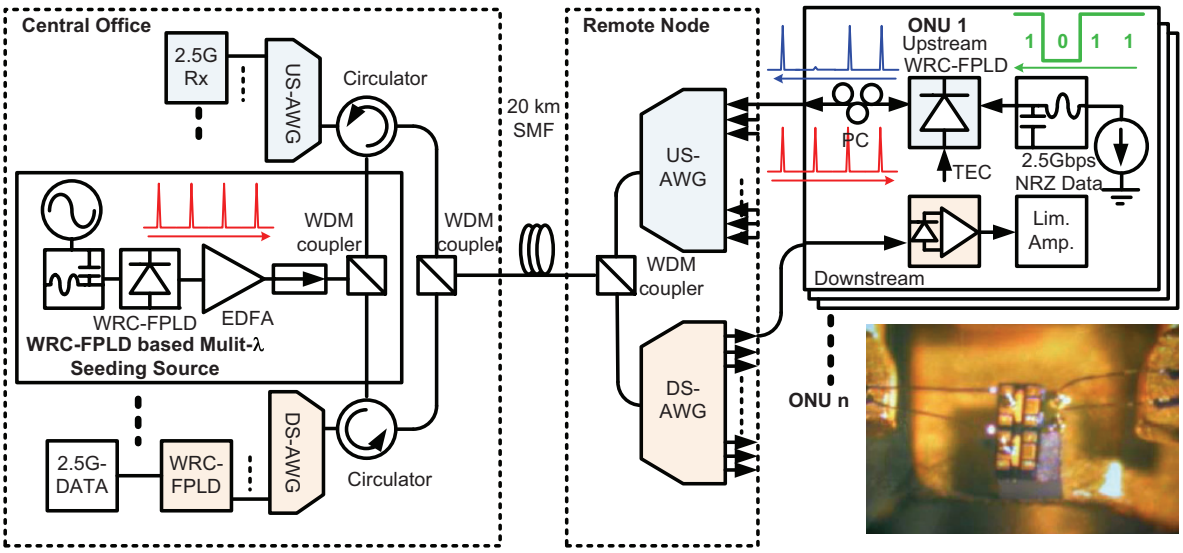

Fig. 4.1 The WRC-FPLD based bi-directional quasi-color-free 2.5-Gb/s RZ WDM-PON with a pulsed WRC-FPLD coherent injection-locker

The master WRC-FPLD with an integrated optical isolator is gain-switched for injection-locking the down- and up-stream slave WRC-FPLDs. The master WRC-FPLD gain-switched at nearly threshold condition exhibits a relative-intensity-noise (RIN) of -130 dB/Hz, which is amplified then by EDFA and channelized by a 200-GHz AWG to function as the multi-wavelength coherent seeding source. The longitudinal-mode wavelength of the master WRC-FPLD is temperature-detuned to match the ITU-T defined DWDM channel. The separation/combination is performed by the band separator/combiner (BS/BC). The design and fabrication of the WRC-FPLDs were modified from a conventional buried heterostructure FPLD without significantly increasing the production cost. Under free-running case, such a WRC-FPLD shows a threshold current up to 27 mA, as shown in Fig. 4.2. The resonant cavity length of all WRC-FPLDs is 600 μm with corresponding longitudinal mode spacing of 0.6 nm. The back and front facet reflectivity of WRC-FPLD are 94% and 1%, respectively. Such a highly asymmetric coating design allows the efficient external injection from the front facet to reduce the power budget and to avoid the power consumption at rear-facet of the WRC-FPLD. The fiber-pigtailing for the TO-56-can packed WRC-FPLD is also supported

by the laser diode manufacturer using laser fusing-splicing technology. For reducing the surface reflectivity, the end face of single-mode fiber (Corning, SMF28) is polished to tilt by 8 degree with respect to its surface normal. The WRC-FPLD is directly modulated by 2.5 Gbit/s pseudorandom binary sequences (PRBS) data stream with pattern length of 2^{23}-1 for transmission performance diagnosis. The Vp-p of the electrical PRBS digital data is 1 V (from -500 mV to 500 mV). All of the BER data were taken by using a commercial receiver (Sanway Optoelectronics tech. Corp. Ltd, SI1525-80ATOS-S) in connection with an error detector (Hewlett Packard, 70842B). Afterward, the temperature of the WRC-FPLD is varied from 20°C to 40°C to adjust the number of the injection-locked modes involved within a single AWG-channelized spectral window.

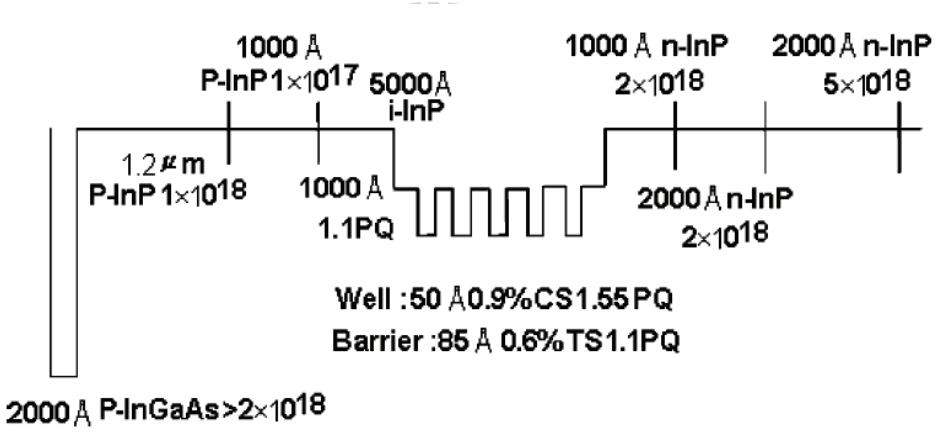

Fig. 4.2. Configuration and band structure of the 1% front-facet AR-coated WRC FPLD.

4.3 Performances and discussions of quasi-color-free 2.5Gb/s RZ WDM-PON

The phenomena of threshold current reduction have been demonstrated under external injection locking [4.10-11]. Nevertheless, the applications of threshold current reduction are usually limited by insufficient injection power. A commercial FPLD exhibits the threshold current reduction of 2 mA, while the injection-locked power needs a further amplification to overcome the end-face transmission loss of the FPLD. In contrast, the power-current

characteristics of the WRC-FPLD under different injection levels are shown in Fig. 4.3(a), which reveals a threshold current reduction by 10 mA with the external injection power increasing up to 9 dB. The related high threshold current of WRC-FPLD is caused by 1-% reflectivity on the front face of the resonance cavity.

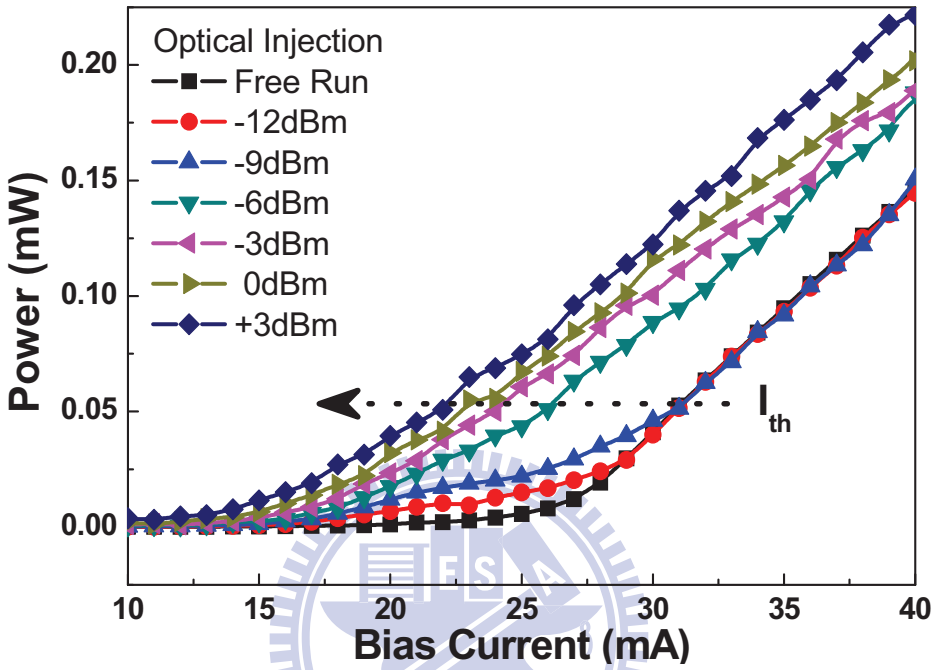

Fig. 4.3(a) The P-I curve of the slave WRC-FPLD under master WRC-FPLD injection-locking with different power levels.

Under such a low end-face reflectivity condition, the external injection compensates the reflection of the resonance cavity, and the lasing phenomenon is easier to be built-up at a lower driving current of WRC-FPLD. The reduction on threshold can be theoretically derived as [4.1]. Note that the power-current slope remains almost constant within the injection power ranged between -12 and +3 dBm, indicating that the reshaping on rising and falling edge of the generated RZ data shape with changing injection level can be negligible in this case. Figure 3(b) illustrates the operating principles of the RZ data-stream generation from slave WRC-FPLD initiated by the external injection from the gain-switched master WRC-FPLD.

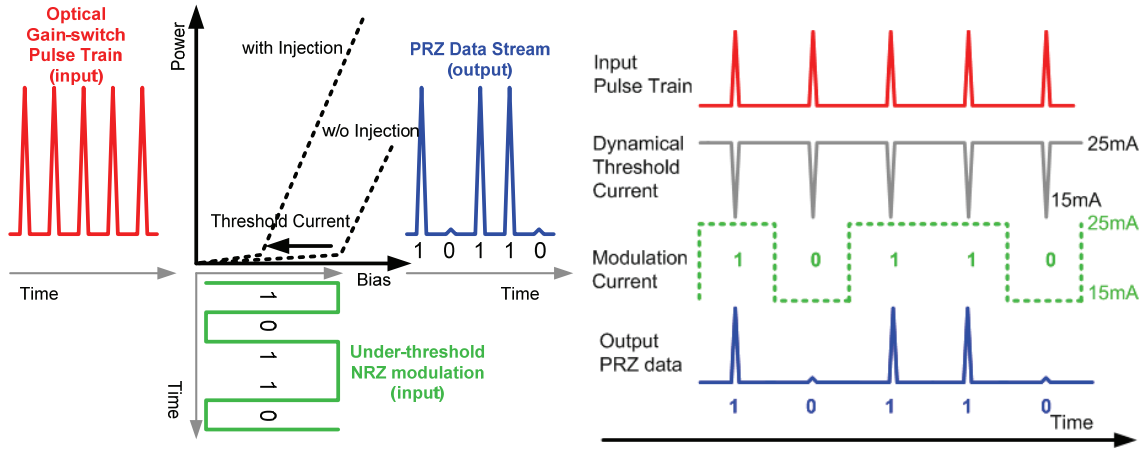

Fig. 4.3(b) Principle of the slave WRC-FPLD RZ transmitter triggered by externally injection from a pulsated master WRC-FPLD and directly modulated by a electrically PRBS data-stream.

As illustrated in Fig. 4.3(b), the external-injection induced pulsed RZ on-off-keying data generation from the slave WRC-FPLD requires the "on" bit of the NRZ-modulated current set at just below threshold current of the WRC-FPLD at free-running condition, and a DC bias is added to offset the modulation at half of threshold. In this case, the slave WRC-FPLD is un-lasing without the coherent injection by the master WRC-FPLD pulse, and the threshold reduction is detuned to switch the mode of the slave WRC-FPLD between spontaneous emission and RZ data transmission with the pulsated master WRC-FPLD carrier injection. The slave WRC-FPLD is directly modulated at 2.5 Gb/s to deliver pulsed RZ data after coherently injection-locked by the channelized master WRC-FPLD. Both the down- and up-stream slave WRC-FPLDs biased at slightly below threshold current are directly modulated by PRBS NRZ data and injection-locked by the channelized master WRC-FPLD gain-switched to deliver a coherent RZ data-stream. The gain-switched master WRC-FPLD pulsewidth can be optimized to 49 ps by setting RF power up to +8 dBm (see Fig. 4.4), which possesses a greatly broadened longitudinal mode after gain-switching to improve the injection-locking wavelength tolerance. The spectral linewidth of the master WRC-FPLD can be broadened from 0.2 (free-running) to 0.8 nm (with maximum RF power), which has

covered the entire AWD channelized spectral window.

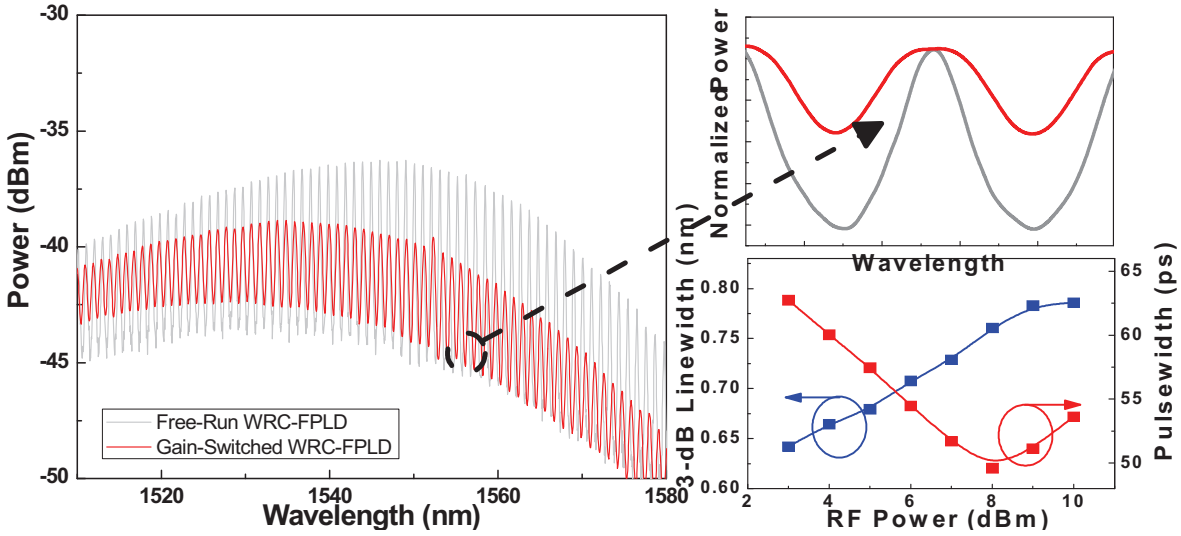

Fig. 4.4 Left: optical spectra of the master WRC-FPLD operated at free-running (gray) and gain-switching (red) condition. Upper right: the normalized mode spectra at free-runing (gray) and gain-switching (red) conditions. Lower right: the linewidth and pulsewidth of the master WRC-FPLD with different RF modulation powers.

Such a pulsated master WRC-FPLD facilitates the slave WRC-FPLD from a wider injected-locking range, and the side-mode-suppression-ratio (SMSR) of the injected-locked WRC-FPLD is confined by both the RF gain-switching and the optical injection powers of the power amplifier and the master WRC-FPLD, respectively. As shown in Fig. 4.5, a relatively weak injection-locked WRC-FPLD output with acceptable noise and SMSR (>28 dB) is achieved even the injecting wavelength is detuned away from the slave WRC-FPLD's longitudinal mode by ±0.6 nm at relatively high injection. The lock-in range of the salve WRC-FPLD slightly shrinks to ±0.4 nm for each longitudinal mode under a low-level injection condition, however, which is already 6-8 times larger than that of a standard FPLD. Since the broadened master WRC-FPLD mode has already fulfilled the spectral window of each AWG sliced DWDM channel, the greatly tolerant injection-locking range essentially benefits the easier lock-in of the slave WRC-FPLD from a worse wavelength mismatching condition. The wide lock-in range greatly releases the need of any restorable wavelength

locker set for the commercial FPLD based up-stream transmitter. After gain-switching, the broadens its each longitudinal mode from 0.2 nm to 0.8 nm, as shown in Figs. 6 (a) and (b). In comparison with the sliced ASE, such a 0.8-nm injection source provides a coherent injection into the slave WRC-FPLD with relatively low intensity noise due to the greatly attenuated spontaneous emission. By injection-locking with the master gain-switched WRC-FPLD, the linewidths of free-running and NRZ modulating slave WRC-FPLD are 0.65 nm and 0.8 nm, as shown in Figs. 4.6 (c) and (d). The narrowing linewidth of the free-running WRC-FPLD is caused by the restraining of the slave longitudinal mode which filters the injection master wavelength. The injection induced dynamic threshold reduction linearly amplifies the modulated slave WRC-FPLD, and the master injection with its spectral linewdith controlled by pulsated master.

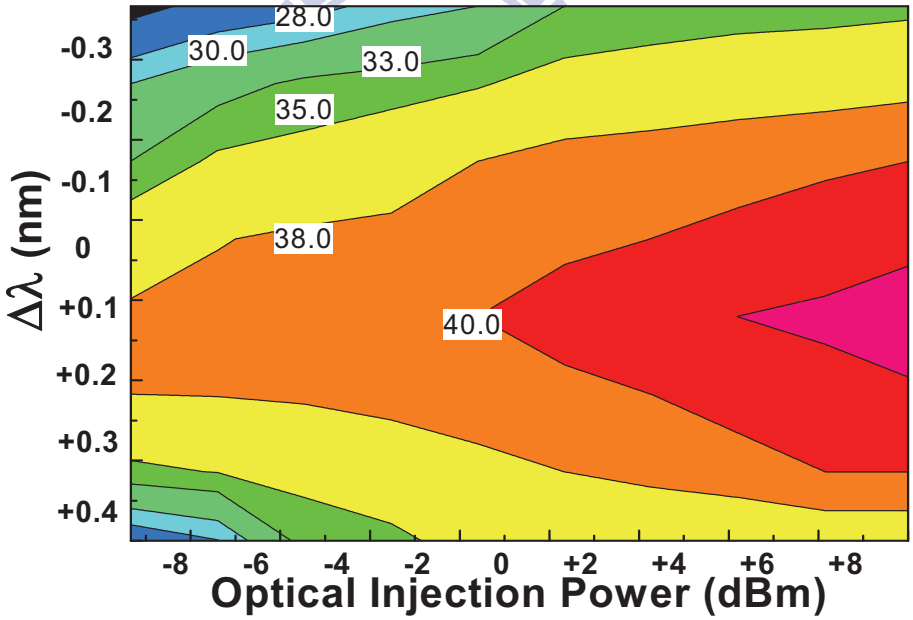

Fig. 4.5 Injection-locking power dependent wavelength lock-in range and corresponding SMSR of the slave WRC-FPLD transmitter.

Since the pulsated master WRC-FPLD has offered a larger injection-locking bandwidth than commercial FPLDs (see Fig. 4.5). The wavelength matching can be significantly optimized without the need of temperature control for the slave WRC-FPLD. The belo-threshold modulation not only releases the temperature and wavelength control of

the slave WRC-FPLD, but also leads to the all-optical NRZ-to-RZ conversion under the optical RZ carrier injection from the pulsed master. To evaluate the temperature influence of the WRC-FPLD, the injection-locked slave WRC-FPLD output spectra are measured at temperature ranging from 21°C to 29°C. The temperature-dependent wavelength red-shift for the slave WRC-FPLD is determined as 0.08 nm/°C. The mode spectrum persistently shifts within the 200-GHz AWG DWDM channel to change the slave WRC-FPLD mode number within each channel between 2 and 3. The AWG filtered mode number oppositely decreases as the temperature further increases to 29°C.

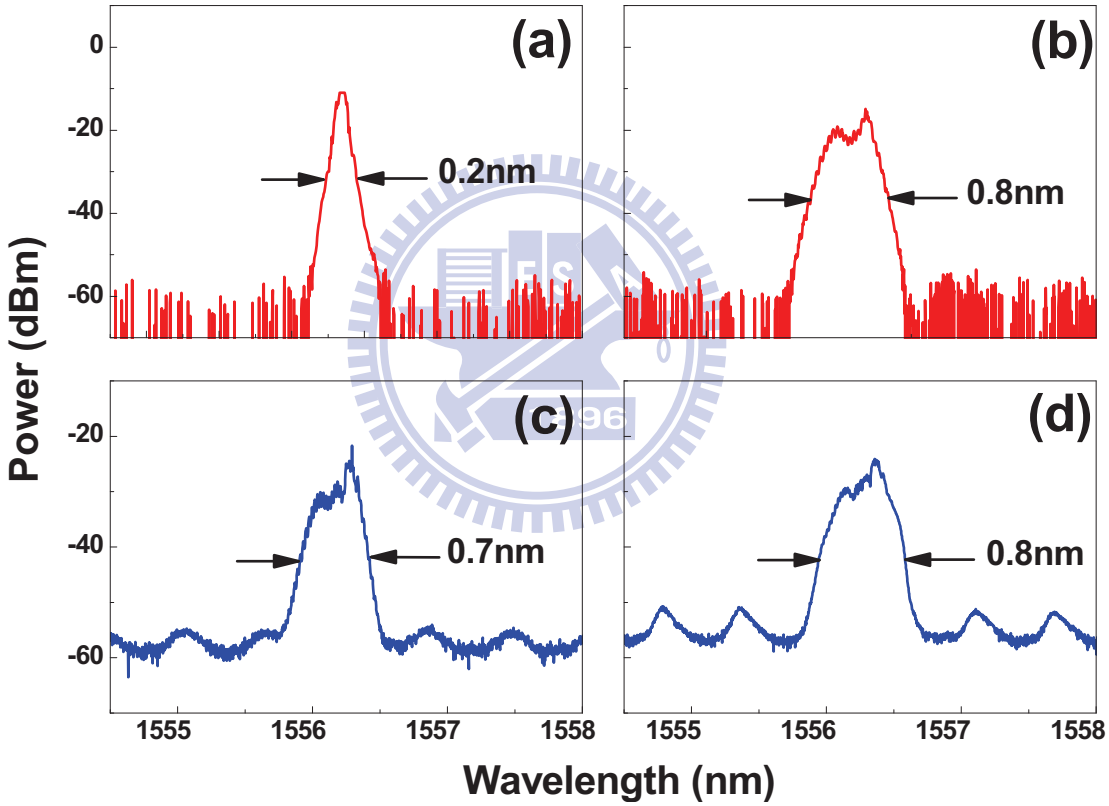

Fig. 4.6 (a) Free-running AWG sliced WRC-FPLD. (b) Gain-switched AWG sliced WRC-FPLD. (c) Free-running slave WRC-FPLD injected by gain-switched WRC-FPLD. (d) NRZ modulated slave WRC-FPLD injected by gain-switched WRC-FPLD.

The red-shift of the longitudinal mode, illustrated in Fig. 4.7, is induced by optical injection, which effectively increases the reflective index and the end-face reflectivity of the slave

WRC-FPLD with increasing intra-cavity photon density. In contrast, the ASE injection-locking technique usually requests relatively high optical injection power due to its non-coherent property and the data-format operation of the WRC-FPLD at NRZ require. Therefore, the required power budget per channel is not easy to achieve if the OLT continuously provides CW optical injection for each ONU. Alternatively, the gain-switched operation of master WRC-FPLD can deliver a much higher peak power by the using the same EDFA, such that not only the lock-in bandwidth but also the injection-locked linewidth can be improved concurrently without sacrificing the power budget per channel. As shown in lower Fig.8, The shifting of longitudinal mode is quickly switching by the injecting optical pulse, and the shift speed is accelerated by the photon lifetime of the slave WRC-FPLD.

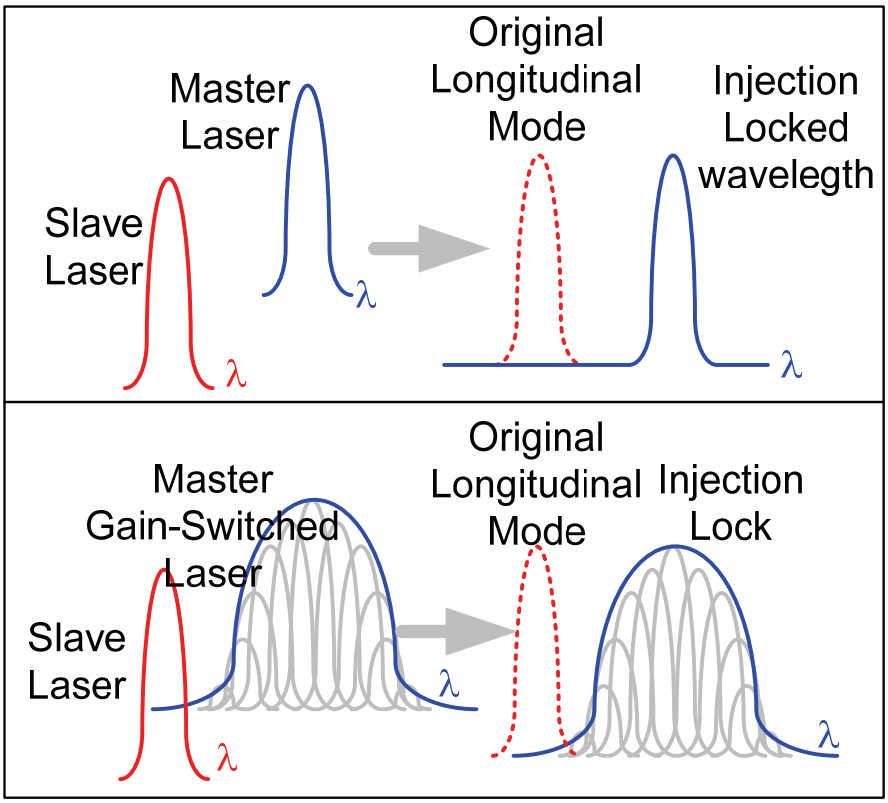

Fig. 4.7 the diagram of single-wavelength injection and gain-switched injection.

With the WRC-FPLD temperature tuning from 21°C to 29°C, the injection-locked slave WRC-FPLD spectrum is stable and invariant with the original wavelength deviation between

the master and slave WRC-FPLDs, as illustrated in Fig. 4.8(a). The shifting longitudinal mode is wavelength-locked by the gain-switched master source even at different matching conditions between the master and slave WRC-FPLDs. Even if the injection power level is higher than the optimized injection-locking power, the wavelength is still hold at the injection wavelength. Since wavelength shifting is induced by changing the inner photon density of WRC-FPLD, the efficiency of optical injection is strongly affected by the Fabry-Perot etalon effect in the WRC-FPLD. Over-power injection induced shifting will be counteracted by lower injection efficiency to maintain the wavelength stability. Such kind of the pulsated master injection-lock slave source behaves like a dynamic wavelength sweeping induced mode-locking between master and slave WRC-FPLDs, and the wavelength-selection can entirely be ignored in such a quasi-color-free WRC-FPLD.

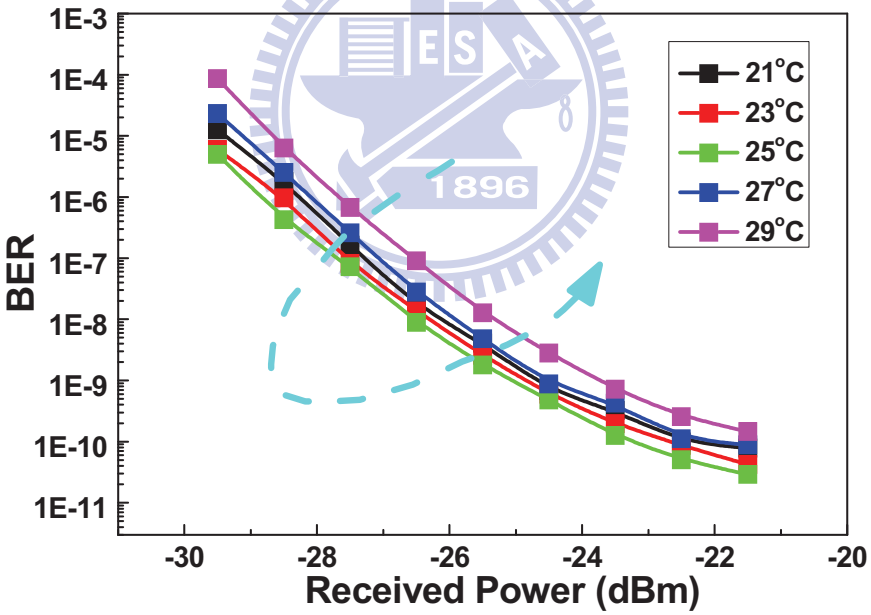

Fig. 4.8 (a) Optical spectrum of injected WRC-FPLD at the temperature from 21°C to 29°C.

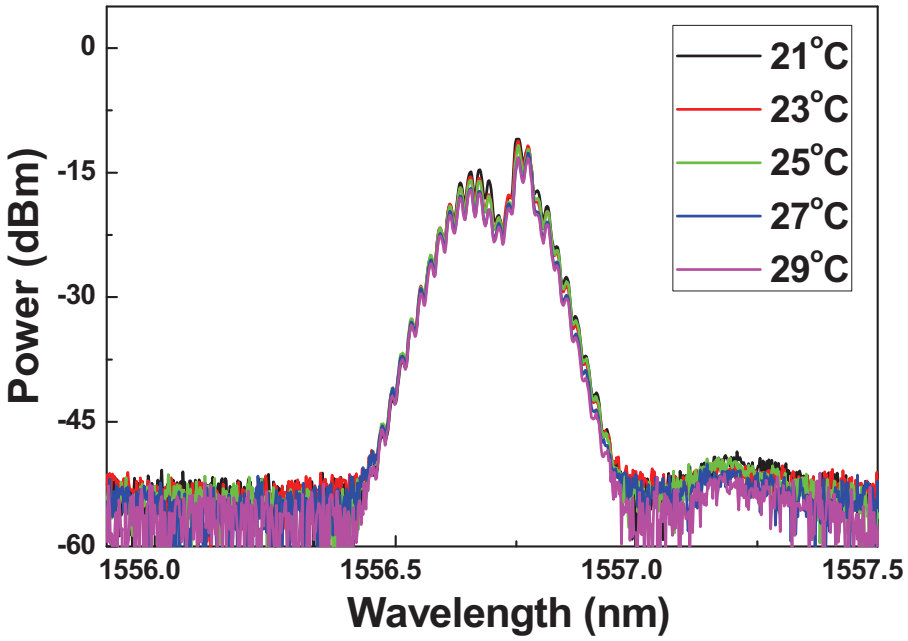

Fig. 4.8 (b) BER of temperature-controlled WRC-FPLD with different injection locked mode number.

As shown in Fig. 4.8(b), there is only a tiny positive power penalty on the BER by 0.6 dB during the WRC-FPLD temperature sweep. Both the spectral shift and the power attenuation concurrently occurs during the change of WRC-FPLD temperature, leading to the different injection-locked mode matching and output powers at different temperatures. Although the WRC-FPLD output power can be affected by both the wavelength matching and the operating temperature, our observations confirm that the temperature effect induced degradation of inner laser efficiency is more pronounced than wavelength matching effect. That is, the receiving power at a specific BER should be inevitably enlarged by increasing the WRC-FPLD operating temperature. Nevertheless, such a degration only induces a power penalty of < 1dB between 21°C to 29°C. The word of "color-free" describes request of the wavelength-matching between master and slave laser. The system can be named color-free while the wavelength-matching can be ignored in the operation. Our proposed system in 4th chap., both the spectral shift and the power attenuation occur during the change of WRC-FPLD temperature, leading to the different injection-locked mode matching and output

powers at different temperatures. The results conclude that there is a positive power penalty on the BER by 0.6 dB which could be ignored of the wavelength-matching. However our proposed system still have 0.6-dB sensitivity penalty that could be described as "quasi-color-free".

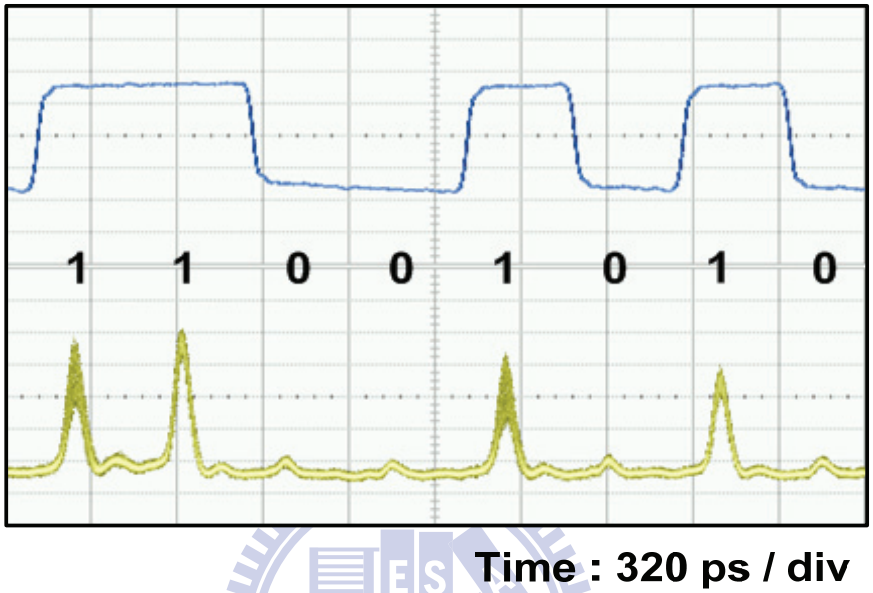

Fig. 4.9(a) Injection-locking power dependent wavelength lock-in range of one longitudinal mode in the slave WRC-FPLD transmitter at the ONU end.

At last, the quasi-color-free RZ transmission performed by the pulsated master WRC-FPLD injection-locked slave WRC-FPLD can be achieved up to 16 DWDM channels. The transmitted RZ data-stream all-optical converted from the modulated NRZ data-stream, and the measured BER transmission performance versus receiving power are shown in Figs. 9(a) and 9(b). A receiving sensitivity for 2.5Gb/s back-to-back transmission at BER<10^{-10} can be -25.6 dBm. A well-opened RZ eye pattern can be obtained with a relatively large dynamic range, in which the rising and falling time (defined as the duration between 20% and 80% of on-level amplitude) are 48 ps and 52 ps, respectively. The best and worst power penalties of the adjacent 16 channels after 25-km SMF propagation are 0.9 dB and 2 dB, respectively. The various power penalties are attributed to linear-dispersion data

transmission distortion and the initial wavelength mismatch. With appropriate temperature tuning of the slave WRC-FPLDs, the variation on receiver sensitivity penalty at BER=10^{-10} can be confined within 1.6 dB under a temperature shift of 15°C. The acceptable tolerance of the wavelength locking bandwidth can be enhanced with increasing RF power to improve gain-switching mode linewidth. By adjusting the cavity length, the longitudinal mode spacing of master WRC-FPLD could be further modified to match the ITU-T defined DWDM channels for practical WDM-PON application.

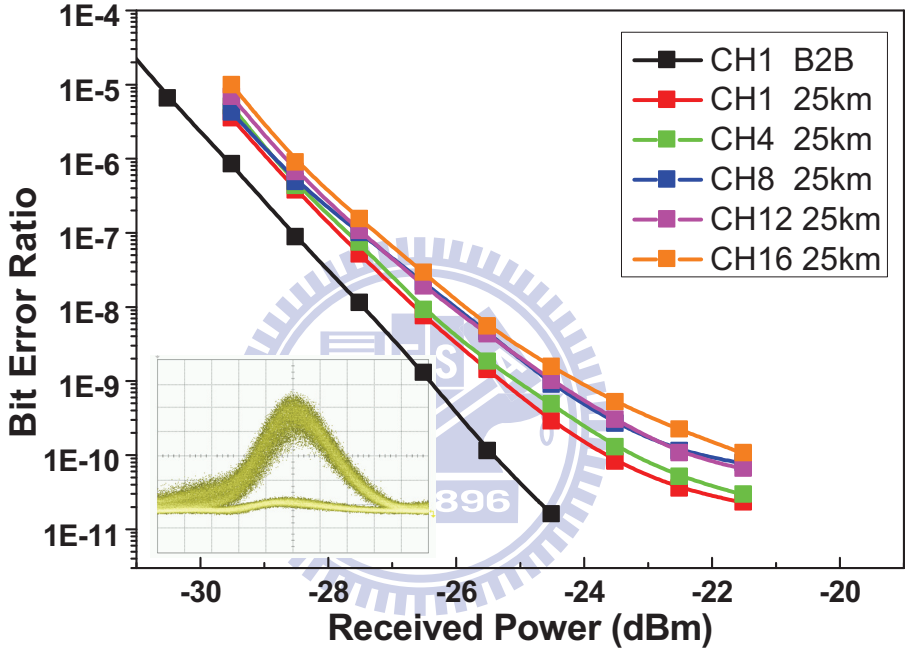

Fig. 4.9(b) BER analysis of wavelength injection locked WRC-FPLD at different channels and measured pulsed RZ eye diagrams (inset)

The power budget in our system could be considered including the fiber loss of 5 dB, the WDM coupler loss of 2 dB, the AWG loss of 4 dB, and the circulator loss of 1 dB. The output optical power of pulse injection WRC-FPLD is -10 dBm. As the transmission receiver sensitivity was measured as -25 dBm, the system allows an additional 3-dB loss for the whole WDM-PON link.

4.4 Summary

We demonstrated a novel bi-directional DWDM-PON with return-to-zero (RZ) data-format at 2.5 Gb/s by using both the down- and up-stream slave WRC-FPLDs coherently injection-locked by a pulsated WRC-FPLD based quasi-colorless master source with more than 10-mA threshold reduction. Both the down- and up-stream slave WRC-FPLDs are directly modulated by PRBS NRZ data and coherently injection-locked by the gain-switched master WRC-FPLD after 200-GHz AWG channelization to perform the bi-directional RZ data transmission at 2.5 Gb/s over 25 km. The proposed scheme involves a gain-switched WRC-FPLD coherent injection source with lower noise than ASE and employs the quasi-color-free WRC-FPLD transmitters with relatively large tolerance on locking bandwidth. Receiving back-to-back and worst transmission sensitivities transmission are -25.6 dBm and -23.6 dBm, respectively, and the rising and falling time of pulsed RZ eye pattern can be obtained with 48 ps and 52 ps. The best side-mode suppression ratio of 42 dB and the lowest timing root-mean-square jitter of 40 dB and 16 ps, respectively, for the pulsed RZ data-stream are observed. This system is an appropriate balance between coherent and incoherent injection solutions. The proposed pulsed RZ network could further be applied to a RZ binary-phase-shift-keying (BPSK) network or hybrid DWDM/OTDM PON architecture.

References

[4.1] S. J. Park, C. H. Lee, K. T. Jeong, H. J. Park, J. G. Ahn, and K. H. Song, "Fiber to the home services based on wavelength division multiplexing passive optical network," *IEEE J. Lightwave Technol.*, **22**, 2582–2591, (2004).

[4.2] K. Lee, J. H. Song, H. K. Lee, and W. V. Sorin, "Multistage access network for bidirectional DWDM transmission using ASE-injected FP-LD," *IEEE Photon. Technol. Lett.*, **18**, 761-763, (2006).

[4.3] W. Lee, M.-Y. Park, S.-H. Cho, J. Lee, C. Kim, G. Jeong, and B.-W. Kim, "Bidirectional WDM-PON based on gain-saturated reflective semiconductor optical amplifiers," *IEEE Photon. Technol. Lett.*, **17**, 2460–2462, (2005).

[4.4] S. C. Lin, S. L. Lee, and C. K. Liu, "Simple approach for bidirectional performance enhancement on WDM-PONs with direct modulation lasers and RSOAs," *Opt. Express*, **16**, 3636–3643, (2008).

[4.5] J. Prat, C. Arellano, V. Polo, and C. Bock, "Optical network unit based on a bidirectional reflective semiconductor optical amplifier for fiber-to-the-home networks," *IEEE Photon. Technol. Lett.*, **17**, 250–252, (2005).

[4.6] G.-R. Lin, T.-K. Cheng, Y.-C. Chi, G.-C. Lin, H.-L. Wang, and Y.-H. Lin, "200-GHz and 50-GHz AWG channelized linewidth dependent transmission of weak-resonant-cavity FPLD injection-locked by spectrally sliced ASE," *Opt. Express*, **17**, 17739-17746, (2009).

[4.7] K.-M. Choi, J.-S. Baik, and C.-H. Lee, "Broad-band light source using mutually injected Fabry–Pérot laser diodes for WDM-PON," *IEEE Photon. Technol. Lett.*, **17**, 2529–2531, (2005).

[4.8] Q. T. Nguyen, P. Besnard, L. Bramerie, A. Shen, C. Kazmierski, P. Chanlou, G.-H. Duan, and J.-C. Simon, "Bidirectional 2.5-Gb/s WDM-PON using FP-LDs wavelength-locked by a multiple-wavelength seeding source based on a mode-locked laser," *IEEE Photon. Technol. Lett.*, **20**, 733-735 (2010).

[4.9] Z. Xu, Y.-J. Wen, W.-D. Zhong, C.-J. Chae, X.-F. Cheng, Y. Wang, C. Lu, and J. Shankar, "High-speed WDM-PON using CW injection-locked Fabry-Pérot laser diodes," *Opt. Express*, **15**, 2953-2962, (2007).

[4.10] Y.-C. Chang, Y.-H. Lin, J. H. Chen, and G.-R. Lin, "All-optical NRZ-to-PRZ format transformer with an injection-locked Fabry-Perot laser diode at unlasing condition", *Opt. Express*, **12**, 4449-4456, (2004).

[4.11] L. Li, “Static and dynamic properties of injection-locked semiconductor lasers,” *IEEE J. Quantum Electron.*, **30**, 1701-1708, (1994).

Chapter 5
Self-restorable injection-locking monitor by integrated photodiode

5.1 Motivation and configuration

The injection-locked Fabry-Perot laser diode (FPLD) has received substantial attention [5.1] as it can produce a single longitudinal mode with a high side-mode suppression ratio (SMSR) for potential applications in the WDM optical communications. In principle, the injection-locking lasers strictly rely on external seeding or self-feedback injecting a continuous-wave (CW) laser to achieve single-mode pulsed generation. Many versatile injection-locking techniques, such as the clock frequency division [5.2], the 10-Gbps WDM passive optical network (PON) [5.3], the parallel transmission and wavelength routing network (Para-Wave NET) [5.4], and the all-optical non-return-to-zero (NRZ) to pseudo-return-to-zero (PRZ) format transformation [5.5], have been demonstrated. All these applications require precisely controlled injection-locked FPLD, but the maintenance as regards its stability and reliability usually requires complicated modules. Therefore, fault management is one of the crucial aspects in network management to enhance the network reliability. Of late, many efforts have been focused on the fault-monitoring methods [5.6] and the self-restorable networks [5.7] to achieve network protection.

In this chapter, a novel in situ injection-locking monitor for real-time and self-restorable tracking the FPLD-based WDM-PON transmitter is shown. Without employing high-speed electronics and instruments, the proposed in situ monitoring and self-restorable architecture uses the integrated MPD, which is usually employed to monitor the optical power illuminated by the FPLD. An embedded 8-bit commercial microcontroller-unit (MCU) is used to achieve the real-time and self-restorable control, which can be easily added

into injection-locking systems for getting higher reliability. It is cost effectively implemented with a minimum amount of redundant network resources and the MPD-based autopower-control (APC) function, which can simultaneously be integrated in the proposed system to optimize the optoelectronic performance of the FPLD.

Figure 1 schematically illustrates an in situ and self-restorable architecture for injection-locked FPLD WDM Transmitter. A fiberoptic WDM transmitter with a standard package of Transistor Outline (TO)-56 can is shown in the inset of Fig. 5.1. The typical front-facet and back-facet reflectivity of their FPLD used in the system is 30% and 90%, respectively. In other words, the front facet of the FPLD is uncoated and the back facet of the FPLD is high-reflection (HR) coated. It is necessary to keep the reflectivity of FPLD at a certain value to make its mode-extinction ratio sufficiently large for distinguishing the lock-in from loose-lock condition. The self-restoration unit cannot work for an FPLD without sufficiently large discrimination between longitudinal modes. The output power of the FPLD chip is 6 mW at 30 mA, and its coupling efficiency to a single-mode fiber is about 15%. The electrical frequency response of the directly modulated FPLD was measured by a lightwave component analyzer (HP, f_{mod}>20GHz, 8703A,) as shown in the Fig. 5.2, and the FPLD exhibits the 3-dB bandwidth of 4.2GHz. The MPD was placed on the HR coated side of the FPLD and the photocurrent is fed back to the MCU-based auto-restorable controller. A tunable laser (TL, ANDO 4321D) with a wavelength resolution of 0.001 nm is employed as the master laser for injection locking the FPLD.

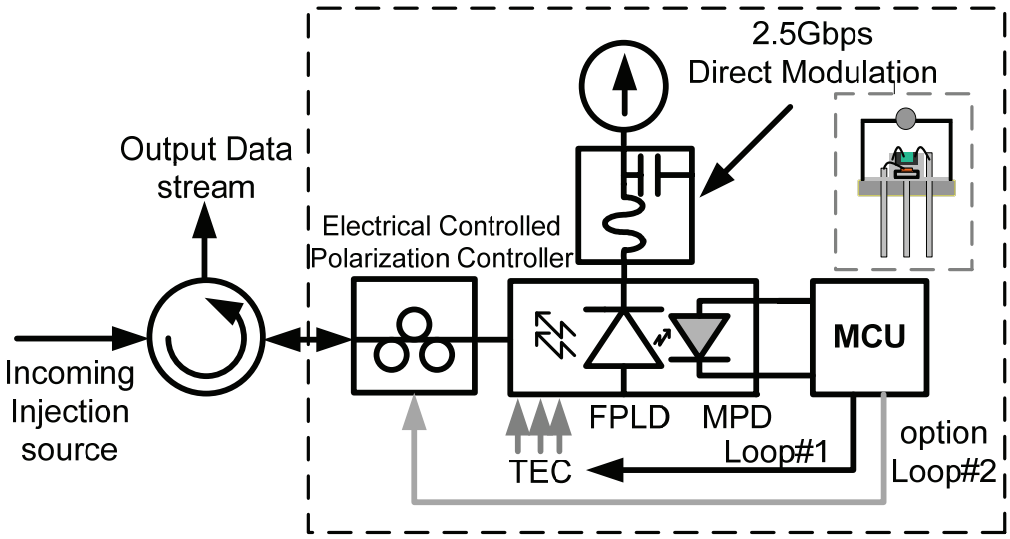

Fig. 5.1 A self-restorable system for injection-locked FPLD with monitor photodiode. The MCU detects the MPD photocurrent and controls the TEC and the polarization controller.

An MCU (ATMEL MEGA88V)-integrated analog-to-digital converter (ADC) recurrently measures the photocurrent of the MPD every 0.1 μs and dynamically controls the temperature of the thermoelectric cooler (TEC). The FPLD exhibits a threshold current of 8.5 mA, a longitudinal mode spacing of 1.15 nm, and a peak wavelength of 1533.5 nm. Herein, the DC bias current of the FPLD is set as 30 mA and the amplitude of the RF signal is set to reach the optical extinction ratio of 10 dB by directly modulating the FPLD. The FPLD temperature is controlled at 30^{o}C with <0.1^{o}C fluctuation to prevent the wavelength drift of each longitudinal mode. The temperature-dependent wavelength shifting slope is 0.06nm/^{o}C. Another function to achieve the self-restoration of the preferred polarization for the FPLD is based on feedback controlling an electronically tunable polarization controller added prior to the FPLD to be injection-locked as shown the loop#2 in Fig.1. The proposed scheme cannot eliminate the polarization sensitive problem accompanied with the injection-locked FPLD, however, the MCU of self-restorable injection locker can concurrently deal both the deviation of FPLD wavelength and the mismatched polarization of

the incoming light.

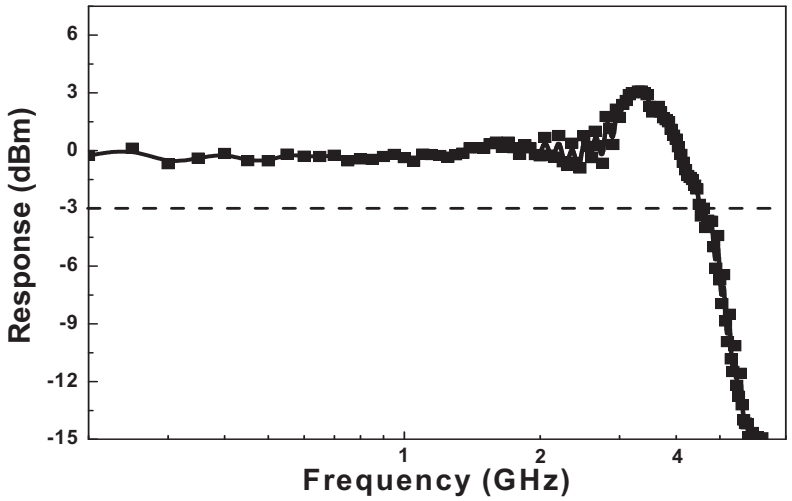

Fig. 5.2 The frequency response of the directly modulated FPLD with 3-dB bandwidth of 4.2GHz

5.2 Modeling and experimental results of MPD-MCU based auto-restorable FPLD transmitter

Figure 3(a) illustrates the injection-locking wavelength evolution by detuning the injection wavelength, in which the black line shows the exact injection locking condition. As a result, the wavelength-locking range of the slave FPLD measured by adopting the modified delayed self-homodyne (MDSH) scheme [5.8], which is used to determine the stability of injection locking by monitoring the reduction of the injection-locked FPLD mode linewidth, is shown in Fig. 5.3(b).

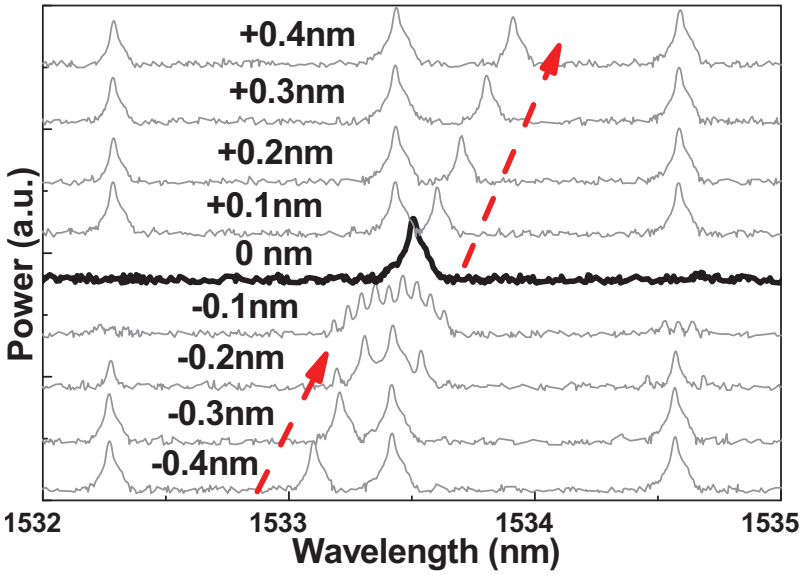

Fig. 5.3 (a) Spectrum evolution of FPLD by detuning per 0.1-nm wavelength.

The detuning wavelength is defined as the wavelength shift of the master TL with respect to one longitudinal mode of the slave FPLD by obtaining SMSR >35 dB. Figure 3(a) shows that <2°C accuracy must be satisfied when using injection-locked FPLD. Figure 3(b) shows that <0.09nm wavelength accuracy must be satisfied at >-3 dBm injection, and the temperature of FPLD should be controlled within 1.5°C. However, the inevitable aging of the FPLD is an important issue in practical telecommunication systems.

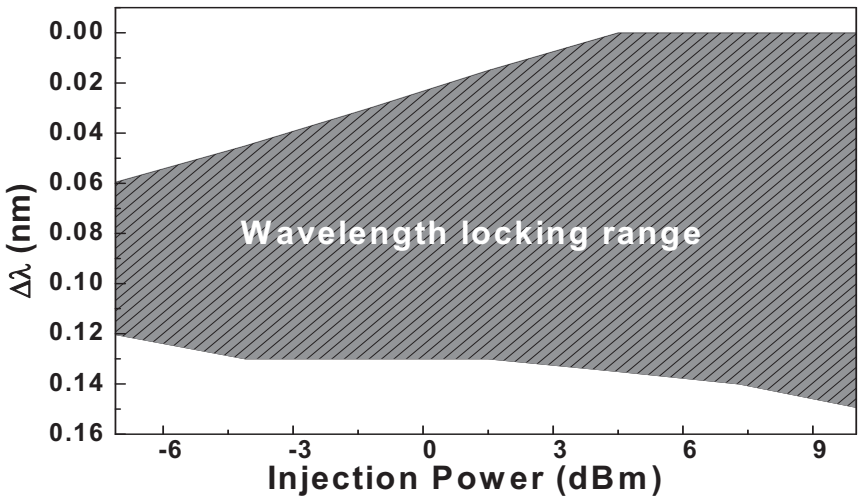

Fig. 5.3 (b) Wavelength locking range of a side mode in the slave FPLD

as a function of injection-locked power.

By adjusting the FPLD driving currents at 25, 30, 35 mA and detuning its wavelength to realize the injection locking, the results shown in Fig. 5.4(a) indicate a notable peak photocurrent at exactly injection locking, which leads to the maximum output power of FPLD. Figure 4(b) illustrates the behavior of the MPD at injection power of + 3, 0, -3, -6, and -9 dBm versus detuning wavelength. A minimum injection power of -9 dBm for all longitudinal modes is required to initiate the wavelength locking. The red-shifted detuning wavelength of the master laser with respect to the free-running longitudinal mode of slave laser was also observed by Bouchoule *et al.* [5.9]. The carrier density of FPLD can be severely depleted at a larger gain region to cause the red shift in locking the wavelength range. In addition, a relatively weak signal with considerable noise generated by multi-longitudinal-mode beating effect has also been found as the injection wavelength is detuned away from the slave FPLD's longitudinal mode by 0.14 nm. The largest illuminated power occurs at the center wavelength of a longitudinal mode exactly located at the injection wavelength to achieve exact injection locking. By detuning injection wavelength, the amplified photocurrent phenomenon at exact injection-locking condition will be reduced by shifting the injection wavelength from the central wavelength of this longitudinal mode. The photon density in the FPLD gradually decays with detuning injection wavelength. Concurrently, the carrier density in the FPLD is persistently depleted under the external injection, even though the injection wavelength deviates from the central wavelength.

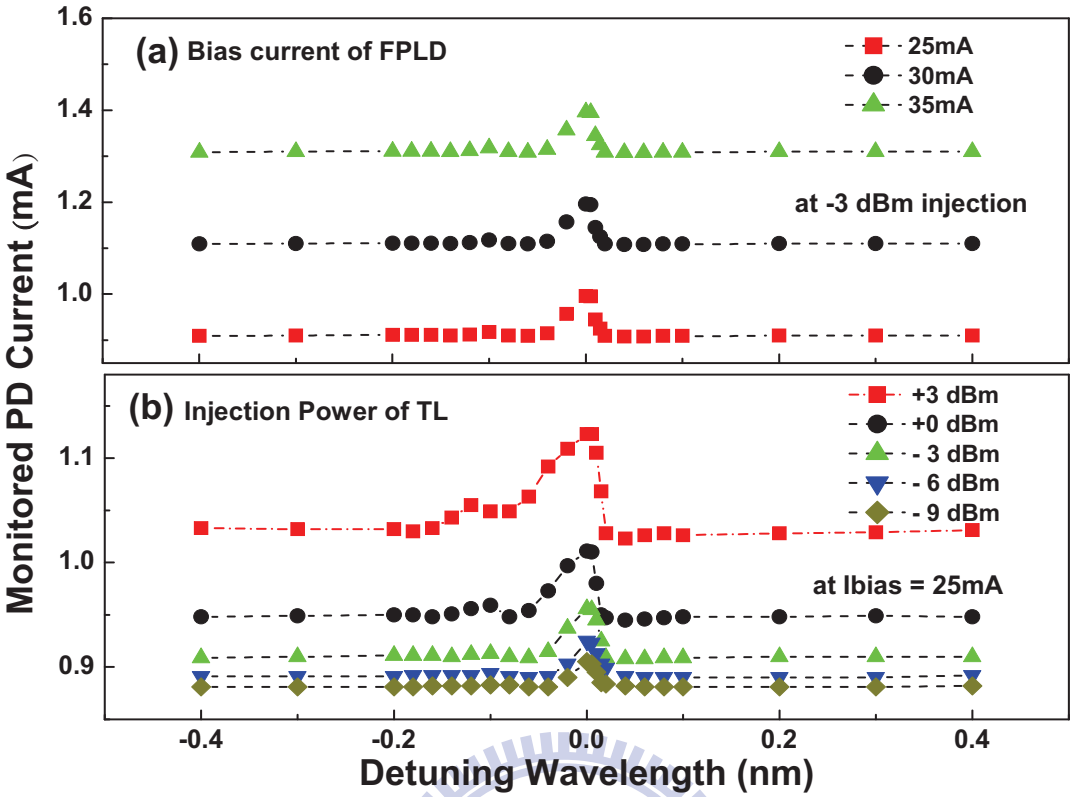

Fig. 5.4 (a) The photocurrent of MPD at the FPLD driving currents of 25, 30, and 35 mA as detuning wavelength. (b) The photocurrent of MPD at the injection power of + 3, 0, -3, -6, and -9 dBm as detuning wavelength

Such a fringe-like photocurrent enhancement effect is mainly caused by the Fabry-Perot etalon. The mode extinction ratio of the FPLD is reduced by attenuating the front or back reflectivity, and thus the sharpness of the transmission function. This clearly elucidates the rapidly decayed gain around central mode wavelength. By injecting each longitudinal mode at -9 dBm, Fig. 5.4(a) illustrates a similarly monitored photodiode (PD) photocurrent feature, where the FP etalon effect dominates the monitored PD photocurrent response. As the FPLD is externally seeded by a single-mode laser source, the carriers in the FPLD were depleted under the external seeding. The power gain of the FPLD lasing mode spectrum by involving the Fabry-Perot etalon effect is described as

$$G_T(\lambda) = G_0 \frac{(1-R_1)R_2}{\left(1-\sqrt{R_1}\sqrt{R_2}e^{2g(\lambda)d}\right)^2} \frac{e^{4g(\lambda)d}}{1+\frac{4\sqrt{R_1}\sqrt{R_2}e^{2g(\lambda)d}}{\left(1-\sqrt{R_1}\sqrt{R_2}e^{2g(\lambda)d}\right)^2}\sin^2\left(\lambda\pi/\Delta\lambda_m\right)}, \quad (1)$$

where g(λ) is the differential gain as a function of wavelength and d the cavity length. R_1 and R_2 are the reflectivity of the front and rare facets, respectively. The phase difference δ in standard Fabry-Perot etalon equation can be replaced by the free spectrum range (FSR) $\Delta\lambda_m$. In particular, the mechanism responsible for gain and output power variations of the FPLD is also discussed, which facilitate the mode discrimination by distinct PD current change between the locking and the unlocking conditions. Assuming one longitudinal mode under external injection-locking condition, the gain of FPLD, G(N,S), can be described as [5.10]

$$\begin{aligned} G\left(N_{inj},S_{inj}\right) &= G_N\left(N_{inj}-N_0\right)\left(1-k_sS_{inj}\right) = G_N\left(N_{th}-N_0\right)+\Delta G \\ &= \frac{1}{\tau_p}+D_G+G_N\Delta N-G_s\Delta S = \frac{1}{\tau_p}-\frac{R_{sp}}{S_{LD}}-\sqrt{\frac{4\alpha^2k_c^2}{\left(1+\alpha^2\right)}}\sqrt{\frac{S_{inj}}{S_{LD}}}, \end{aligned} \quad (2)$$

where N_{inj} is the carrier number of the FPLD under external injection locking, S_{inj} the externally injected photon number, N_0 the transparent carrier number, N_{th} the threshold carrier number, ΔG the gain change, τ_p the photon lifetime, D_G the normalized gain difference, G_N and G_s are the differential gain coefficients for ΔN and ΔS denoting the variations of carrier and photon numbers, respectively. R_{sp} denotes the spontaneous emission rate, and S_{LD} the total photon number at the injection-locked mode, α the linewidth broadening factor, and k_c the coupling coefficient of the FPLD for external injection. The derivation indicates that the gain of FPLD is reduced under the external injection-locking condition. On the other hand, the variation on threshold current (I_{th}) of FPLD from the change of carrier number under external injection-locking condition is given in [5.5, 10, 11]

$$N_{th,inj} = \frac{G\left(N_{inj},S_{inj}\right)}{G_N}+N_0 = \frac{1}{G_N}\left[\frac{1}{\tau_p}-\frac{R_{sp}}{S_{LD}}-\sqrt{\frac{4\alpha^2k_c^2}{\left(1+\alpha^2\right)}}\sqrt{\frac{S_{inj}}{S_{LD}}}\right]+N_0, \quad (3)$$

$$I_{th,inj} = \frac{q}{\eta_i \tau_c} N_{th,inj} = \frac{q}{\eta_i \tau_c}\left[\frac{1}{G_N}\left(\frac{1}{\tau_p} - \frac{R_{sp}}{S_{LD}} - \sqrt{\frac{4\alpha^2 k_c^2}{(1+\alpha^2)}}\sqrt{\frac{S_{inj}}{S_{LD}}}\right) + N_0\right]$$
$$= \frac{q}{\eta_i \tau_c}\left(\frac{1}{G_N \tau_p} + N_0\right) - \frac{q}{\eta_i \tau_c G_N}\left(\frac{R_{sp}}{S_{LD}} + \sqrt{\frac{4\alpha^2 k_c^2}{(1+\alpha^2)}}\sqrt{\frac{S_{inj}}{S_{LD}}}\right), \quad (4)$$

where q denotes the electron charge, η_i the internal quantum efficiency, and τ_c the carrier lifetime. The threshold current of FPLD is also decreased due to the external injection. The output power of the FPLD can thus be written as

$$P_{out,inj} = \eta_d \frac{h\nu}{q}\left(I - I_{th,inj}\right)$$
$$= \eta_d \frac{h\nu}{q}\left\{I - \frac{q}{\eta_i \tau_c}\left(\frac{1}{G_N \tau_p} + N_0\right) + \frac{q}{\eta_i \tau_c G_N}\left(\frac{R_{sp}}{S_{LD}} + \sqrt{\frac{4\alpha^2 k_c^2}{(1+\alpha^2)}}\sqrt{\frac{S_{inj}}{S_{LD}}}\right)\right\}, \quad (5)$$
$$= \eta_d \frac{h\nu}{q}\left(I - I_{th,0}\right) + \eta_d \frac{h\nu}{q}\Delta I_{inj} \equiv P_{out,0} + \Delta P$$

where η_d is indeed the differential quantum efficiency, $h\nu$ the energy per photon, and I_{th} the threshold current. Both the gain and the threshold current of the FPLD are decreased under external injection-locking condition. The reduced gain fails to amplify the injected signal, whereas the improvement on the output power of the FPLD is completely due to threshold current reduction.

The seeding reduces the threshold current of laser and therefore the output power for lasing will increase under constant current condition. The relative importances of these two effects are coming from the same rate equation to our best knowledge. As we known, we use the output power to represent the photocurrent due to their relationship of direct proportion. The threshold current and output power of the FPLD under injection-locking condition can be described by the following equations. To include the possible excitation of the neighboring mode with increasing detuning, we present a rate equation for the photon

number *Sp* in that mode (unlocked mode) as

$$\dot{S}_p = \left(G-1\right)S_p/\tau_p + R_s \tag{6}$$

The equation for the carrier density *n* is

$$\dot{n} = J/eV - n/\tau_s - GS/\tau_p V \tag{7}$$

where *J* is the bias current of the laser, *e* is the electron charge, *V* is the volume of the active region, τ_s is the carrier lifetime. When the external field is injected, the carrier density is changed from its free-running value n_o, by Δn. The gain *G(n, S)* can be expanded as [5.10]

$$G\left(n,S\right) \simeq G\left(n_{0S},S_{0S}\right) + \Delta G \simeq 1 + G_n\Delta n - k_s\Delta S\,, \tag{8}$$

where $G_n = v_g\tau_s\delta g/\delta n$ and α is the linewidth broadening factor, and *G(n_{0S}, S_{0S})* is the normalized gain in the free-running laser. $\Delta S = S - S_{os}$, S_{os} is the photon number without external light injection. The static locking properties can be obtained according to:

$$\Delta S\left(1/\tau_p - G_S S_L\right) + \Delta N/\tau_e = 0\,, \tag{9}$$

The optical injection induced the threshold current decrease was exhibited by Chang *et. al.* [5.5] as

$$\begin{aligned} I_{th,ui} &= \frac{qV}{\eta_i\tau}n_{th,ui} = \frac{qV}{\eta_i\tau}\left[\frac{\left(\frac{1}{\tau_p} - \frac{R_{sp}}{S_{Lm}} - \sqrt{\frac{4\alpha^2k_c^2S_i}{\left(1+\alpha^2\right)S_{Lm}}}\right)\Big/\left(1/v_g\tau_p\right)}{G_n} + n_{tr}\right] \\ &= \frac{qV}{\eta_i\tau}\left(\frac{g_{th}}{a} + n_{tr}\right) - \frac{qV}{\tau\eta_i a}\left(\frac{R_{sp}}{S_{Lm}} + \sqrt{\frac{4\alpha^2}{\left(1+\alpha^2\right)}}\sqrt{S_{iLm}}\right) \\ &= I_{th,free-running} - \Delta I_{injection} \end{aligned}\,, \tag{10}$$

,where S_{iLm} is the injection strength factor, and the decreasing threshold current will increase

the output power. By combing Eqs. (9), and (10), the photon number difference ΔS_{Ith} caused by threshold current reduction can be expressed as

$$\begin{aligned}\Delta S_{Ith} &= \tau_p \Delta N_{th} / \tau_e \left(G_S S_L - 1\right) \\ &= \tau_p \left(\Delta I_{th} \tau_e / qV\right) / \tau_e \left(G_S S_L - 1\right) \\ &= \tau_p \left[\frac{qV}{\tau_e \eta_i a} \left(\frac{R_{sp}}{S_L} + \sqrt{\frac{4\alpha^2}{\left(1+\alpha^2\right)}} \sqrt{S_{iL}} \right) \tau_e / qV \right] / \tau_e \left(G_S S_L - 1\right) \\ &= \frac{\tau_p}{\eta_i a \tau_e \left(G_{(n_{0S}, S_{0S})} k_s S_{Lm} / \tau_p - 1\right)} \left(\frac{R_{sp}}{S_L} + \sqrt{\frac{4\alpha^2}{\left(1+\alpha^2\right)}} \sqrt{S_{iLm}} \right)\end{aligned}, \quad (11)$$

On the other hand, the total gain difference T_G from the threshold value can be increased by the external light injection locking as

$$\begin{aligned}T_G &= D_G + \Delta G_m = D_G + G_N \Delta N_m - G_S \Delta S_m \\ &= -\frac{R_{sp}}{S_{Lm}} - \sqrt{\frac{4\alpha^2 k_c^2 S_i}{\left(1+\alpha^2\right) S_{Lm}}}\end{aligned}, \quad (12)$$

where the gain difference D_G is for the free-running laser biased below or far above threshold. Thus, the total gain difference T_G will be increased under the condition external injection locking. Certainly, the external injection light is amplified by the active region of the FPLD at resonant condition, and the external injection shall increase the total output power of the FPLD. If we consider the FP resonance effect that amplifies the external injection light, the increased photon number caused by amplified external injection light ΔS_{ext} can be described by T_G as

$$\begin{aligned}\Delta S_{ext} &= S_i \bullet k_c^2 \bullet T_G \\ &= S_i k_c^2 \left(\frac{R_{sp}}{S_L} + \sqrt{\frac{4\alpha^2}{\left(1+\alpha^2\right)}} \sqrt{S_{iL}} \right),\end{aligned} \quad (13)$$

In order to realize the relative importance for power increasing of the review mentioned two effects, the comparison between ΔS_{ext} and ΔS_{Ith} as following equation.

$$\frac{\Delta S_{ext}}{\Delta S_{Ith}} = \frac{S_i k_c^2 \eta_i G_{(n_{0S}, S_{0S})} \tau_e \left(G_{(n_{0S}, S_{0S})} k_s S_L / \tau_p - 1 \right)}{\nu_g \tau_p^2}, \tag{14}$$

We discuss the condition that the injected wavelength locates at peak of the longitudinal mode, and it induces the maximum gain change due to external injection. Although the FP resonance effect amplification and decreasing threshold interact with each other, we can realize the relationship between the two effect by fixing the photon number externally injected into the laser cavity S_i or photon number in the locked mode S_L as the Eq(9) shown. Assuming the photon number in the locked mode and the normalized gain in the free-running laser are constant, the FP resonance effect will be more effective as increasing the photon number externally injected into the laser cavity. For a fixed injection power, increasing biased current is another method to let the FP resonance effect be more effective.

5.3 Concept and circuit design

The concept of the in situ PD and MCU-based self-restoration system is derived from the fault-finding and restoration functions comprehensively used in optical time-domain reflectometry (OTDR) system for maintaining the cabling system's functionality. The principle of self-restoration in a conventional OTDR is based on to the transmission-line theory, which detects impedance or reflectance change of the optical pulse when reflecting from the break-up node along a fiber cable. Such an impedance change is reflected back and the OTDR measures the time taken for the reflection to return and converts this into distance along the fiber cable. An MCU is usually employed for the time-distance conversion in the OTDR; however, there is no requirement on the additional feedback circuitry for further control. Based on this concept, the flow chart for designing such a PD-MCU link in our

system is plotted in Fig. 5.5. In the injection-locked laser diode system, the slave laser output power is a function of independent variables, such as the master laser injecting wavelength and the specific longitudinal-mode wavelength of slave laser (which is tunable with the changing temperature). Thus, the PD-MCU system is constructed in response to the input signal from the injection-locked slave laser by producing an error signal feedback to control the temperature of the slave laser diode.

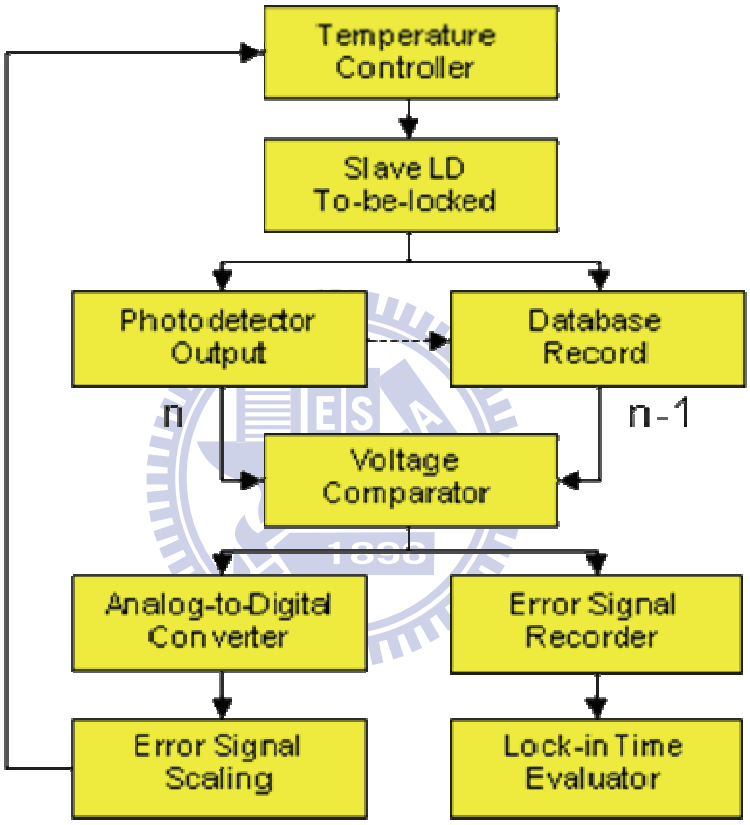

Fig. 5.5 The conceptual flow chart for designing the PD-MCU link based self-restoration unit.

In more detail, the signal input to the MCU is obtained by optoelectronically converting the injection-locked laser diode output power via the photodetector, and the converted voltage signal is used as the input to a microcontroller unit (MCU) with a program for an automated diagnosis of injection-locking condition. The MCU compares the input signal amplitude with the recorded amplitude in its memory, and then responds by producing an error signal to

feedback control the operating temperature of the laser diode. As a result, the wavelength of the gain spectrum as well as the longitudinal modes in the laser diode can be shifted by the feedback temperature control, thus providing an improved injection locking with the incoming master laser signal at a deviated wavelength. After a relatively short duration, the voltage comparator in MCU delivers zero-error voltage when the converted output signal amplitude from the injection-locked laser diode no longer changes, as the initiation of feedback control by the PD-MCU based self-restoration system has eventually forced the longitudinal wavelength laser diode coincident with the incoming master wavelength. The digital/discrete circuit blocks are used to process these signals in the MCU, which is converted back to analog/continuous signals for temperature control afterward. This results in the self-restoration of the wavelength of the injection-locked slave laser diode. Such a PD-MCU link essentially enhances the real-time wavelength restoration and error-noise suppression abilities through the digitized voltage comparator and feedback controller. The circuit block for building such a PD-MCU link is illustrated in Fig. 5.6.

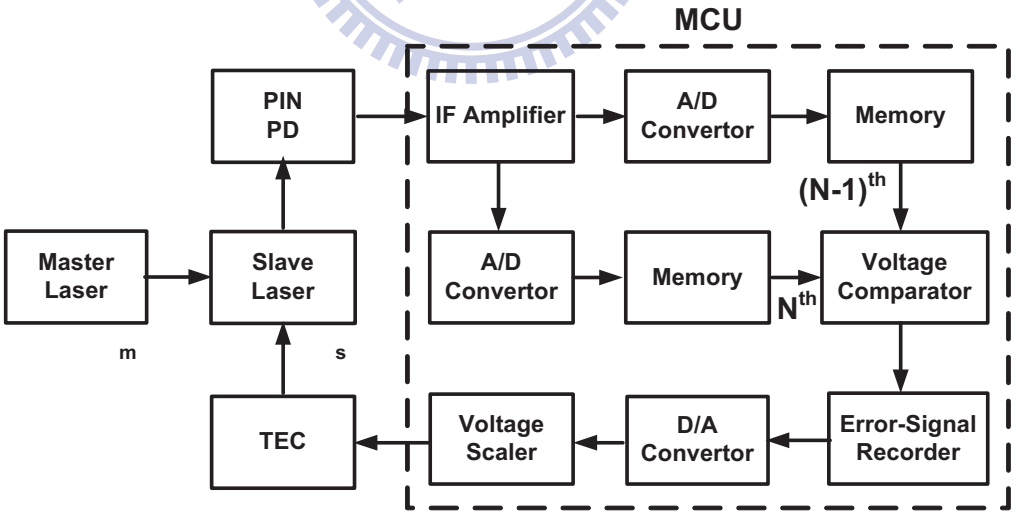

Fig. 5.6 The circuit block for building a PD-MCU link based self-restoration unit.

Indeed, such injection-locked laser diodes still exhibit a benefit on narrow linewidth,

long transmission distance, and especially the enhanced modulation bandwidth when comparing with other kinds of injection-locked sources. Nevertheless, both of wavelength matching and polarization matching are the important issues of the injection-locked FPLD for its application on communication network systems. In particular, the polarization control is the unique and inherent problem when utilizing the injection locking technique to control the laser diode wavelength. If the polarization state of the external injection is vertical to that of the FPLD, the eye diagram is worse than the injection-locked case and the BER is slightly degraded with a power penalty of 3 dB. However, the FPLD can still be used for data transmission since which is operated at free-running mode as compared to the injection-locked mode in this case. If the wavelength of the incoming light is also deviated without self-restoration, the bit-error-ratio (BER) performance of the FPLD under polarization mismatched condition is almost identical to that of the FPLD works at free-running condition. That is, the polarization degree directly affects the injection efficiency, which is a little bit different from the wavelength detuning effect. The requested power of optical injection into the FPLD could be greatly increased due to the deviation of the injected polarization from the preferred state of the FPLD. In our self-restorable design, the concept to achieve the self-restoration of the preferred polarization for the FPLD is based on feedback controlling an electronically tunable polarization controller added prior to the FPLD to be injection-locked. The MPD current of the FPLD is monitored during operation for feedback controlling the polarization controller to obtain the maximum output power from the injection-locked FPLD. After comparing the monitored MPD current with previous value, the MCU sends a controlling signal to detune incoming polarization via a polarization controller (see loop#2 in Fig.1). With the same feedback control loop, the two important issues of wavelength locking and polarization matching can be concurrently implemented for the practical self-restorable injection locker. Based on the proposed self-restorable injection locker for the injection-locked FPLD, both the wavelength deviation and polarization mismatch

between the FPLD and the incoming light can be effectively feedback controlled to optimize the injection-locking performance, which makes the self-restorable injection-locked FPLD more practical for data transmission in network system.

5.4 Injection-locking monitor of self-restoration

Later on, the analysis of auto-restorable architecture is performed to characterize the auto-injection-locking performance of a directly modulated FPLD in a 2.5-Gbit/s WDM fiberoptic network. To achieve auto-restoration, the MCU plays an important role in detecting and calculating the MPD photocurrent, and decides whether to increase or decrease the slave-FPLD temperature by feedback TEC. The TO-can of FPLD is clamped to the aluminum block to ensure the TO-can at the ambient temperature. While a sudden unlocking event occurs with a monitored photocurrent located in gradient MPD current region, the MCU can correctly determine the detuning direction by comparing the derivative photocurrent. However, if the sudden unlocking wavelength is located in the flattened gain region, the auto-restoration will directly control the slave FPLD wavelength toward the next longitudinal mode to be injection locked. The positive-wavelength searching further benefits from the early wavelength peak detection in most conditions. In experiment, the injection wavelength is blue-shifted by 0.8 nm and the injection power is set at -9 dBm to simulate the practical condition at the unlocking state. The 0.8-nm shift is indeed a relatively worse case for demonstrating the self-restoration system with a positive wavelength searching function (increase temperature). Concurrently, the mode spacing and the temperature drift rate were preset in the MCU.

For each slave FPLD under self-restoration operation, all the parameters are not necessarily calibrated as the MCU can automatically lock-in the desired mode by detecting the optimized point. The MPD current remains almost constant when the self-restoration is completed by tuning the FPLD longitudinal mode coincidently with the injecting wavelength,

as shown in Fig. 5.7(a). By detuning the injecting source at different wavelengths, the injection-locked output spectra can be obtained and shown in Fig. 5.7(b). As tuning over the specific longitudinal mode, the photocurrent is rapidly decayed due to the Fabry-Perot etalon enhanced gain competition effect. Overheating instead of the gradient variation searching method was used in our system to enhance the locking time, while the MCU program performs more like a binary searching function to reach the mode restoration within three damping cycles. In general, such a self-restoration can be achieved within 10 seconds (limited by the TEC tuning speed). Even with such a bad case for a slave FPLD with an external TEC module, the injection locking can still be obtained within 50 seconds and the correct temperature can be recovered with 0.1°C resolution, as shown in Fig. 5.6. This figure is obtained with an injecting power of -3 dBm with a monitored PD current of about 1 mA at stabilized injection-locking condition. In the system proposed here, the lowest injection power can be -9.0 dBm, which is limited by the background noise level and by the resolution of the ADC circuit in MCU.

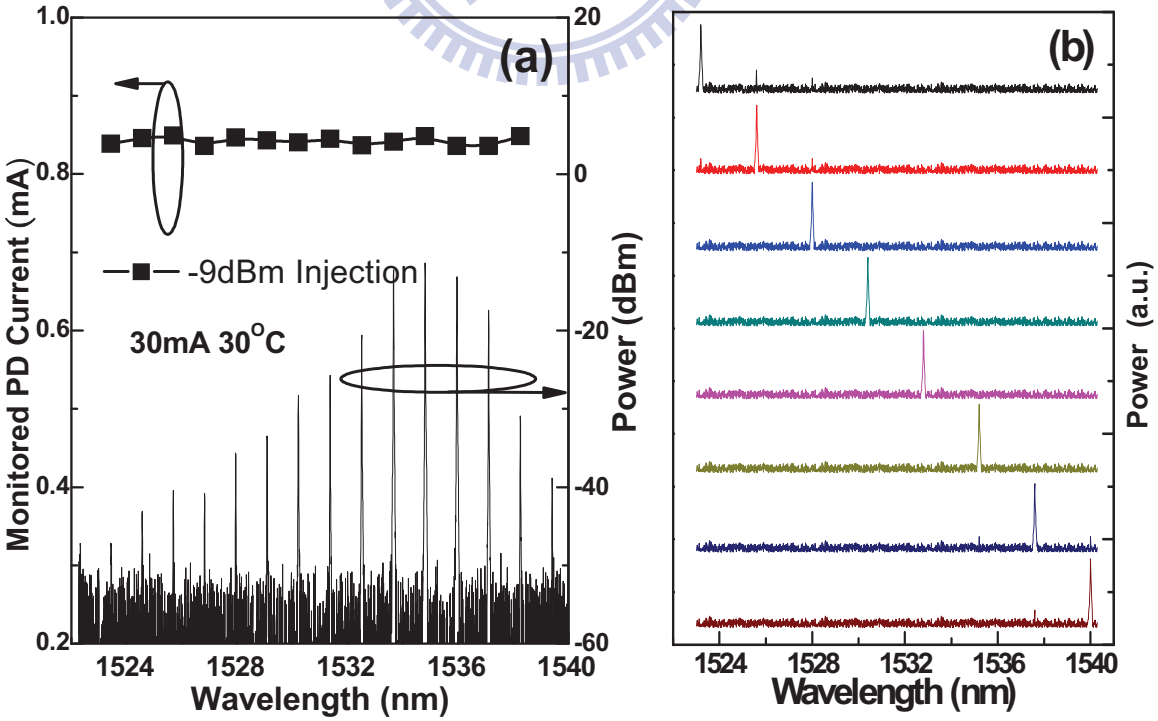

Fig. 5.7 (a) The monitored PD current (upper, square-dotted curve) and

the free-running FPLD spectrum (lower, block lines); (b) the spectra of the FPLD transmitter injection locked at different longitudinal modes (color lines at right part).

On the other hand, the injection power cannot be increased too high as it may damage the coupling end-face of the FPLD transmitter. Moreover, the additional reflectance from the FPLD coupling end-face is up to 1.5% (assume the coupling efficiency of the TO-can ball lens is 15%, and the front-face reflectivity of the FPLD is 70%). The FPLD output power could saturate at higher injection levels, whereas the reflection from coupling end does not saturate with increasing injection power. As a result, the FPLD transmitted data stream will be carried by a DC offset due to the additional coupling end-face reflection. In this case, the extinction ratio of the transmitted data gradually decreases with increasing injection level, which seriously degrades the noise and the bit-error-rate performance. If the transmitted data stream is further monitored, the intensity noise raised by the beating between incoming laser and local FPLD could occur. This phenomenon could also induce an interfered signal inside the FPLD transmitter. In particular, when the injecting wavelength is slightly deviated from the mode wavelength, the interference occurs to greatly enlarge the relative intensity noise of the transmitted data and thus induces additional chirp for output data stream. This is why the external injection is limited to below +3 dBm. Otherwise, such an interference problem becomes so serious as to degrade the transmitted data performance.

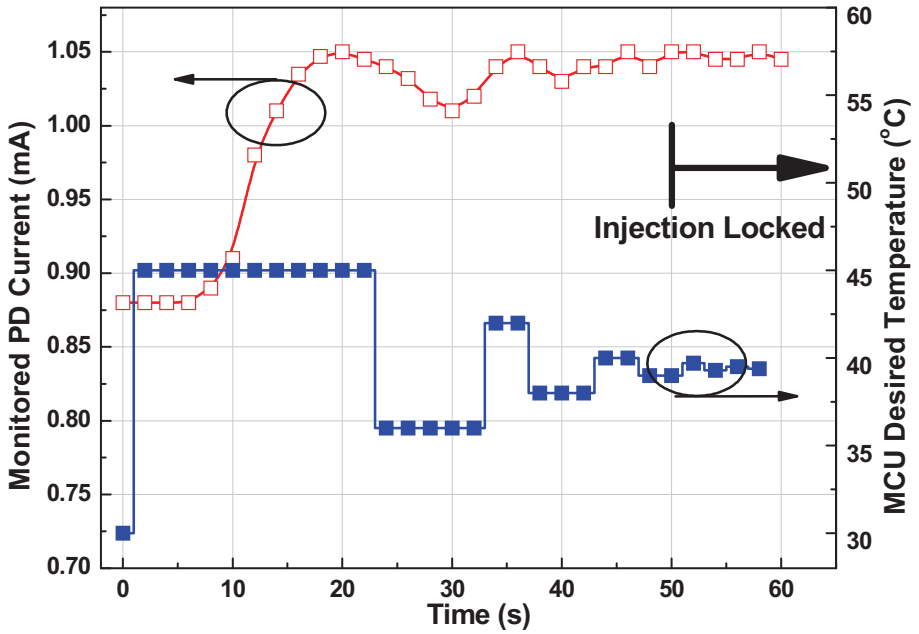

Fig. 5.8 The recovery experience of the self-restorable unlocked FPLD and corresponding MPD current controlled by MCU.

5.5 System performances of the MCU-based auto-restorable injection-locking transmitter

To obtain the BER performance, the DC bias current of the FPLD is set as 30 mA and the amplitude of the pseudo random binary sequence (PRBS) data stream to directly modulate the FPLD is set to reach an on/off extinction ratio of 10 dB. The FPLD temperature is controlled at 25°C. In the Fig. 5.9, the BER performance was analyzed at back-to-back condition without the use of any WDM filter between FPLD and receiver, as shown in the Fig. 5.1 of the manuscript. First of all, the BER performances of the FPLD working at free-running and manually operated to reach a perfectly injection-locking condition are measured and shown as the blue and green curves, respectively. Without perfect matching between the FPLD mode and the external injection wavelength (i.e. the loose injection-locking condition), the BER significantly degrades with its response curve located between those of the free-running and manually injection-locking cases. The BER response

obtained when detuning the injection wavelength away from the FPLD mode by only 0.03 nm is shown as the red curve in Fig. 5.9.

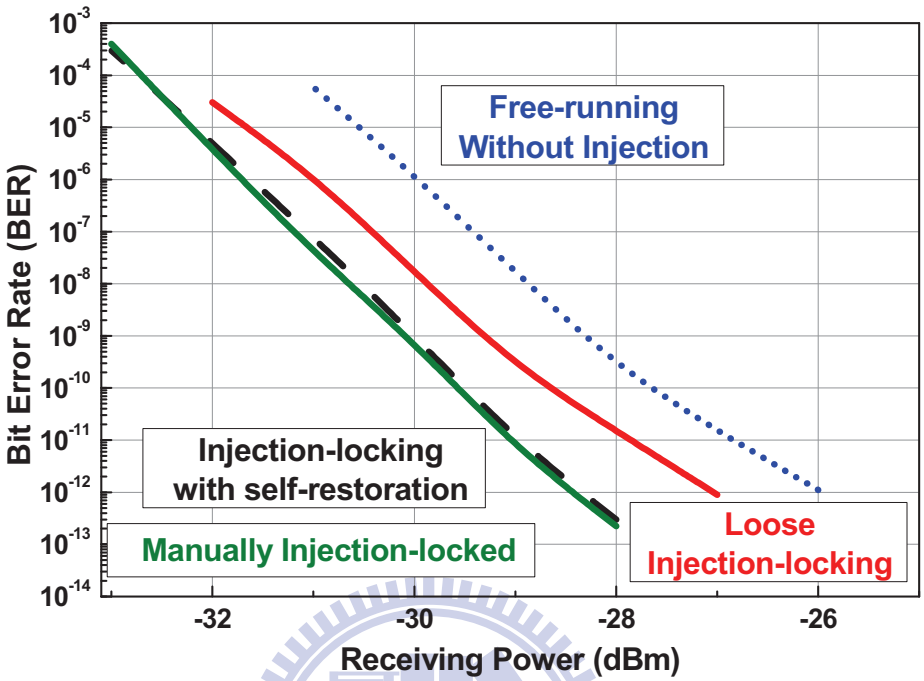

Fig. 5.9 The BER of the FPLD transmitter measured at three different conditions.

Afterwards, the MPD-MCU based self-restorable injection-locker is initiated to achieve auto-restoration injection-locking, and the measured BER response (black dashed curve) shows almost identical response with the best case obtained at manually injection-locking condition. Note that the auto-restoration speed strictly depends on the cooling/heating efficiency of the TEC and the environmental temperature. Such a long lock-in time is the worst case only when the TEC chip for controlling the temperature of the FPLD is located outside the transmitter module. Therefore, a delayed temperature compensating response is inevitably observed, which can be greatly improved by adding high-power or built-in TEC. A commercially available FPLD TO-can module with a built-in TEC device [5.12] has been introduced recently in the market, which could greatly shorten the temperature compensation response as well as the lock-in speed through the proposed self-restoration scheme. In

addition, the measured BER of the optical transmitting eye diagram can accurately calculate from the recorded Q factor [5.13]. At 2.5 Gbit/s, the BER of the injection-locked FPLD modulated by PRBS data-steam with 2^{31}-1 pattern length is 10^{-12} at a receiving power of -25 dBm. After the self-restoration, the Q factor measured from the optical eye histogram is as much as 8.2, providing a reachable BER of 1.1×10^{-16} at a data rate of 2.5 Gbit/s.

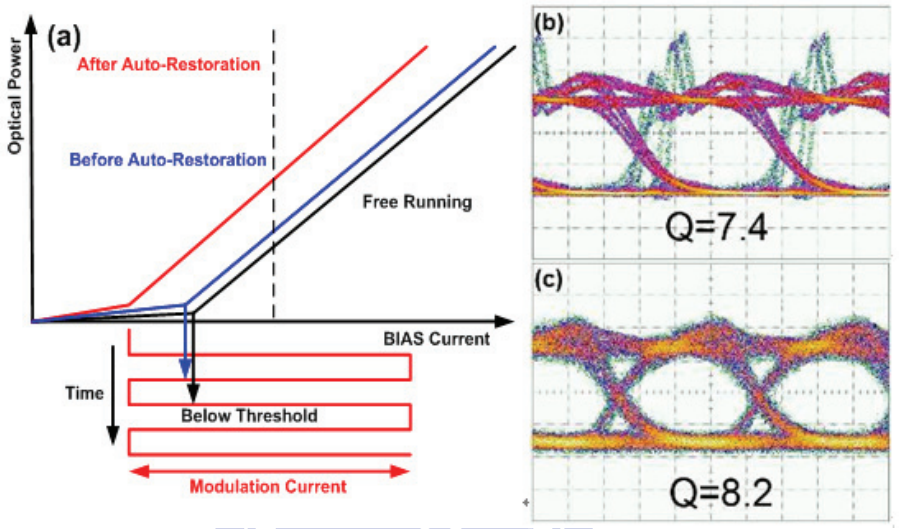

Fig. 5.10 Left: (a) Threshold current of FPLD before and after self-restoration. Right: The Optical eye-diagrams (b) before and (c) after auto-restoration.

The optical eye-diagram and Q value of before and after auto-restoration are shown in Fig. 5.10. The lower Q value of about 7.4 caused by the significant overshoot of the FPLD transmitted data-stream is obtained before auto-restoration condition, which is mainly attributed to the lower bias point and modulation base below the FPLD threshold current as shown in Figs. 10(a) and 10(b). After auto-restorable injection-locking operation, the threshold current of FPLD is effectively decreased due to the optical injection at a proper wavelength coincident with the longitudinal mode of the FPLD [5.5], such that the overshoot problem observed on the eye-diagram is solved and the Q value can be further promoted to 8.2 or larger as shown in Fig. 5.10(c). We have also measured the BER performances by

slightly detuning the wavelength of incoming source away from that of the free-running FPLD at very beginning, then comparing the receiving sensitivity of FPLD before and after self-restoration control, as shown in Fig. 5.11. Without self-restoration scheme, the degradation on BER performance of the injected FPLD transmitter becomes serious with increasing wavelength deviation. In comparison, the power penalty for obtaining the same BER at 10^{-9} from the injection-locked FPLD transmitter without a self-restoration control greatly increases from 0.8 to 1.9 dB as the deviated wavelength enlarges from 0.02 to 0.04 nm. After self-restoration control, the mode wavelength of the FPLD eventually coincides with that of the incoming source to results in a receiving sensitivity of -30.1 and -28.2 dBm at BER of 10^{-9} and 10^{-12}, respectively.

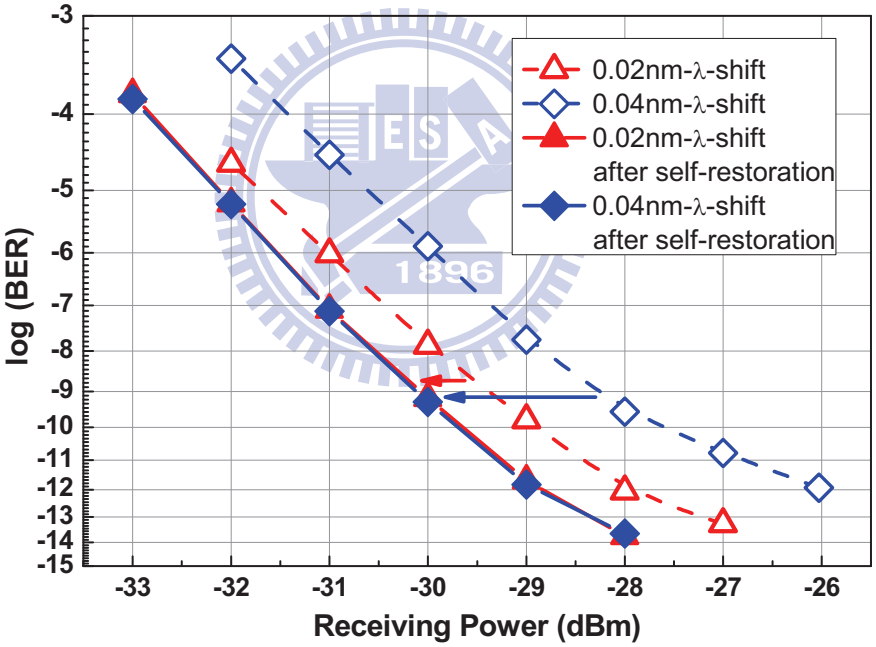

Fig. 5.11 The BER of the FPLD transmitter before and after self-restoration at different wavelength-deviation conditions.

The additional cost is an important issue for the implementation of the self-restorable injection-locked FPLD in practical networks. The component expense of the proposed self-restorable injection-locking FPLD scheme is briefly listed as Table I, which is compared with the reflective semiconductor optical amplifier (RSOA) based injection-locked transmitter

[5.14] and the traditional coherent wavelength injection locked FPLD without self-restorable function. As compared with the ROSA (OA-RL-OEC-1550, CIP) based injection-locked transmitter, a great reduction on the cost at the light source is reached due to the use of a commercially available FPLD in our scheme. The TEC cooler and controller are necessary for all architectures. Only the cost of an ADC/DAC integrated MCU controller is added into the proposed scheme, but the market price of a popular MCU (such as the ATMEL MEGA88V) used in commercial systems is just US$ 1.

TABLE 1. Expense comparison of the injection-locked transmitter solutions between RSOA and FPLD with/without self-restoration.

System Expense	RSOA WDM-PON	Injection-locked FPLD with Self-Restoration	Injection-locked FPLD without Self-Restoration
Light Source	US$500~1000	US$5~20	US$5~20
TEC controller	US$10	US$10	US$10
MPD-MCU	-	**US$ ~1**	-

For the future integration of optical transceiver in the proposed system, a schematic diagram was modified from a typical 2.5-Gbps small-form-factor-pluggable (SFP) optical transceiver (SI1525-40ATO, SANOC). Most of the components in the system are commercial and ready-to-use parts in a typical SFP transceiver application. For example, the laser diode driver, limiting amplifier, TEC controller, MCU, and PIN-TIA receiver were chosen as MAX3738 (MAXIM), MAX3747 (MAXIM), MAX8521 (MAXIM), ATMEGA88 (ATMEL), and TRR-1F41-320 (Truelight), respectively. In particular, the proposed system needs to control the temperature of the FPLD and a TEC cooler should be integrated in the transceiver. A commercial laser TO-can module built-in TEC cooler [5.12] with a maximum diameter of

5.6mm and a total length of 12.7 mm was demonstrated by Sumitomo Electric Industries, Ltd. as shown in Fig. 5.12. By implanting such a transmitter, the system could be achieved in a compact-size module such as a typical SFP optical transceiver for future access networks and LAN application.

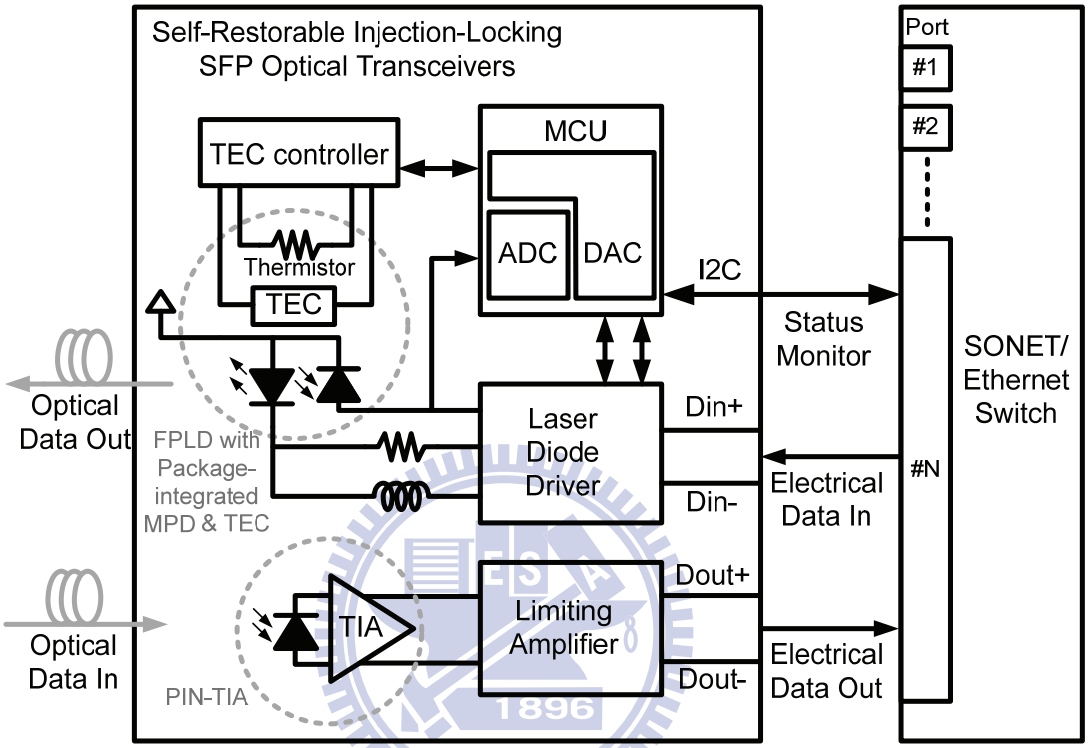

Fig. 5.12 Future system of the MPD-MCU based self-restoration unit.

However, some degradation on the eye-diagram and BER when detuning the polarization state of the external injection to be orthogonal to the preferred polarization state of the FPLD was observed. In practical application, such a problem relies on the self-restoration of the preferred polarization for the injection-locked FPLD, which can be achieved by feedback controlling an electronically tunable polarization controller added prior to the WRC-FPLD. Our proposed scheme cannot eliminate the polarization sensitive problem accompanied with the injection-locked FPLD, however, and the MCU of self-restorable injection locker can concurrently deal both the deviation of FPLD wavelength and the mismatched polarization of the incoming light. The schematic Fig. 5.14 of the self-restorable injection locker modified to involve the input polarization function is shown as below. The polarization degree

directly affects the injection efficiency, which is a little bit different from the wavelength detuning effect. That is, the requested power of optical injection into the FPLD could be greatly increased due to the deviation of the injected polarization from the preferred state of the FPLD. In our self-restorable design, the concept to achieve the self-restoration of the preferred polarization for the FPLD is based on feedback controlling an electronically tunable polarization controller added prior to the FPLD to be injection-locked. The MPD current of the FPLD is monitored during operation for feedback controlling the polarization controller to obtain the maximum output power from the injection-locked FPLD. After comparing the monitored MPD current with previous value, the MCU sends a controlling signal to detune incoming polarization via a polarization controller. With the same feedback control loop, the two important issues of wavelength locking and polarization matching can be concurrently implemented for the practical self-restorable injection locker. In particular, the polarization control is the unique and inherent problem when utilizing the injection locking technique to control the laser diode wavelength. Nevertheless, such injection-locked laser diodes still exhibit a benefit on narrow linewidth, long transmission distance, and especially the enhanced modulation bandwidth when comparing with other kinds of injection-locked sources.

5.6 Summary

In this chapter, a novel in situ and self-restorable scheme has been demonstrated for the injection-locking FPLD-based WDM transmitter by an integrated MPD in connection with an MCU controlling unit. The injection-locking and self-restoration characteristics such as the locking-in wavelength range and the illuminated power dependent MPD current of the injection-locked FPLD are analyzed. The integrated MCU calculates the monitored photocurrent from the MPD and dynamically controls the FPLD temperature via a TEC controller. After self-restorable injection locking, the transmitter exhibits a Q factor of 8.2 to provide a reachable BER as low as 1.1 10^{-16}, and an SMSR of >35 dB. The FPLD directly

modulated by a PRBS datasteam can be self-restoration injection-locked within 50 seconds, achieving a BER of 10^{-12} at a data rate of 2.5 Gbit/s with a receiving power as low as -25 dBm. With the self-restorable injection-locking scheme, the APC function that was prohibited in the injection-locked FPLDs can be added into future FPLD-based optical networks with a vastly improved stability and reliability. The proposed scheme works for most of the injection-locking FPLDs and can be cost effectively implemented using a minimum amount of redundant network resources.

References

[5.1] C. Henry, “Locking range and stability of injection locked 1.54 μm InGaAsP semiconductor laser,” *IEEE J. Quantum Electron*. **21**, 1152, (1985).

[5.2] Y. Matsui, S. Kutsuzawa, S. Arahira, Y. Ogawa, and A. Suzuki, “Bifurcation in 20-GHz gain-switched 1.55-μm MQW lasers and its control by CW injection seeding,” *IEEE J. Quantum Electron*. 34, 1213, (1998).

[5.3] Z. Xu, Y.-J. Wen, W.-D. Zhong, C.-J. Chae, X.-F. Cheng, Y. Wang, C. Lu, and J. Shankar, “High-speed WDM-PON using CW injectionlocked Fabry-Pérot laser diodes,” *Opt. Express*. **15**, 2953, (2007).

[5.4] N. Kashima, S. Yamaguchi, and S. Ishii, “Optical transmitter using side-mode injection locking for high-speed photonic LANs,” *IEEE J. Lightwave Technol.* **22**, 550, (2004).

[5.5] Y.-C. Chang, Y.-H. Lin, J. H. Chen, and G.-R. Lin, "All-optical NRZ-to-PRZ format transformer with an injection-locked Fabry-Perot laser diode at unlasing condition", *Opt. Express.* **12**, 4449, (2004).

[5.6] C. K. Chan, F. Tong, L. K. Chen, K. P. Ho, and D. Lam, “Fiber-fault identification for branched access networks using a wavelength-sweeping monitoring source,” *IEEE Photon. Technol. Lett.* **5**, 614, (1999).

[5.7] K. Lee, S. B. Lee, J. H. Lee, Y. -G. Han, S. -G. Mun, S. -M. Lee, and C. -H. Lee, "A self-restorable architecture for bidirectional wavelength-division-multiplexed passive optical network with colorless ONUs," *Opt. Express*, **15**, 4863, (2007).

[5.8] R. D. Esman and L. Goldberg, “Simple measurement of laser diode spectral linewidth using modulation sidebands,” *Electron. Lett.* **24**, 1393, (1988).

[5.9] S. Bouchoule, N. Stelmakh, M. Cavelier, and J.-M. Lourtioz, “Highly attenuating external cavity for picosecond-tunable pulse generation from gain/Q-switched laser diodes,” *IEEE J. Quantum Electron.* **29**, 1693, (1993).

[5.10] L. Li, “Static and dynamic properties of injection-locked semiconductor lasers,” *IEEE J. Quantum Electron.* **30**, 1701, (1994).

[5.11] K. Petermann, “*Laser Diode Modulation and Noise,*” Publishers Dordrecht, The Nitherlands: Kluwer Academic, (1998).

[5.12] M. Ichino, S. Yoshikawa, H. Oomori, Y. Maeda, N. Nishiyama, T. Takayama, T. Mizue, I. Tounai, and M. Nishie, “Small Form Factor Pluggable Optical Transceiver Module with Extremely Low Power Consumption for Dense Wavelength Division

Multiplexing Applications," *Proceedings of 2005 Electronic Components and Technology Conferenc*e, **1**, 1044, (2005).

[5.13] N. S. Bergano, F. W. Kerfoot, C. R. Davidsion, "Margin measurements in optical amplifier system," *IEEE Photon. Technol. Lett.* **5**, 304, (1993).

[5.14] W. Lee, M.-Y. Park, S.-H. Cho, J. Lee, C. Kim, G. Jeong, and B.-W. Kim, "Bidirectional WDM-PON Based on Gain-Saturated Reflective Semiconductor Optical Amplifiers," *IEEE Photon. Technol. Lett.* **17**, 2460, (2005).

Chapter 6
Conclusions

6.1 Summary

In this dissertation, we investigated four novel design of weak-resonant-cavity-Fabry-Perot-laser-diode (WRC-FPLD) in the wavelength division multiplexer passive optical network (WDM-PON) systems. The side-mode injection-locked FPLD transmission diagnosis of a multi-channel selectable transmitter is introduced in chapter 2. The WRC-FPLD with enhanced injection-locking bandwidth is introduced in chapter 3. The pulsating master and injected slave weak-resonant-cavity laser diodes based quasi-color-free 2.5Gb/s WDM-PON is introduced in chapter 4. The self-restorable injection-locking monitor by integrated photodiode for FPLD WDM Transmitter is introduced in chapter 5. From these researches performed in this dissertation, some valuable feature and contribution can be briefly summarized as following.

(1) Side-mode injection-locked FPLD transmission diagnosis of a multichannel selectable

- The effect of the injection-locking power and side-longitudinal-mode order on the linewidth, SMSR, and BER characteristics of a slave FPLD injected by another spectrally sliced master FPLD are theoretically analyzed.
- The back-to-back and 25km-SMF transmission performances of the 2.5-Gbit/s directly modulated FPLD based WDM-PON transmitter under side-mode injection-locking is demonstrated.
- The maximum usable channels of the side-mode injection-locking FPLD are 22, covering a wavelength-locking range up to 24 nm.

- A BER of $<10^{-12}$ is obtained for the nearest 13 modes and a 10^{-10} error rate can be achieved for all of the 22 injection-locked modes.

(2) Weak-resonant-cavity Fabry-Perot laser diode with Enhanced Injection-locking Bandwidth

- The effects of the front-facet reflectivity of the WRC-FPLD on the injection locking range, the spontaneous emission dependent SNR and Q-factor, and the BER transmission response are theoretically and experimentally investigated
- As a result, the 30-nm wavelength-locking capacity of the directly modulated AR-FPLA based ONU transmitter with 1% front0facet reflectivity under side-mode injection-locking condition is demonstrated for 2.5-Gbit/s DWDM-PON application.
- The largest SMSR up to 40 dB and a least Q factor of 9.5 is achieved when injection-locking the central mode with a seeding power level of -3 dBm, which provides a receiving sensitivity of -24.4 dBm at BER of 10^{-12}.

(3) Pulsating master and injected slave weak-resonant-cavity laser diodes based quasi-color-free 2.5Gb/s WDM-PON

- The quasi-color-free pulsed RZ transmission can be achieved up to 16 DWDM channels. The acceptable tolerance of wavelength locking bandwidth can be enhanced with increasing RF power to improve gain-switching mode linewidth.
- A receiving sensitivity for 2.5Gbs/s back-to-back transmission at BER$<10^{-10}$ can be -25.6 dBm. With appropriate temperature tuning of the slave WRC-FPLDs, the variation on receiver sensitivity penalty at BER=10^{-10} can be confined within 1.6 dB under a temperature shift of 15^{o}C.
- A well-opened eye pattern can be obtained with a relatively large dynamic range, in which the rising and falling time (defined as the duration between 20% and 80% of

on-level amplitude) are 48 ps and 52 ps.

(4) Self-Restorable Injection-Locking Monitor by Integrated Photodiode for FPLD WDM Transmitter

- A novel in situ and self-restorable scheme has been demonstrated for the injection-locking FPLD-based WDM transmitter by an integrated MPD in connection with an MCU controlling unit. The injection-locking and self-restoration characteristics such as the locking-in wavelength range and the illuminated power dependent MPD current of the injection-locked FPLD are analyzed.
- The FPLD directly modulated by a PRBS datasteam can be self-restoration injection-locked within 50 seconds, achieving a BER of 10^{-12} at a data rate of 2.5 Gbit/s with a receiving power as low as -25 dBm.
- After self-restorable injection locking, the transmitter exhibits a Q factor of 8.2 to provide a reachable BER as low as 1.1×10^{-16}, and an SMSR of >35 dB.
- With the self-restorable injection-locking scheme, the APC function that was prohibited in the injection-locked FPLDs can be added into future FPLD-based optical networks with a vastly improved stability and reliability.
- The proposed scheme works for most of the injection-locking FPLDs and can be cost effectively implemented using a minimum amount of redundant network resources.

As our best knowledge, the commercial TO-can package could meet the request of 10-Gb/s application. However, in order to enhance the locking bandwidth and injection efficiency, the weak-resonant cavity of our proposed laser is unfavorable for high speed operation. Our proposed WRC-FPLD is specially designed for WDM-PON application, and the investigated results exhibits many benefits such as data rate of 2.5G/s, 30-nm injection range, and quasi-color-free operation. In order to take the advantages, the bandwidth of WRC-FPLD was measured at 3 GHz. Some of the remarkable researches on similar transmitters of

WDM-PON solutions are summarized as below table. In comparison with the results of ASE light source injected FPLD, the incoherent light injection usually brings a relatively high intensity noise to limit the achievable bit rate or transmission distance. The WDM-PON transmitters based on such an injection source can provide a highest data rate up to 1.25 Gbps with the minimum WDM channel spacing of 100 GHz. With the use of coherent light source injection, the WRC-FPLD based WDM-PON transmitter becomes a potential candidate for achieving 2.5-Gbps transmission in WDM-PON system with channel spacing of 50 GHz [3]. Although a 10-Gbps WDM-PON injected by DFB laser diode was previously demonstrated [4], which only allows a wavelength-detuning range of 3.6 GHz (0.029 nm) at BER of 10-9, and the wavelength matching and temperature controlling circuitry is mandatory. Since the temperature-dependent wavelength shifting slope of a regular commercial FPLD is 0.06 nm/oC, and the temperature of FPLD with locking range of 0.029 nm should be maintained within +/-0.25 ^{o}C. This is not an easy approach to deal with the locking range and the BER performance within such a tiny temperature tolerance. There is always a tradeoff between intensity noise and coherence of the injection-locked FPLD or WRC-FPLD based transmitters in the WDM-PON architectures. Our proposed pulsating injected WRC-FPLD system is the only quasi-color-free WDM-PON system with the data-rate over 2.5Gb/s.

Injection-locked WDM-PON solutions	**Max Data Rate**		**Distance**	**Locking bandwidth**		**Channel Spacing**
ASE injected FPLD	1.25 Gbps	Low	20km	N.A.	Poor	100 GHz
ASE injected RSOA	1.25 Gbps	Low	20km	**Color-Free**	**Best**	100 GHz
QD-MLL injected FP	**2.5 Gbps**	**Good**	25km	0.27nm	Poor	50 GHz
DFB injected FP 10Gbps	**10 Gbps**	**Best**	10km	0.029nm	Very poor	N.A.
ASE injected WRC-FPLD	1.25 Gbps	Low	25km	**Quasi-Color-Free (3.2dB penalty)**	**Good**	200 GHz
Pulsating injected WRC-FPLD	**2.5 Gbps**	**Good**	25km	**Quasi-Color-Free (1dB penalty)**	**Good**	**100 GHz**

6.2 Suggestions for Future Work

There are -possible direction for future work:

1. This system is an appropriate balance between coherent and incoherent injection solutions. The proposed pulsed RZ network could further be applied to a RZ binary-phase-shift-keying (BPSK) network or hybrid DWDM/OTDM PON architecture.

Curriculum Vitae

姓名：廖育聖 Liao, Yu-Sheng

出生地：台灣 台北市 Taiwan, Taipei

出生日期：1978/07/10

學歷 *Academic Background*：

國立交通大學應用數學學系與電子工程學系 雙學士學位

國立台北科技大學光電工程研究所 碩士學位

國立交通大學光電工程研究所 博士學位

比賽獲獎 *Awards*：

1. "External feedback injection controlled 2.5 Gbps on/off keying of a single-mode gain-switched laser diode" was a warded "the Best Paper Award" **(最佳論文獎)** at ***OPT2003* (台灣光電科技研討會)**.
2. "簡化型通訊用光偵測器靈敏度與誤碼率分析系統" was awarded at **教育部 91 學年度大專校院通訊科技專題製作競賽 晉級複賽**
3. "OC-192 光通訊用注入鎖定半導體雷射權光訊號格是轉換邏輯閘" was awarded at **教育部 93 學年度大專校院通訊科技專題製作競賽 晉級複賽**
4. "脈衝光梳時鐘注入半導體光法大器為基礎之 OC-192 全光格式轉換器" was awarded at **教育部 94 學年度大專校院通訊科技專題製作競賽 優等**

專利 *Patents*:

1. **廖育聖**、廖宗添、林恭如,"發明自耦同步調制技術以量測光接收機之等效靈敏度與誤碼率", **中華民國專利, 發明第 I 226762 號, 2005 年 1 月 11 日**
2. **廖育聖**, "光纖傳輸模組之發光二極體結構改良", **中華民國專利, 新型第 M 318193 號, 2007 年 9 月 1 日**
3. **廖育聖**、廖宗添、孫秀杏,"透鏡整合式光纖接頭", **中華民國專利, 新型第 M 347575 號, 2008 年 12 月 21 日**
4. **廖育聖**、廖宗添、孫秀杏, "光學透鏡整合模組", **中華民國專利, 新型第 M 347576 號, 2008 年 12 月 21 日**

博士論文 *Doctor Dissertation*：

利用弱共振腔費比布洛雷射二極體於被動式分波多工光纖網路之研究

Studies on Weak-Resonant-Cavity-Fabry-Perot-Laser-Diode-based Wavelength Division Multiplexer Passive Optical Network

指導教授：林恭如、郭浩中

碩士論文 *Master Thesis*：

反向光注入鎖模半導體光放大器光纖雷射之研究

Study of Backward-Optical-Injection Mode-Locked Semiconductor Optical Amplifier Fiber Lasers

指導教授：林恭如、徐巍峰

Publication List

國際期刊論文與研討會論文投稿及發表紀錄：

學術期刊 *Journal Paper*：

碩士期間:

1. Gong-Ru Lin, **Yu-Sheng Liao** and GuangQun Xia "Dvnamics of optical backward injection induced gain-deplete ion modulation and modulation an mode-locking in semiconductor optical amplifier fiber laser", Vol. 12 pp. 2017-2026, ***Opt. Express,*** Apr. 2004. ***Selected by Virtual Journal of Ultrafast Science, Vol. 3, No. 6, June 2004.***
2. Gong-Ru Lin and **Yu-Sheng Liao** "Harmonic Injection-locking Behavior of Frequency-Detuned Optical Pulse in Erbium-Doped Fiber Laser ", ***Jpn. J. Appl, Phys.***, Vol. 43, Issue: 8A, pp. 5204-5208, Aug. 2004.
3. Gong-Ru Lin, Pai-Shen Hsueh, Hsiao-Hua Wu, and **Yu-Sheng Liao**, "The Detuning Characteristics of Rational Harmonic Mode-Locked Semiconductor Optical Amplifier Fiber-Ring Laser Using Backward Optical Sinusoidal-Wave Injection Modulation", ***J. Lightwave Technol.***, Vol. 23, No. 3, pp. 1325-1333, Mar. 2005.

博士期間:

4. Gong-Ru Lin and **Yu-Sheng Liao** "Sensitivity evaluation of fiber optic OC-48 p-i-n transimpedance amplifier receivers using sweep-frequency modulation and intermixing diagnostics", ***Optical Engineering***, Vol, 44, No.4, pp. 044002-1-044002-5, Apr. 2005.
5. Yung-Cheng Chang, Yu-Huang Lin, **Yu-Sheng Liao**, and Gong-Ru Lin, "Switchable dual-wavelength NRZ-to-RZ data-format transformer using non-DC-biased and synchronously modulated laser diode", ***IEICE Trans. Electron.***, Vol. E88-C, No. 5, pp. 981-983, May 2005.
6. **Yu-Sheng Liao** and Gong-Ru Lin, "Comparison on the Sensitivity of Fiber-optic SONET OC-48 PIN-TIA Receivers Measured by Using Synchronous Modulation Inter-Mixing Technique and Bit-Error-Rate Tester", ***IEEE Trans. Instrum. Meas.,*** Vol. 55, No. 6, pp. 2172-2175, Dec. 2006.
7. **Yu-Sheng Liao**, Gong-Ru Lin, Hao-Chung Kuo, Kai-Ming Feng, and M. Feng, "10Gbit/s Operation of an $In_{0.53}Ga_{0.47}As$ p-i-n Photodiode on Metamorphic InGaP Buffered Semi-Insulating GaAs Substrate", ***IEEE Photonics Technol. Lett.,*** Vol. 18, No. 17, pp. 1822-1824, Sep. 2006.
8. **Yu-Sheng Liao**, Jin-Wei Shi, Y.-S. Wu, Hao-Chung Kuo, M. Feng, and Gong-Ru Lin, "Optically heterodyne diagnosis of a high-saration-power undoped InP sandwiche InGaAs p-i-n photodiode grown on GaAs" ***Opt. Express,*** Vol. 14, No.12, pp. 5031-5037 Jun. 2006.
9. Gong-Ru Lin, Jun-Yuan Chang, **Yu-Sheng Liao**, and Hai-Han Lu, "L-Band Erbium-Doped Fiber Laser with Coupling-Ratio Controlled Wavelength Tunability", ***Opt. Express,*** Vol. 14, No. 21, pp. 9743-9749, Oct. 2006.
10. Gong-Ru Lin, Kun-Chieh Yu, Ci-Ling Pan, and **Yu-Sheng Liao**, "All-Optical Decision-Gating of 10Gbit/s RZ Data in a Semiconductor Optical Amplifier Temporally Gain-Shaped with Dark-Optical-Comb", ***J. Lightwave Technol.***, Vol. 25, No. 7, pp. 1651-1658 Jul. 2007.
11. **Yu-Sheng Liao**, Hao-Chung Kuo, Yung-Jui Chen, and Gong-Ru Lin, "Side-mode transmission diagnosis of a multichannel selectable injection-locked Fabry-Perot Laser Diode with anti-reflection coated front facet," ***Opt. Express,*** Vol. 17, No. 6, pp. 4859-4867, Mar. 2009.
12. Gong-Ru Lin, **Yu-Sheng Liao**, Yu-Chieh Chi, Hao-Chung Kuo, Gong-Cheng Lin, Hai-Lin Wang, and Yung-Jui

Chen, “Long-cavity Fabry-Perot Laser Amplifier Transmitter with Enhanced Injection-locking Bandwidth for WDM-PON Application” ***J. Lightwave Technol.***, Vol. 28, No. 20, pp. 2925-2932, Oct., 2010.

13. **Yu-Sheng Liao**, Hao-Chung Kuo, and Gong-Ru Lin, "In Situ and Self-Restorable Injection-Locking Monitor by Integrated Photodiode for FPLD WDM Transmitter," ***IEEE J. Quantum Electron.,*** Accepted.

國際研討會 *International Conference Paper*：

碩士期間:

1. Gong-Ru Lin and **Yu-Sheng Liao**, “Comparison on the Sensitivity of Fiber-Optic SONET OC-48 PIN-TIA Receivers Measured by using Synchronous Modulation Inter-Mixing Technique and Bit-Error-Rate Tester”, ***Conference on Asia-Pacific Optical and Wireless Communications***, Wuhen, China, October 14-18, 2003. **invited talk** (邀請演講)
2. Gong-Ru Lin and **Yu-Sheng Liao**, “A Synchronous Modulation and Inter-Mixing Technique for Sensitivity and Error-Rate Analysis of SONET OC-3/155Mbps PIN-TIA”, ***The Fifth Pacific Rim Conference on Lasers and Electro-Optics (CLEO/PR 2003)***, oral paper, Taipei, Taiwan, December 15-19, 2003.
3. **Yu-Sheng Liao** and Gong-Ru Lin, “5 GHz optically cross-gain modulation induced mode-locking of semiconductor optical amplifier”, ***International Conference on Laser and Electro-Optics Society Annual Meeting (CLEO2004)***, post paper CWA76, San Francisco, USA, May 15-19, 2004.
4. **Yu-Sheng Liao** and Gong-Ru Lin, “Detuning the Duty Cycle of Backward Optical Injection for Optimized Mode-Locking in Semiconductor Optical Amplifier Fiber Laser”, ***Ninth Optoelectronics and Communications Conference/Third International Conference on Optical Internet (OECC/COIN2004)***, Poster session, paper 13p-100, Yokohama, Japan, July12-16, 2004.
5. Yu-Huang Lin, Yung-Cheng Chang, **Yu-Sheng Liao**, and Gong-Ru Lin, “Optically triggered on/off keying of 10-Gbit/s single-mode return-to-zero data pulse-train from Fabry-Perot laser diode”, ***Ninth Optoelectronics and Communications Conference/Third International Conference on Optical Internet (OECC/COIN2004)***, Poster session, paper 13p-68, Yokohama, Japan, July12-16, 2004.
6. Yung-Cheng Chang, Yu-Huang Lin, **Yu-Sheng Liao**, and Gong-Ru Lin, “Tunable Dual-Wavelength NRZ-to-RZ Data-Format Transformer at 10 Gbps Using Non-DC-Biased and Synchronously Modulated Laser Diode”, ***Ninth Optoelectronics and Communications Conference/Third International Conference on Optical Internet (OECC/COIN2004)***, Poster session, paper 13p-106, Yokohama, Japan, July12-16, 2004.

博士期間:

7. Chi-Kuang Lin, **Yu-Sheng Liao**, Hao-Chung Kuo, and Gong-Ru Lin, “Low-leakage $In_{0.53}Ga_{0.47}As$ p-i-n photodetector fabricated on GaAs substrate with linearly graded metamorphic InxGa1-xP buffer”, ***2004 Asia-Pacific Optical and Wireless Communications Conference and Exhibition (APOC2004)***, paper. 5624-61, Beijing, China, November 7-11, 2004.
8. Yi-Hsiang Chiu, **Yu-Sheng Liao**, and Gong-Ru Lin, “The effect of backward injecting wavelength on the mode-locking dynamics of a semiconductor amplifier based fiber laser”, ***2004 Asia-Pacific Optical and Wireless Communications Conference and Exhibition (APOC2004)***, paper. 5624-61, Beijing, China, November 7-11, 2004.

9. I-Hsiang Chiu, **Yu-Sheng Liao**, Yung-Cheng Chang, and Gong-Ru Lin, "A 3.5-ps Mode-Locked Semiconductor Optical Amplifier Fiber Laser generated by 60-ps Backward Optical Dark Pulse-Train Injection", ***Photonics West 2005, Symposia: Lasers and Applications in Science and Engineering***, San Jose, California, 22-27 January 2005.
10. **Yu-Sheng Liao**, and Gong-Ru Lin, "Beyond 10-Gbps operation of a metamorphic InGaP buffered In0.53Ga0.47As p-i-n photodetector grown on GaAs substrate", ***2005 Asia-Pacific Optical and Wireless Communications Conference and Exhibition (APOC2005)***, oral paper 6020-75, Shanghai China, November 6-10, 2005.
11. **Yu-Sheng Liao**, Hao-Chung Kuo, M. Feng, and Gong-Ru Lin, "Metamorphic InGaP buffered $In_{0.53}Ga_{0.47}As$ p-i-n photodetector grown on GaAs substrate for 10Gbit/s and beyond", Conference on Semiconductor Photodetectors III, part of the ***SPIE Integrated Optoelectronic Devices 2006 Symposium***, San Jose, California, USA, January 21-26, 2006.
12. **Yu-Sheng Liao**, Gong-Ru Lin, Hao-Chung Kuo, Kai-Ming Feng, Milton Feng, "A 10-Gbps $In_{0.53}Ga_{0.47}As$ p-i-n Photodiode Receiver on Metamorphic InGaP Buffered GaAs Substrate", ***OSA/IEEE Conference on Laser and Electro-Optics (CLEO2006)*****,** Oral Session CThD - Receivers and Detectors, Paper CThD1, Long Beach, California USA, May 21-26, 2006.
13. **Yu-Sheng Liao**, I-Shiang Chiu, and Gong-Ru Lin, "Femtosecond Harmonically Optical-Injection Mode-Locked Semiconductor Optical Amplifier Based Fiber Lasers", ***2006 Asia-Pacific Optical and Wireless Communications Conference and Exhibition (APOC2006)***, Session APOC01, paper 6351-7, Gwangju Korea, September 3-7, 2006.
14. Jun-Yuan Chang, **Yu-Sheng Liao**, Hai-Han Lu, and Gong-Ru Lin, "Wavelength control of L-band erbium-doped fiber laser with tunable-ratio output couplers", ***2006 Asia-Pacific Optical and Wireless Communications Conference and Exhibition (APOC2006)***, Session APOC02, paper 6351-71, Gwangju Korea, September 3-7, 2006.
15. Kun-Chieh Yu, **Yu-Sheng Liao**, and Gong-Ru Lin, "Self Optical Decision Gating of Degraded RZ Data Stream at 10Gbits/s with a Optical-Clock-Injected Semiconductor Optical Amplifier", ***2006 Asia-Pacific Optical and Wireless Communications Conference and Exhibition (APOC2006)***, Session APOC03, paper 6353-42, Gwangju Korea, September 3-7, 2006.
16. **Yu-Sheng Liao** and Gong-Ru Lin, "22-Channel Detuning Capacity of a Side-Mode Injection Locked FPLD for Directly Modulated 2.5Gbit/s DWDM-PON", ***Optical Fiber Communication Conference and Exhibit (OFC2006)***, Session OMS, Oral paper OMS8, Anaheim, California, March 25-29, 2007.
17. **Yu-Sheng Liao**, Yung-Jui Chen, and Gong-Ru Lin, "22-Channel Capacity of 2.5Gbit/s DWDM-PON ONU transmitter by Direct-Modularly Side-Mode Injection Locked FPLD", ***2006 Asia-Pacific Optical and Wireless Communications Conference and Exhibition (APOC2007)***, Oral paper. 6783-90, Wuhan, China, Nov. 5, 2007.
18. Gong-Cheng Lin, Sun-Chien Ko, Yin-Hsun Huang, Hai-Lin Wang, **Yu-Sheng Liao**, and Gong-Ru Lin, "Self-seeding injection of anti-reflection coated FP laser amplifier based transmitters for wavelength division multiplexing PON", ***2006 Asia-Pacific Optical and Wireless Communications Conference and Exhibition (APOC2007)***, Oral paper. 6783-96, Wuhan, China, Nov. 5, 2007.

19. **Yu-Sheng Liao**, Yung-Jui Chen, Yin-Hsun Huang, Hai-Lin Wang, Sun-Chien Ko, Gong-Cheng Lin, Gong-Ru Lin, "A Novel Anti-Reflecton Coated FP Laser Amplifier for 2.5Gbit/s DWDM-PON Transmission" ***Conference on Lasers and Electro-Optics (CLEO2007)***, paper JTuA121, Baltimore Maryland, USA, May 6-11, 2007.
20. Kun-Chieh Yu, **Yu-Sheng Liao**, and Gong-Ru Lin, "Duty-Cycle and Chirp Diagnosis of All-Optical Format Conversion Data in Multi- and Single-Wavelength Inverse Optical Comb Injected Semiconductor Optical Amplifier," ***Conference on Lasers and Electro-Optics (CLEO2007)***, paper JTuA121, Baltimore Maryland, USA, May 6-11, 2007.
21. **Yu-Sheng Liao**, and Gong-Ru Lin, "Integrated Photodiode Based On-Line and Self-Restorable Injection-Locking FPLD Monitor for WDM Optical Networks," ***Conference on Lasers and Electro-Optics (CLEO2008)***, San Jose, CA, MAY 04-09, 2008.
22. **Yu-Sheng Liao**, Yu-Chieh Chi, Hao-Chung Kuo, and Gong-Ru Lin, "Pulsating master and injected slave weak-resonant-cavity laser diodes based quasi-color-free 2.5Gb/s RZ DWDM-PON" ***Optical Fiber Communication Conference and Exposition (OFC2011),*** Los Angeles, CA, USA, March 8-10, 2011.